Coherent X-ray Imaging

Ian McNulty

Center for Nanoscale Materials

18 June 2014

16th National School on Neutron and X-ray Scattering

Argonne National Laboratory

Outline

1. Fundamentals

contrast

resolution

coherence

x-ray sources, optics, detectors

imaging regimes, coherent scattering

2. Direct methods

projection

full-field

3. Indirect methods

coherent diffractive imaging

scanning CDI (ptychography)

holography

Imaging

image [ˈɪmɪdʒ]

Noun:
The optical counterpart of an object produced by an optical device (as a lens or mirror) or an electronic device

Verb:
Make a visual representation of (something) by scanning it with a detector or electromagnetic beam.

- *Merriam-Webster Dictionary*

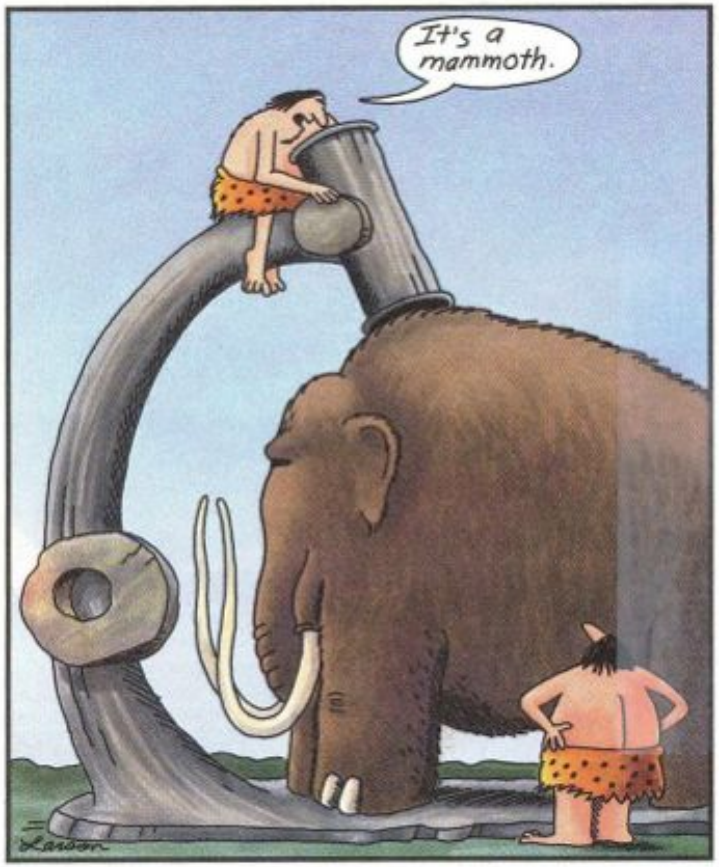

Early microscope

Contrast mechanisms in x-ray imaging

Access a wealth of information

- Absorption — measure electron density
- Phase — measure real part of refractive index
- Fluorescence — measure elemental distribution
- Spectroscopy — measure chemical state, atomic neighborhood
- Diffraction — probe atomic lattice structure and strain
- Polarization — probe magnetic and orbital states

- Natural sample contrast is possible; staining not required
- Image structure of thick samples, sectioning not required
- More penetrating, less damage, less charging than with electrons

Refractive index and contrast in the x-ray region

$$n = 1 - \delta - i\beta = 1 - \frac{r_e}{2\pi}\lambda^2 \sum_i n_i f_i(0)$$

$$A = A_0 \exp(-inkt)$$

$$k = 2\pi / \lambda$$

- Absorption contrast:

  sensitive to *Im(n)*

  $$\sim 4\pi\beta(x,y)t/\lambda$$

- Phase contrast:

  sensitive to *Re(n)*

  $$\sim 2\pi\delta(x,y)t/\lambda$$

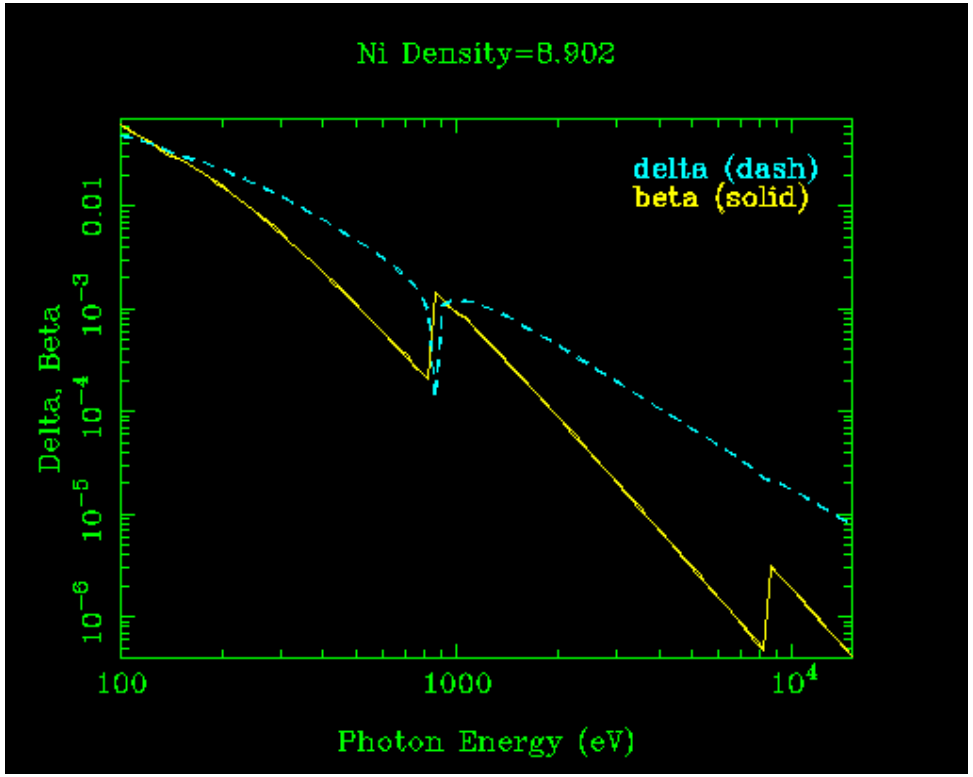

Absorption edges provide elemental and chemical specificity

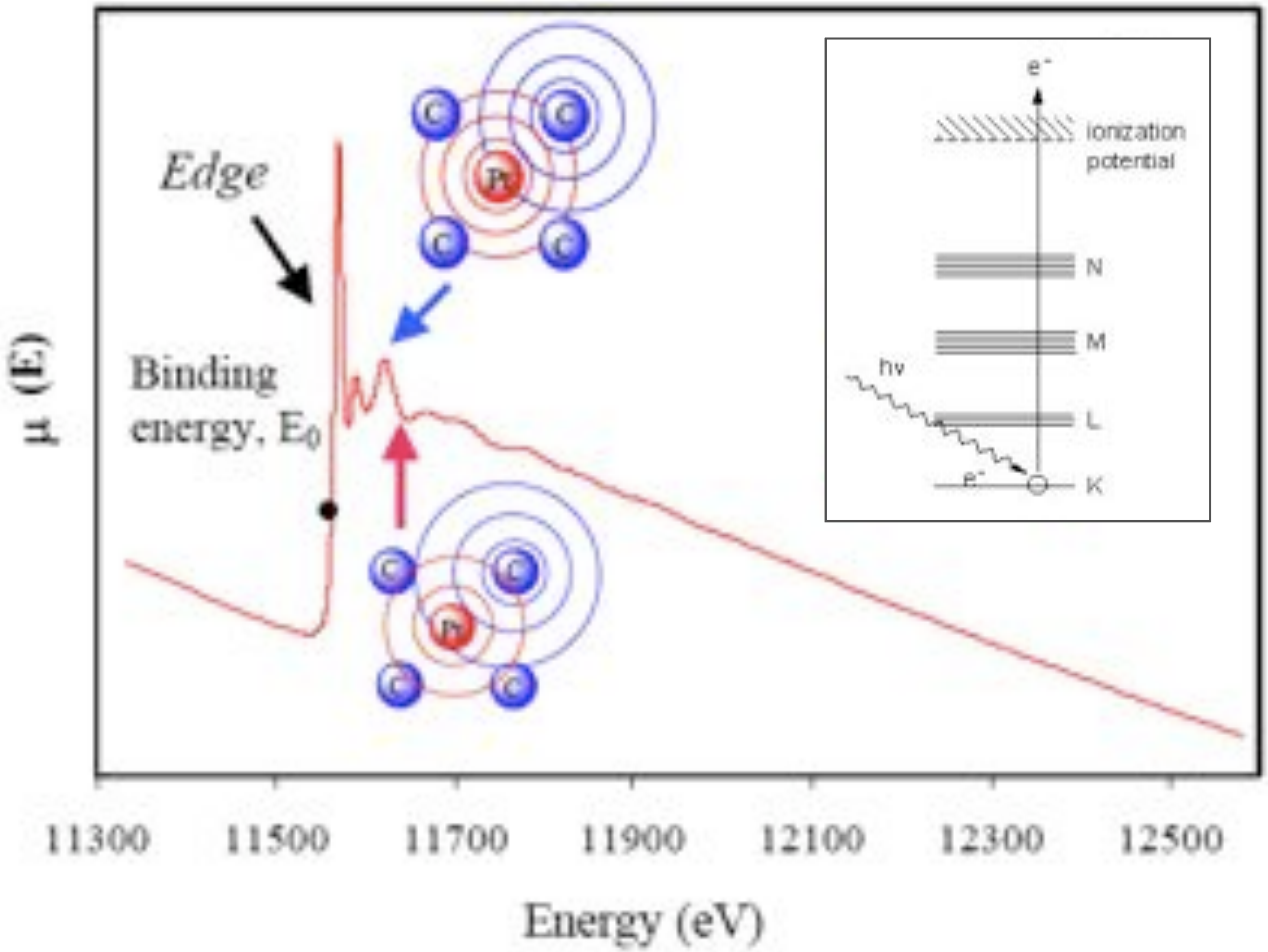

Polarized x-rays give sensitivity to electron spin

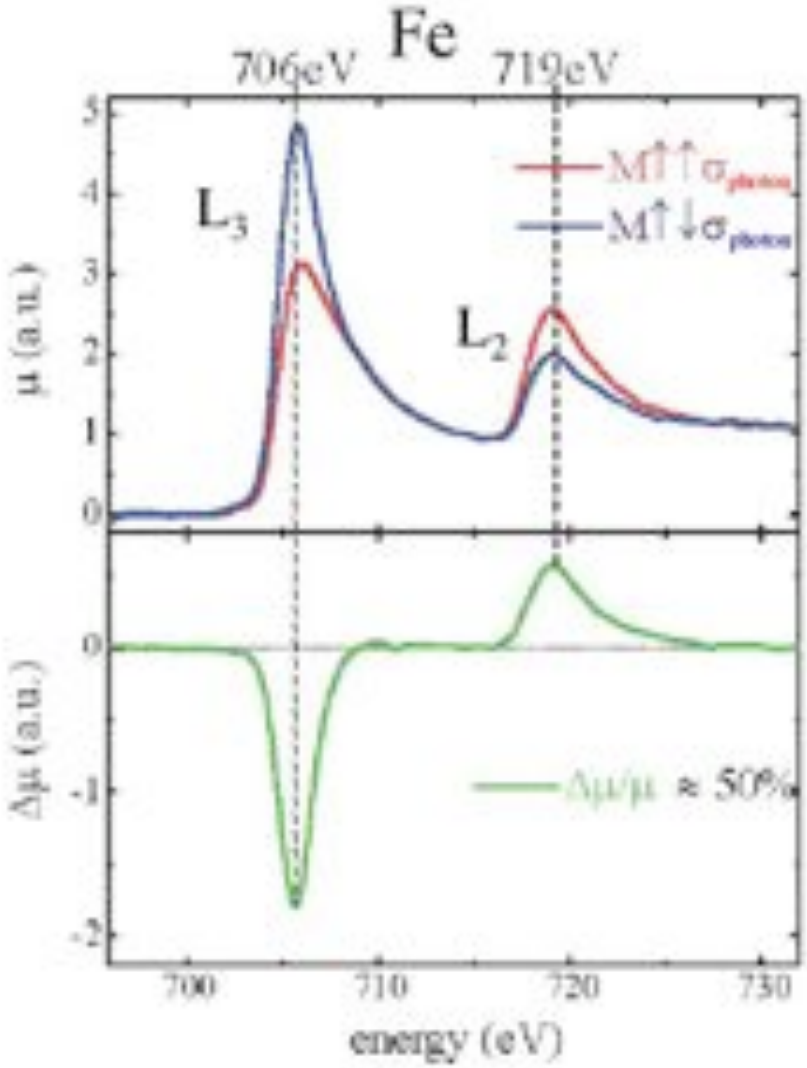

Image formation as a scattering process

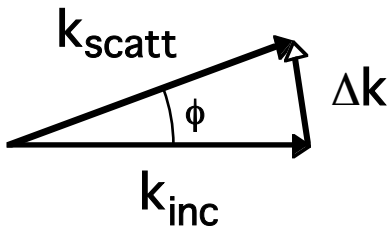

Incident waves with initial momentum k_{inc} are elastically scattered into new direction k_{scatt} with momentum transfer Δk.

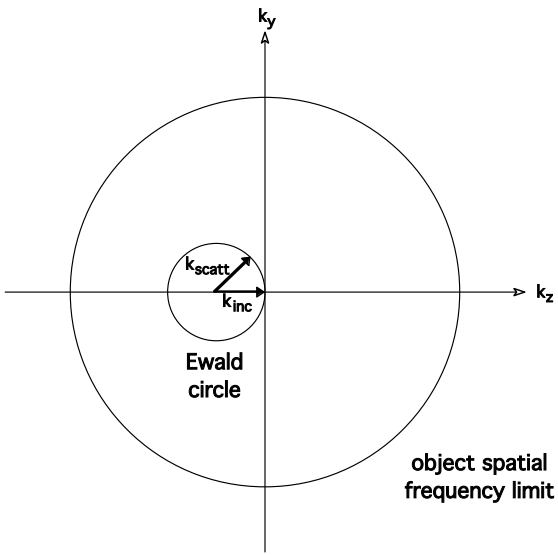

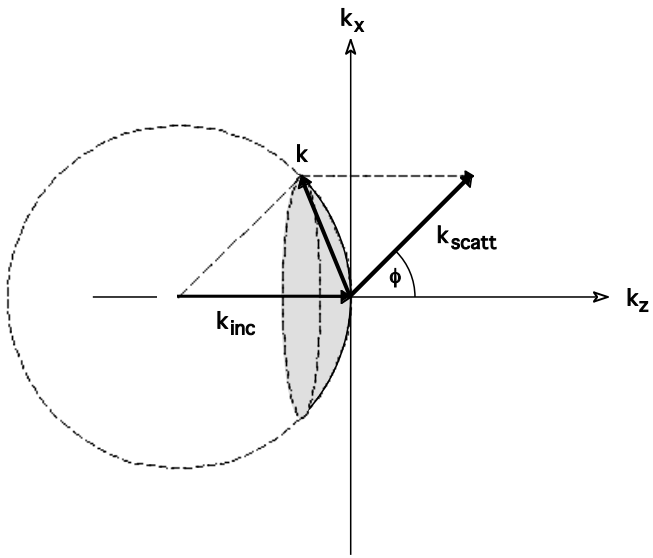

Ewald sphere is defined by conservation of momentum. Only spatial frequencies on the Ewald sphere are accessible to the imaging process, limiting attainable resolution.

Diffraction limits to resolution

Point-spread function

$$P(x,y) = \frac{\sin x}{x}\,\frac{\sin y}{y}$$

with $x = \frac{kax}{z}$, $y = \frac{kay}{z}$

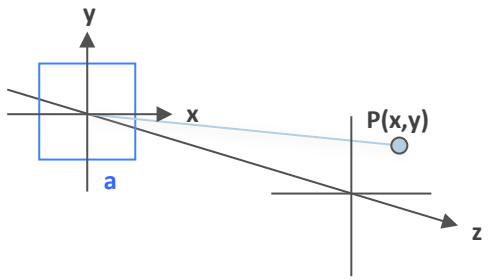

Transverse $\boxed{R = 0.5\,\frac{\lambda}{NA}}$

where $NA \sim \frac{a}{z}$

$$k = \frac{2\pi}{\lambda}$$

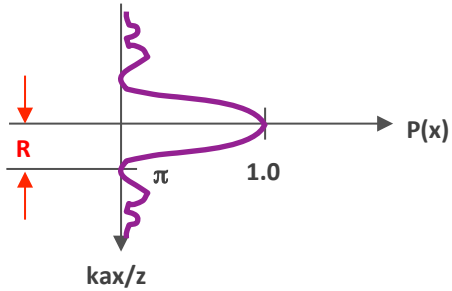

Bragg's law

$$\Delta\vec{k} = \vec{k}_{inc} - \vec{k}_{scatt} \qquad (0 \le \Delta k \le 2k_{inc}) \qquad k_x^2 + k_y^2 + (k_z + k_{inc})^2 = k_{inc}^2$$

For extreme-angle ray (xz plane, $k_y = 0$) with $k_x = \frac{2\pi}{2R} = \frac{2\pi}{\lambda}NA$

Longitudinal $\boxed{DOF = \frac{\lambda}{(NA)^2}}$ and $k_z = \frac{k_x^2}{2k_{inc}} \qquad (k_z << k_{inc})$

What do we mean by "resolution"?

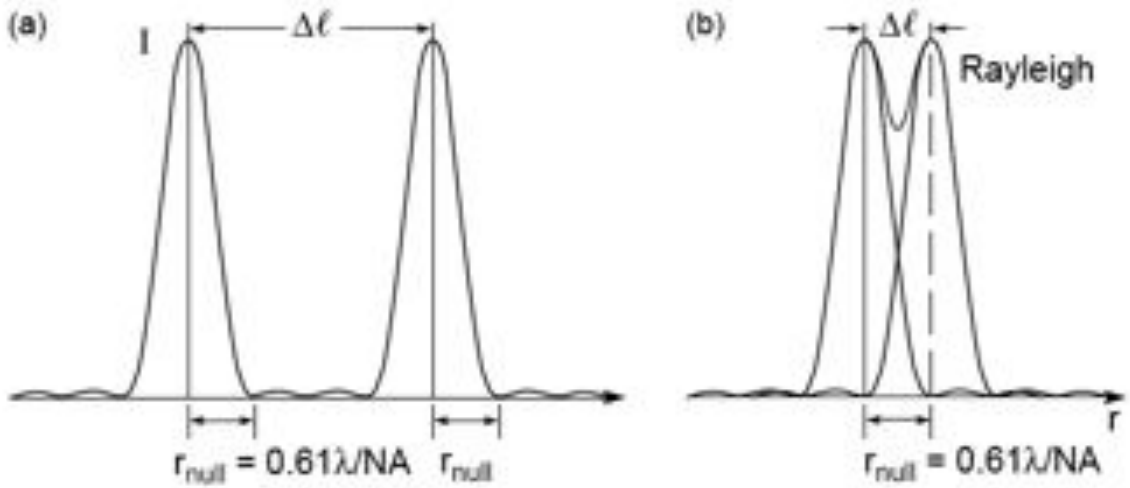

- Point sources are spatially coherent
- Mutually incoherent
- Intensities add
- Rayleigh criterion (26.5% dip)

Conclusion: With spatially coherent illumination, objects are "just resolvable" when

$$\mathrm{Res}|_{coh} = \frac{0.61\,\lambda}{\mathrm{NA}} = 1.22\,\Delta r$$

Coherence

longitudinal coherence

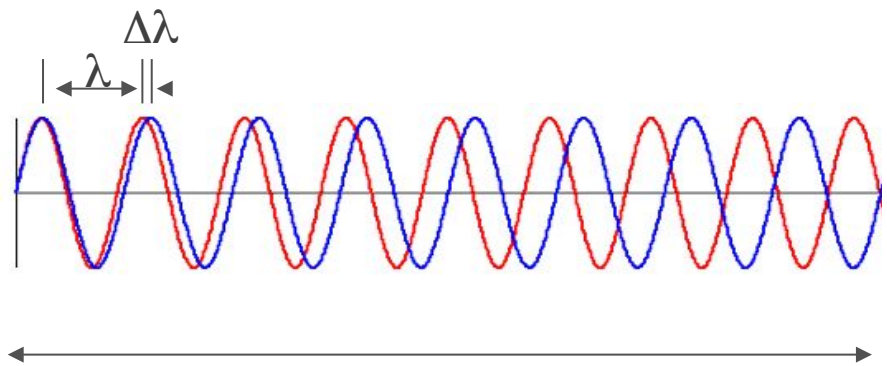

$$l_c \sim \frac{\lambda^2}{\Delta\lambda}$$

$$\tau_c \sim \frac{\lambda^2}{c\Delta\lambda}$$

transverse coherence

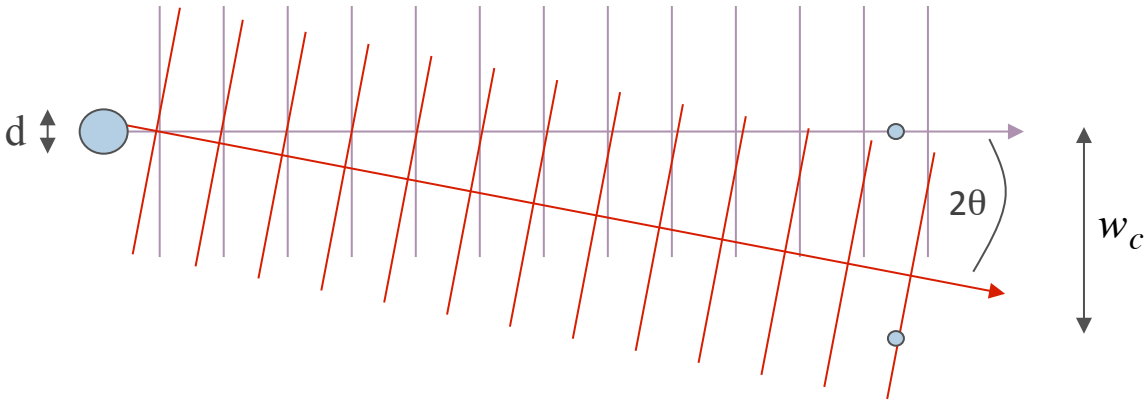

$$w_c \sim \frac{\lambda z}{d}$$

$$d \cdot \theta = \lambda / 2\pi$$

$$\Delta x \, \Delta p \geq \hbar / 2$$

Coherent vs. incoherent

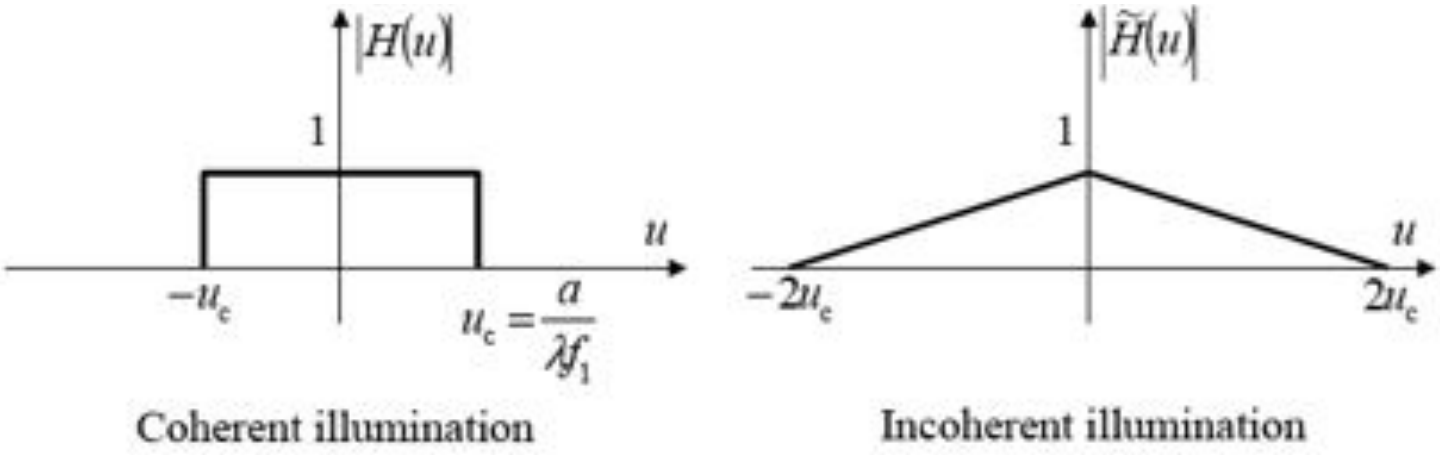

Scanning and full-field microscopy are *incoherent* methods

- Transfer function is linear in the field *intensities*
- Characterized by sloping function down to 2NA

Diffraction and holographic microscopy are *coherent* methods

- Transfer function is linear in the field *amplitudes*
- Characterized by flat top, sharp cutoff at limiting NA

Why use synchrotron radiation?

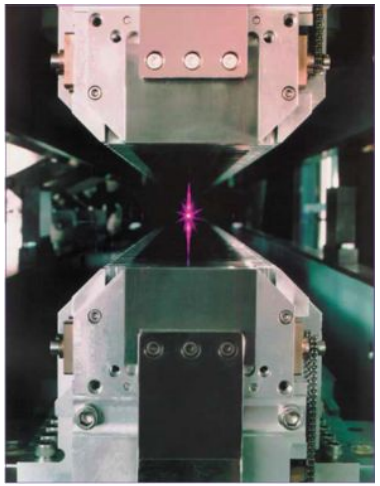

Synchrotron sources offer:

- Brightnesss (small source, collimated)
- Tunability (IR to hard x-rays)
- Polarization (linear, circular)
- Time structure (short pulses)

➢ Source brightness is the key figure of merit for coherent imaging

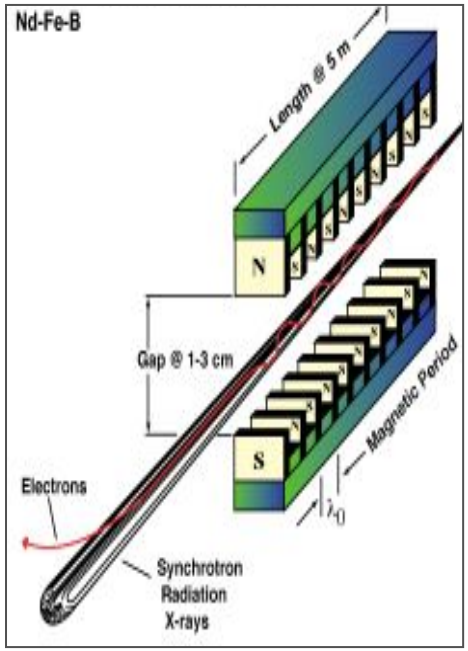

B = photons/source area, divergence, bandwidth

$F_c \sim \lambda^2 B$

Coherent flux from synchrotron sources

- SR sources (except FELs) are incoherent, but highly forward directed due to relativistic effects $\theta \sim 1/\gamma$

- Spatial and temporal filtering (pinholes, monochromators) are needed to select the coherent flux $F_c \sim \lambda^2 B$

- Only the coherent flux can be focused into a diffraction-limited spot or be used to form interference fringes

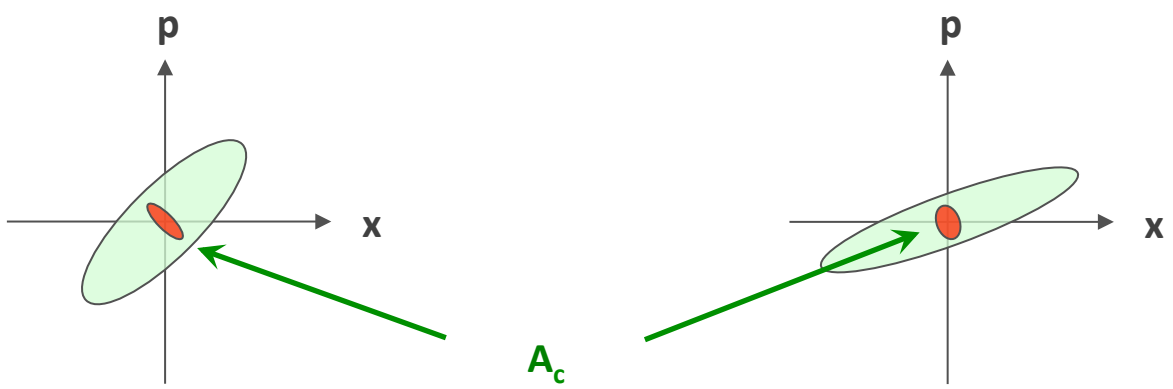

X-ray source brightness

Flux per spatially coherent mode: $F_c = B\,\lambda^2/4$

Discovery of x-rays

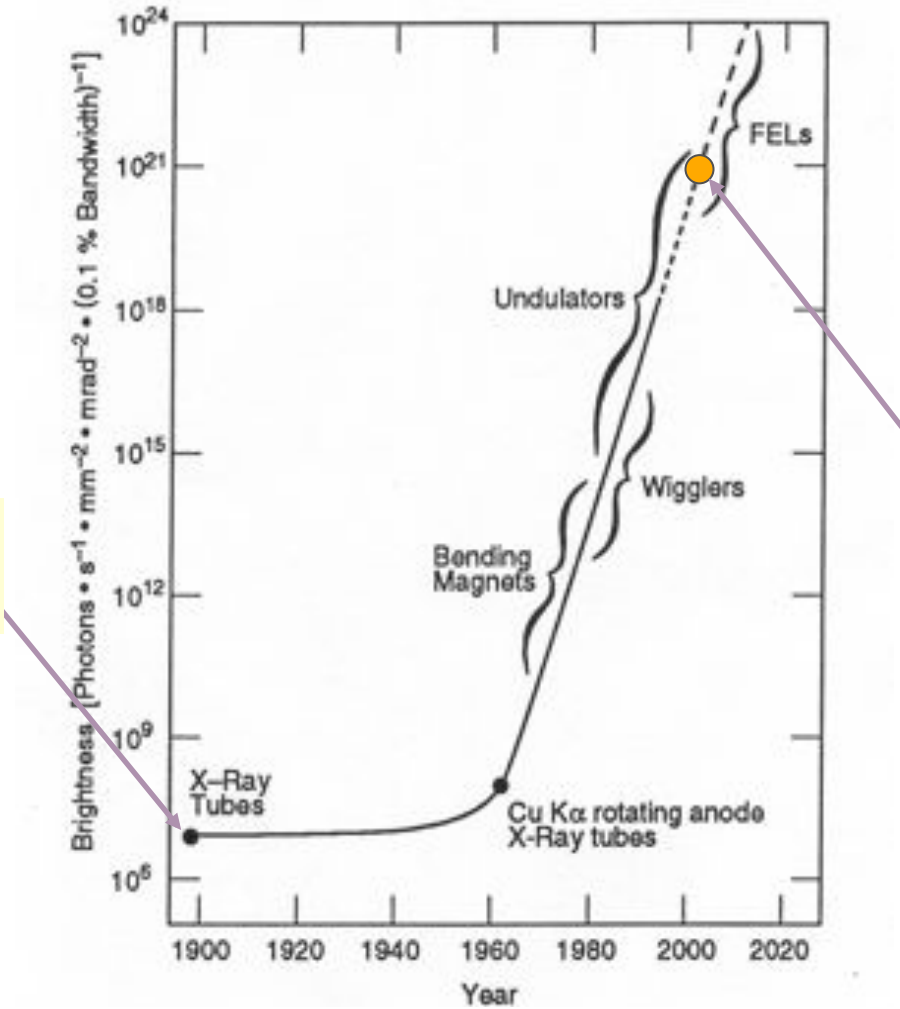

We are here

H. Winick, "Synchrotron Radiation Sources: A Primer," (1994)

Diffraction limited focusing requires coherent light

Achieving high NA is challenging because x-rays interact weakly

$n = 1 - \delta - i\beta$ $\quad$ $\delta,\beta \sim 10^{-3}$ to 10^{-6} $\quad$ $\Rightarrow$ $\quad$ $|n| \approx 1$

Refractive (compound refractive lenses) ~ 50 nm

Low efficiency, highly chromatic, aberrations

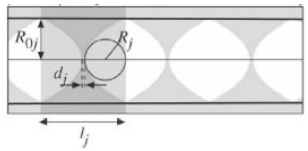

Reflective (Kirkpatrick-Baez mirrors) ~ 40 nm

High efficiency, achromatic, limited to ~10 nm

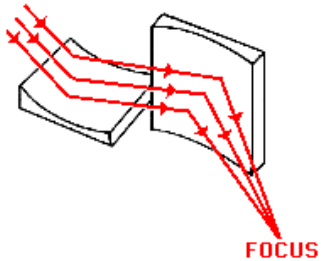

Diffractive (Fresnel zone plates, MLLs) ~ 15 nm

Moderate efficiency, limited to ~10 nm except MLL

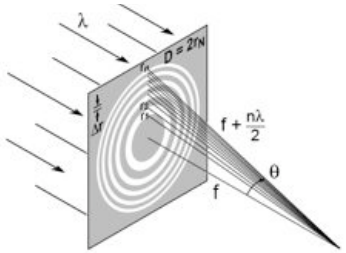

Waveguides ~ 10 nm

Low efficiency, 2D is challenging

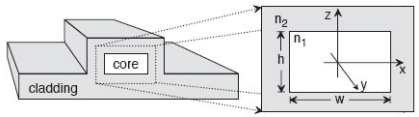

Fresnel zone plate

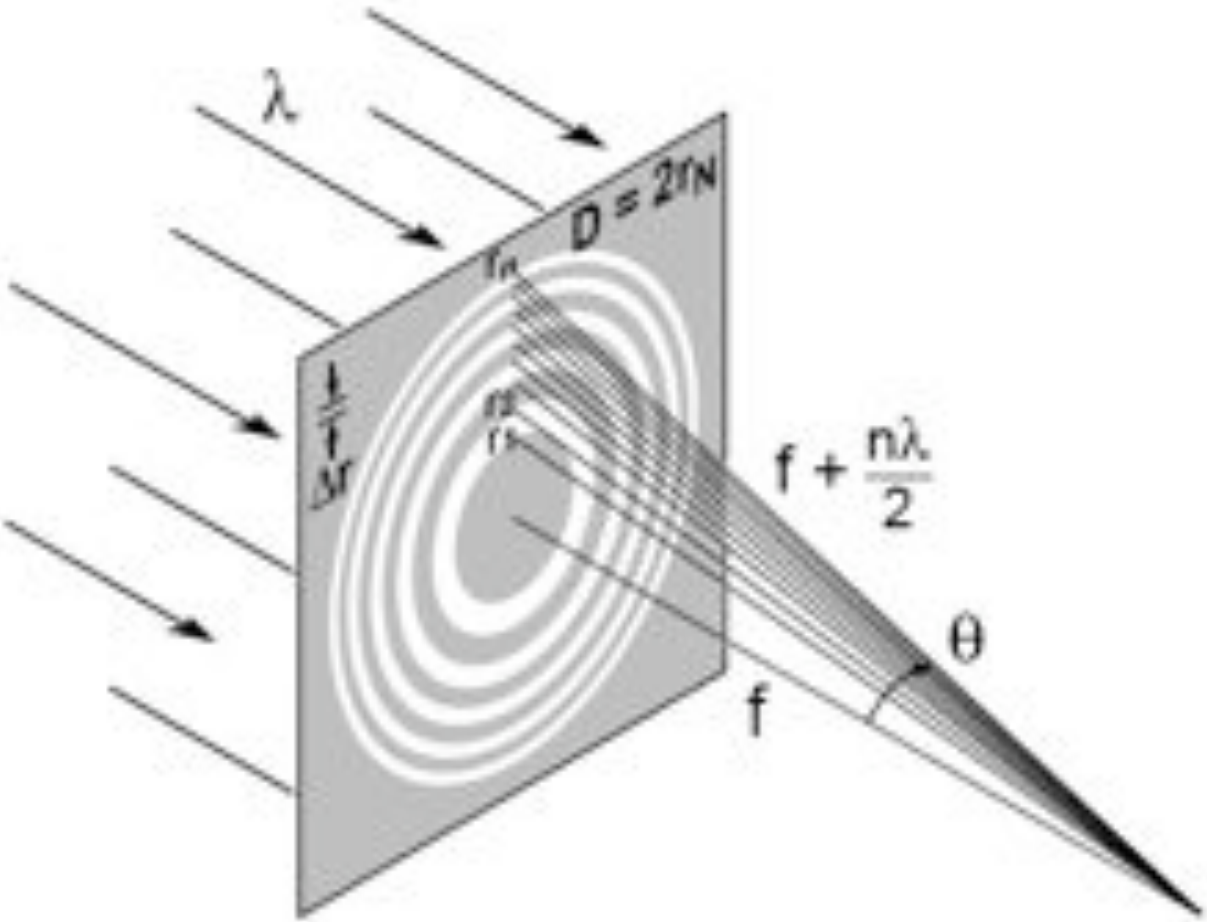

$$f^2 + r_n^2 = \left(f + \frac{n\lambda}{2}\right)^2$$

$$r_n^2 = nf\lambda + \frac{n^2\lambda^2}{4}$$

$$r_n \approx \sqrt{nf\lambda}$$

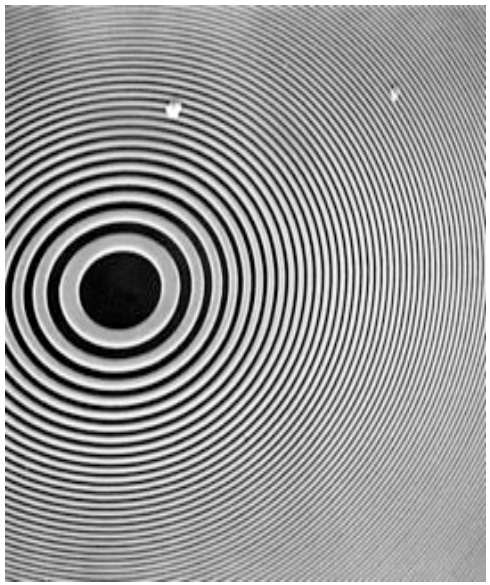

J.L. Soret. Arch. Sci. Phys. Nat. 52. 320 (1875).
R.W. Wood, Physical Optics, (Macmillan, New York, 1934), p. 37.
J. Kirz, J. Opt. Soc. Am. 64, 301 (1974).

Large-format, single-photon sensitive x-ray CCD cameras opened the door to coherent x-ray imaging

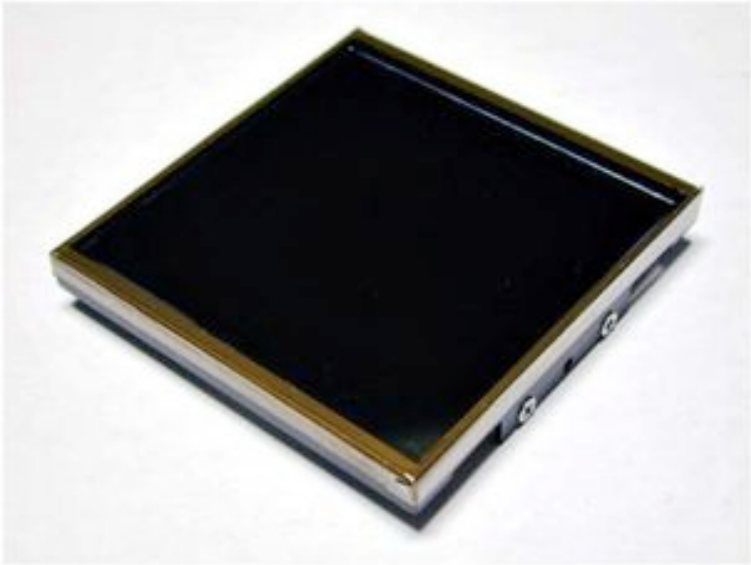

Fairchild Peregrine 486 CCD Camera

- 4K x 4K pixel array (61.4 mm square area)
- 15 µm pixels, 100% fill factor
- Back-illuminated for up to 80% QE
- Readout noise < 5 e- at 50 Kpixels/s
- Dynamic range > 86 dB in MPP
- 6 s readout with four on-chip amplifiers
- Pixel binning for more rapid readout
- Peltier-cooled to -50 C for low dark current

Pixel array detectors: revolutionizing coherent imaging

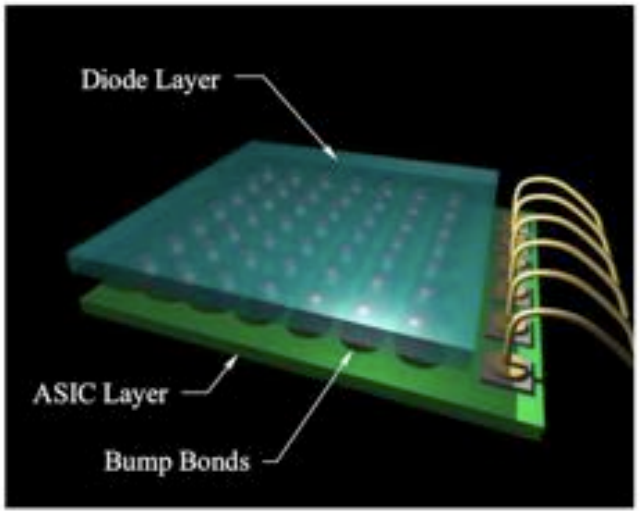

D. Schuette, S. Gruner (Cornell)

A Three Layer Hybrid Device

- Diode layer → converts x-rays to photocurrent.
- ASIC layer → custom signal processing electronics.
- A layer of metallic interconnects (bump bonds) between corre-sponding pixels on the diode and ASIC layers.

Pilatus 6M detector
(PSI/Dectris)

PADs can be read out in ~1 ms (CCDs take seconds!)

PAD pixels are 55-150 µm. (CCDs are 12-24 µm)

Imaging regimes with coherent x-rays

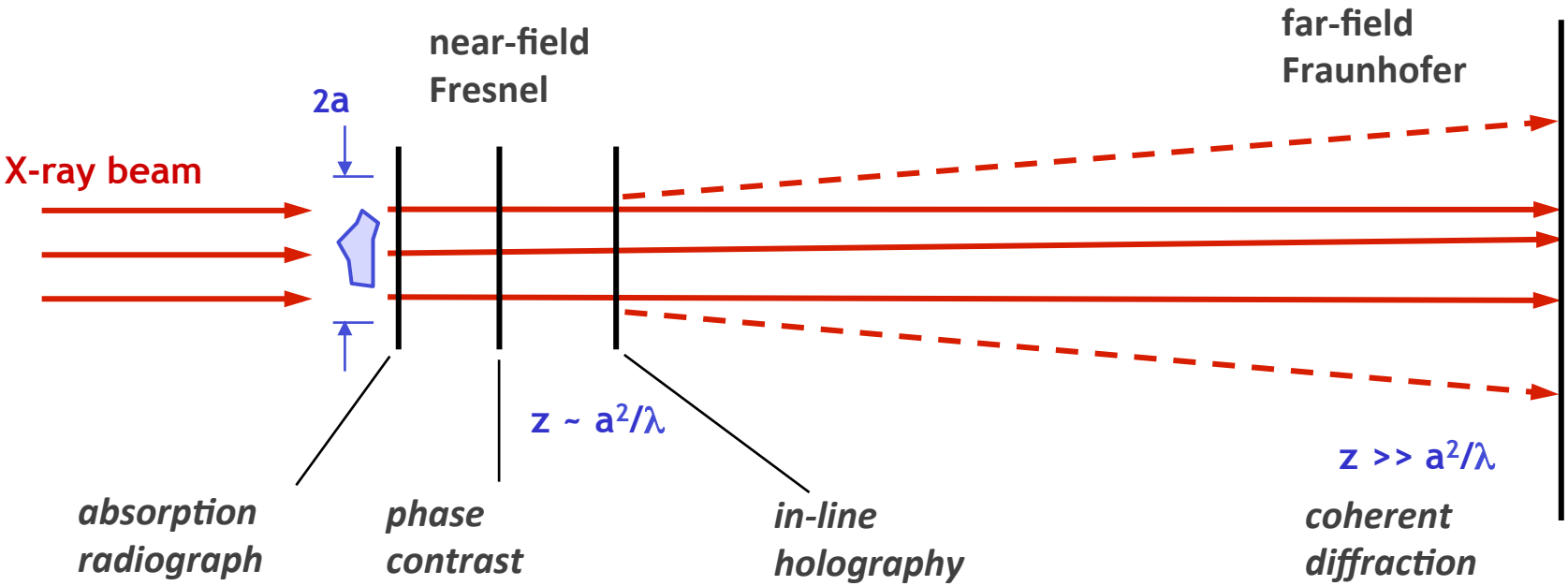

Kagoshima (1999)

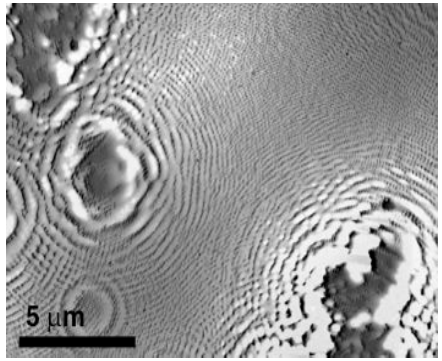

Jacobsen (1990)

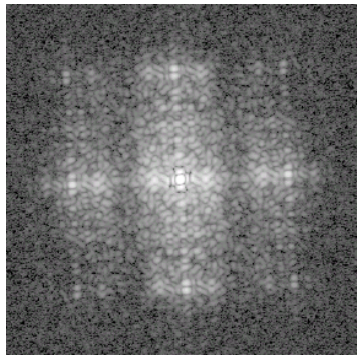

Miao (1999)

X-ray scattering from a disordered sample

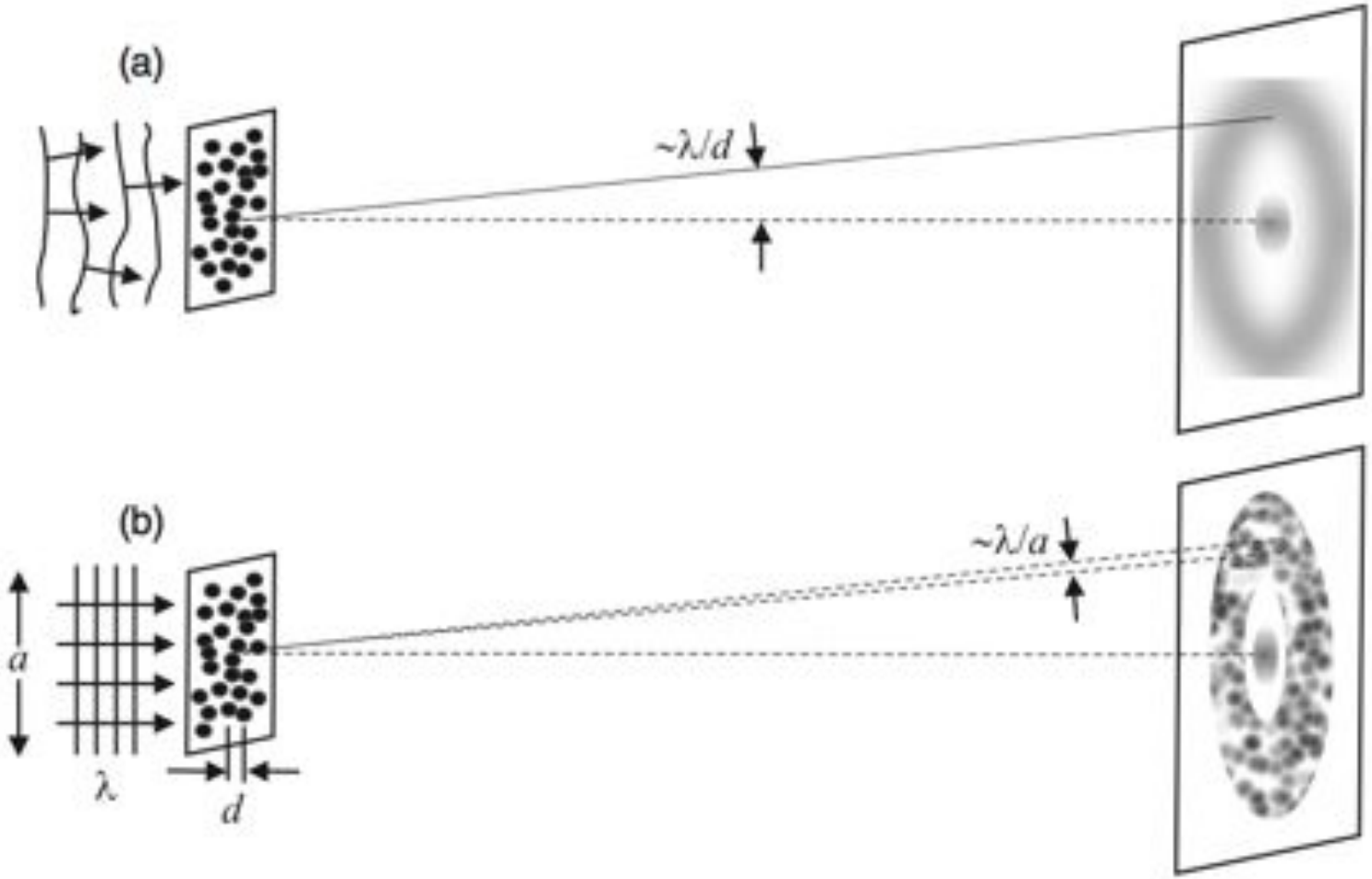

X-ray diffraction from a disordered medium with particle distance d and object size a.
(a) **Incoherent scattering**, giving rise to a continuous diffraction ring.
(b) **Coherent scattering**, resulting in a speckled diffraction ring.

F. van der Veen and F. Pfeiffer, J. Phys. Cond. Mater. 16, 5003 (2004)

2. Direct methods

- **Imaging regimes with coherent light**
- **Projection imaging**
- **Full-field imaging**

References:

1. M. Howells, "Soft-x-ray microscopes," Physics Today 38, 22 (Aug. 1985).
2. J. Kirz and H. Rarback, "Soft xray microscopes," Rev. Sci. Instrum. 56, 1 (1985).
3. J. Als-Nielsen and D. McMorrow, *Elements of Modern X-ray Physics* (Wiley, New York, 2000).
4. D. Attwood, *Soft X-Rays and Extreme Ultraviolet Radiation: Principles and Applications* (Cambridge, 2007).
5. J. Goodman, *Introduction to Fourier Optics*, 3rd ed. (Roberts and Company, 2005).

Direct methods

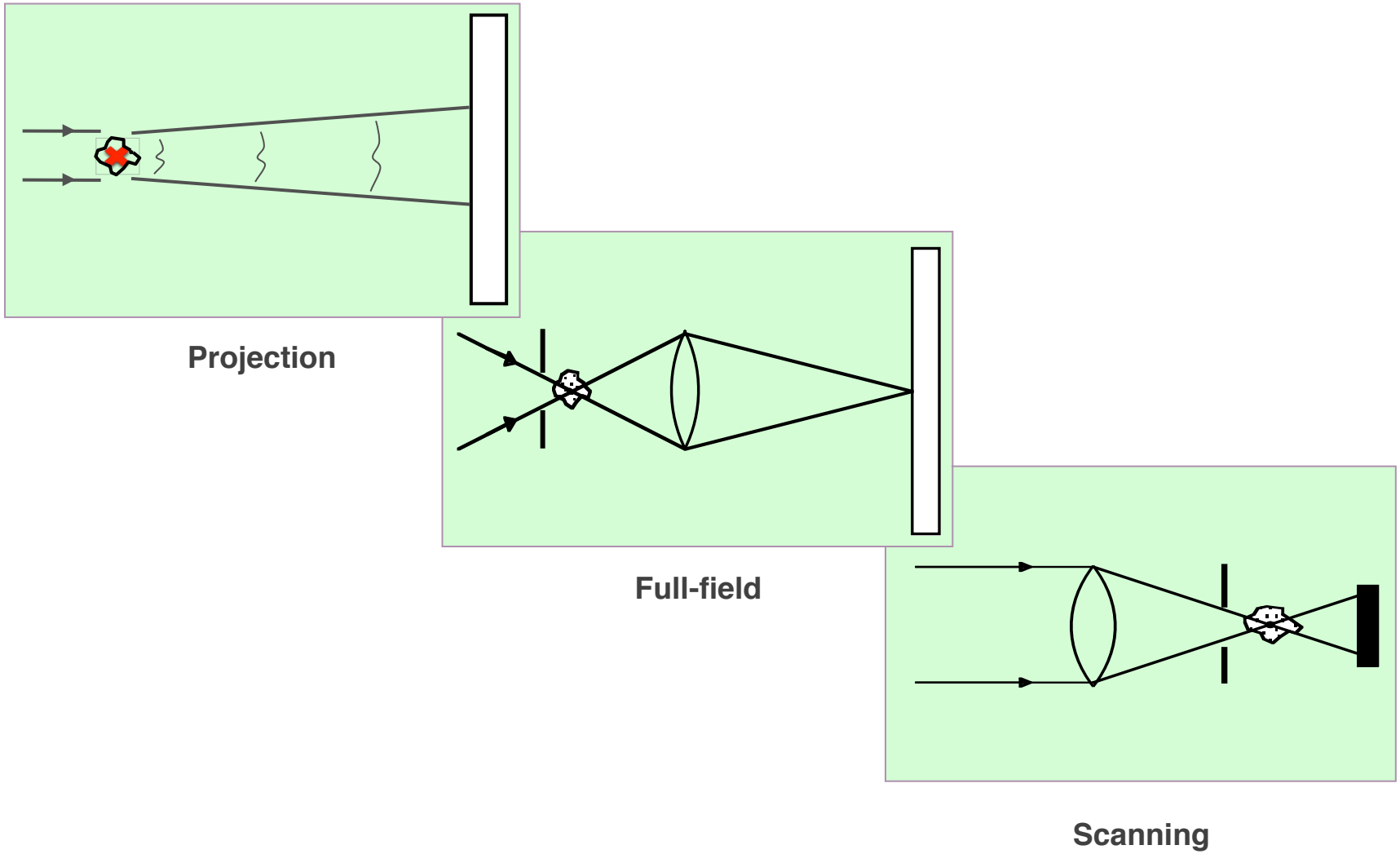

Phase contrast: tool of choice for low absorption samples

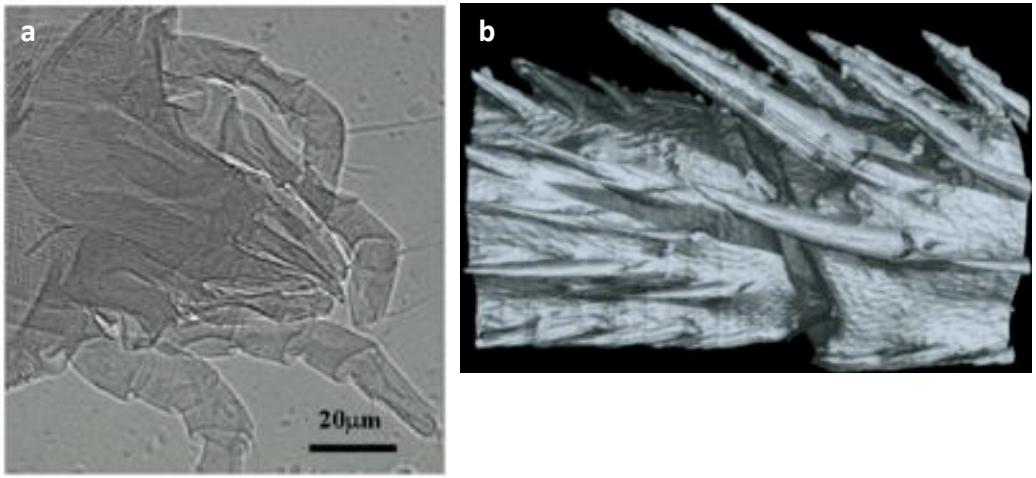

(a) Dust mite and (b) tomographically reconstructed fly leg joint, recorded with ~8 keV x-rays and propagation phase contrast.

S. Mayo, Opt. Express 11, 2289 (2003)

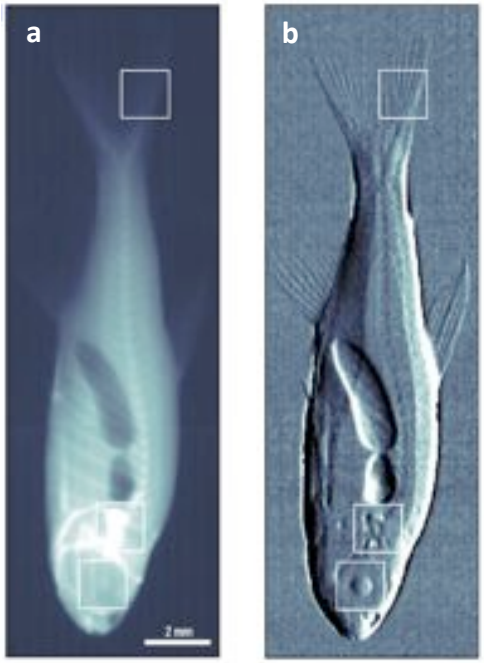

Small fish, recorded with three-grating method and standard x-ray tube (40 kV/25 mA). (a) Transmission. (b) Differential phase.

F. Pfeiffer, Nature Phys. 2, 258 (2006)

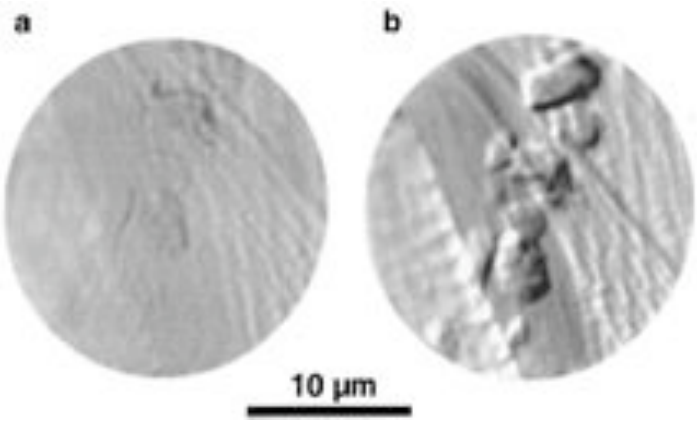

Moth wing, recorded with 4 keV x-rays.
(a) Bright-field. (b) Differential interference contrast.

B. Kaulich, T. Wilhein, JOSA A19, 797 (2002)

Full-field x-ray microscope

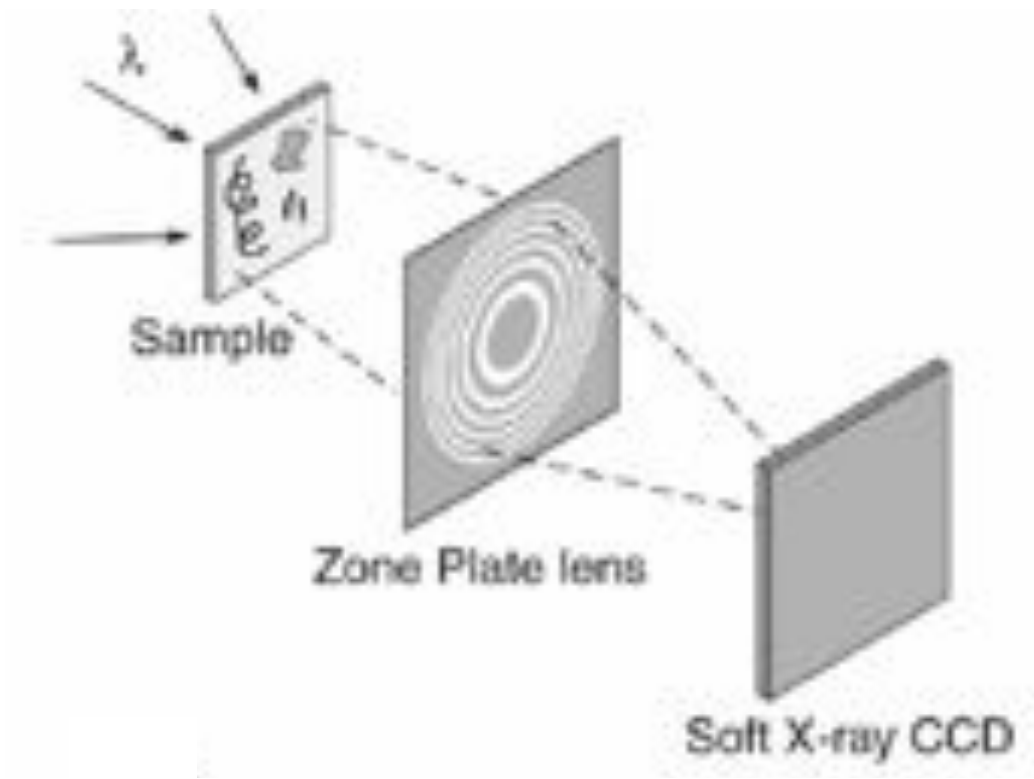

0. Rudolph and G. Schmahl, Ann. N. Y. Acad. Sci. 342, 94 (1980)

Resolution of a Fresnel zone plate lens

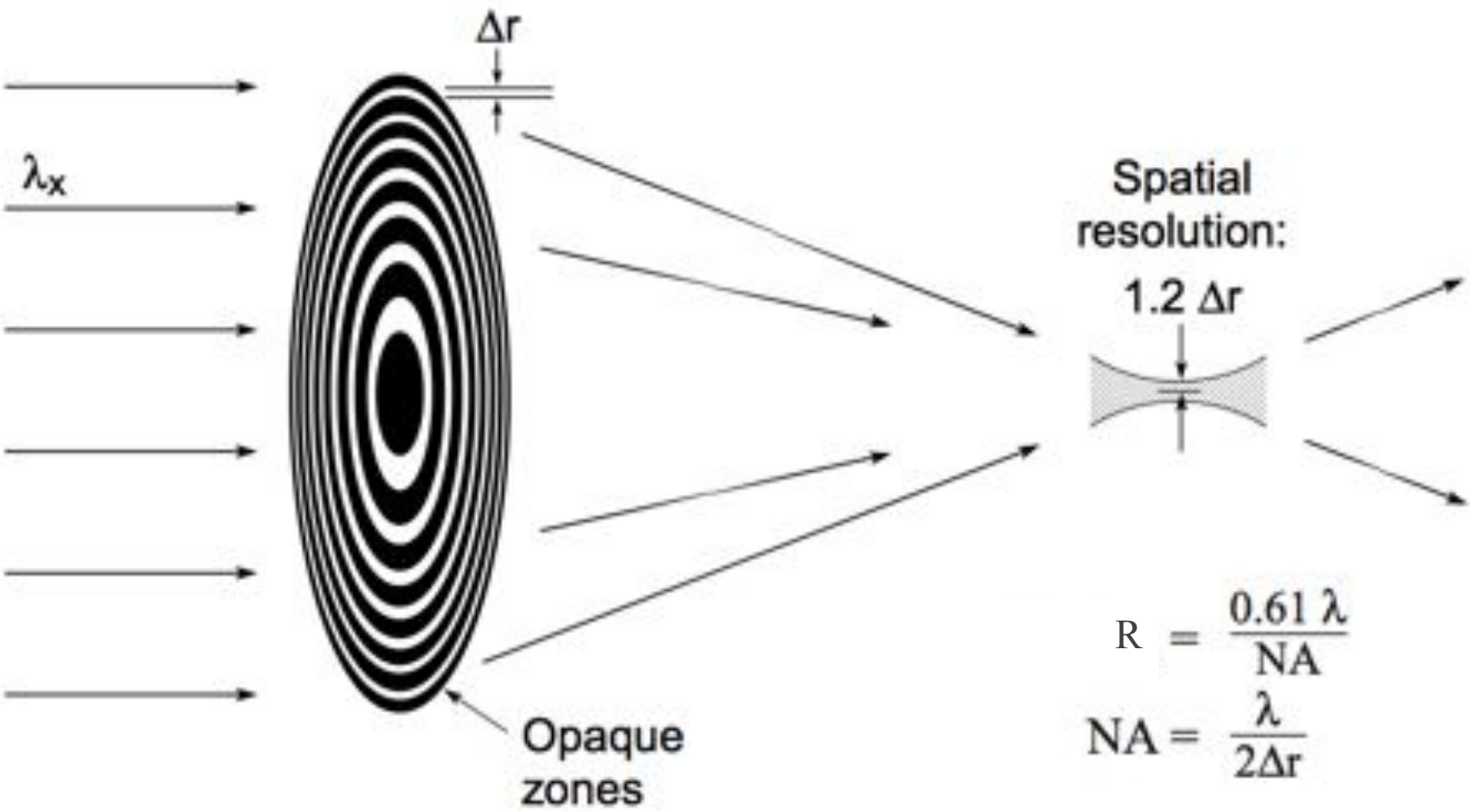

$$R = \frac{0.61\,\lambda}{NA}$$

$$NA = \frac{\lambda}{2\Delta r}$$

Quantitative phase tomography

- Defocus series (a, b, c) and phase (d) of a silicon AFM tip
- Quantitative 3D reconstructions of real part of refractive index from ±70° tomographic projections through tip
- **Calculated $\delta = 5.1 \times 10^{-5}$**

  Measured $\delta = 5.0 \pm 0.5 \times 10^{-5}$

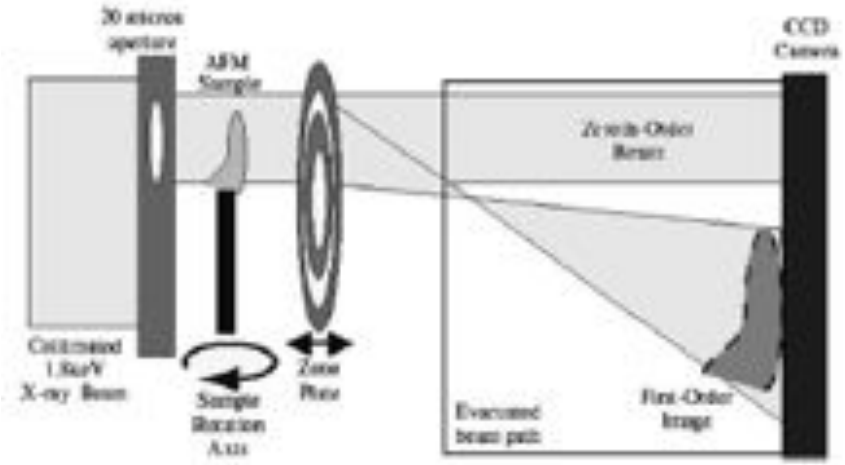

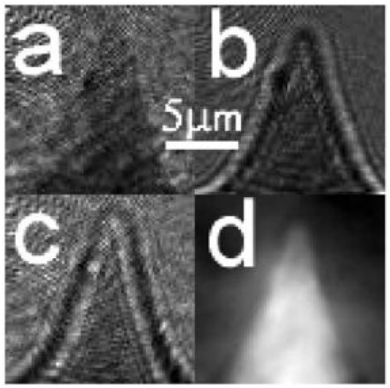

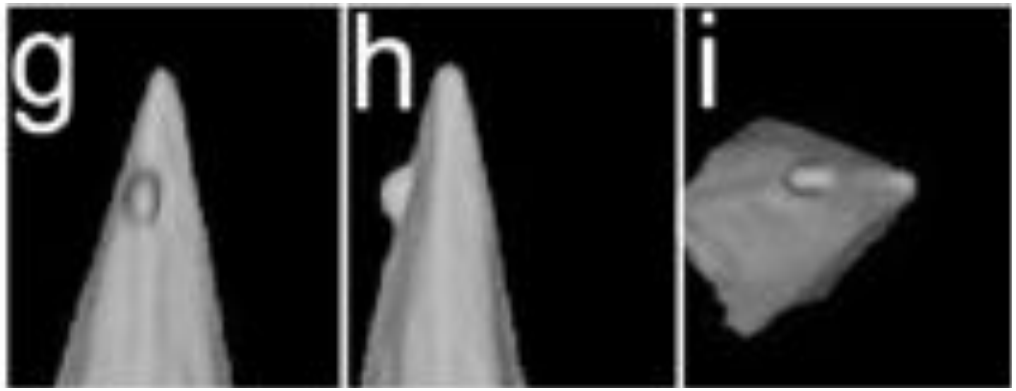

P. McMahon, Opt. Commun. 217, 53 (2003)

3. Indirect methods

- **Coherent diffractive imaging**
  - **Isolated sample (single-view)**
  - **Extended sample (ptychography)**
- **Bragg coherent diffractive imaging**
- **Holography**
- **Time-resolved imaging**

References:

1. J. Als-Nielsen and D. McMorrow, *Elements of Modern X-ray Physics* (Wiley, New York, 2000).
2. F. van der Veen and F. Pfeiffer, "Coherent x-ray scattering," J. Phys. Condens. Mat. 16, 5003 (2004).
3. J.R. Fienup, "Phase retrieval algorithms: a comparison," Appl. Opt. 21, 2758 (1982)
4. I. Robinson and R. Harder, "Coherent X-ray diffraction imaging of strain at the nanoscale," Nature Mater. 8, 291 (2009)
5. J. Stöhr and H.C. Siegmann, *Magnetism* (Springer, Berlin, 2006).

Indirect methods: CDI and holography: "Lensless" imaging

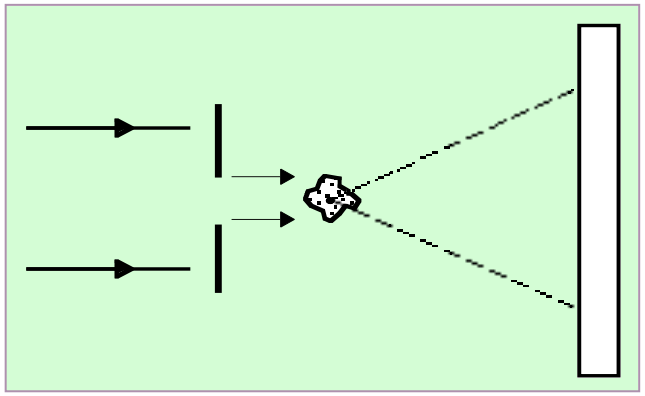

Coherent Diffraction

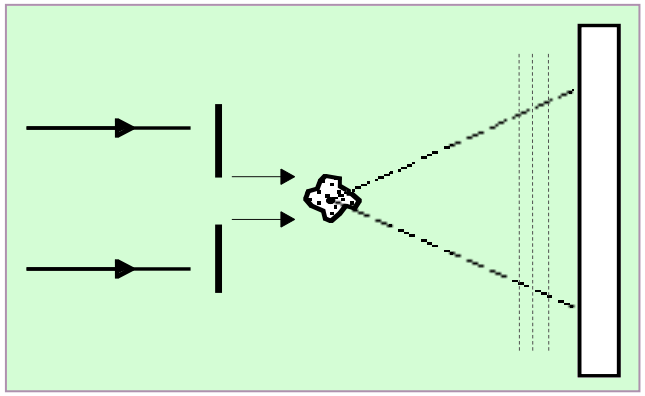

Holography

- Object wave (diffraction) is detected directly
- Diffraction intensity corresponds to autocorrelation of object

- Coherent reference wave interferes with object wave to form hologram
- Hologram intensity corresponds to convolution of object and reference

Resolution:	transverse	$\sim \lambda/NA$
	longitudinal	$\sim \lambda/(NA)^2$
Contrast:		$\propto \lvert f_1^2 + f_2^2 \rvert$

Coherent diffractive imaging

***Lensless* method**

Resolution ~ λ / angular size **limited only by wavelength and signal**

- Two-step process: record coherent diffraction pattern, recover object structure numerically (iterative phase retrieval)
- Sensitive to phase as well as absorption of the specimen
- Get 3D by tomographic methods; no depth of field limit
- But: must assume some information to recover phase, e.g. known object extent or illumination profile

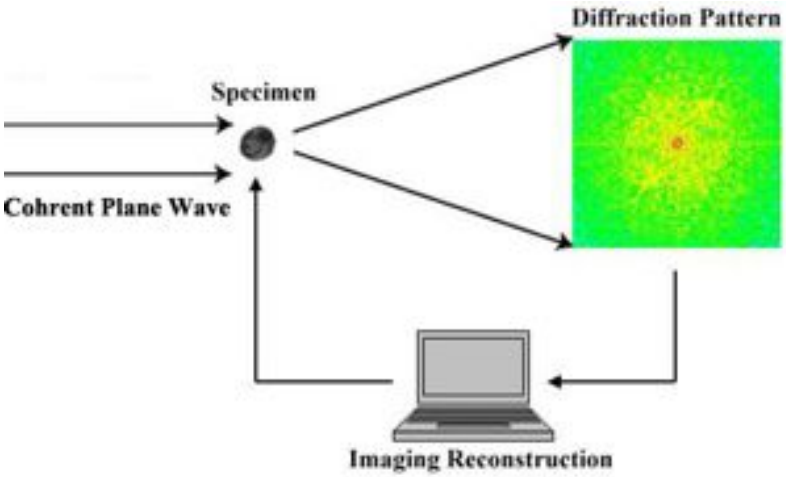

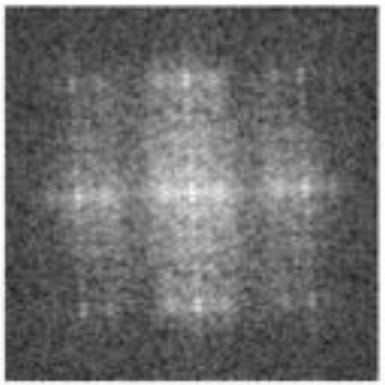

Diffraction pattern

Reconstruction

J. Miao, Nature 400, 342 (1999)

Iterative phase retrieval

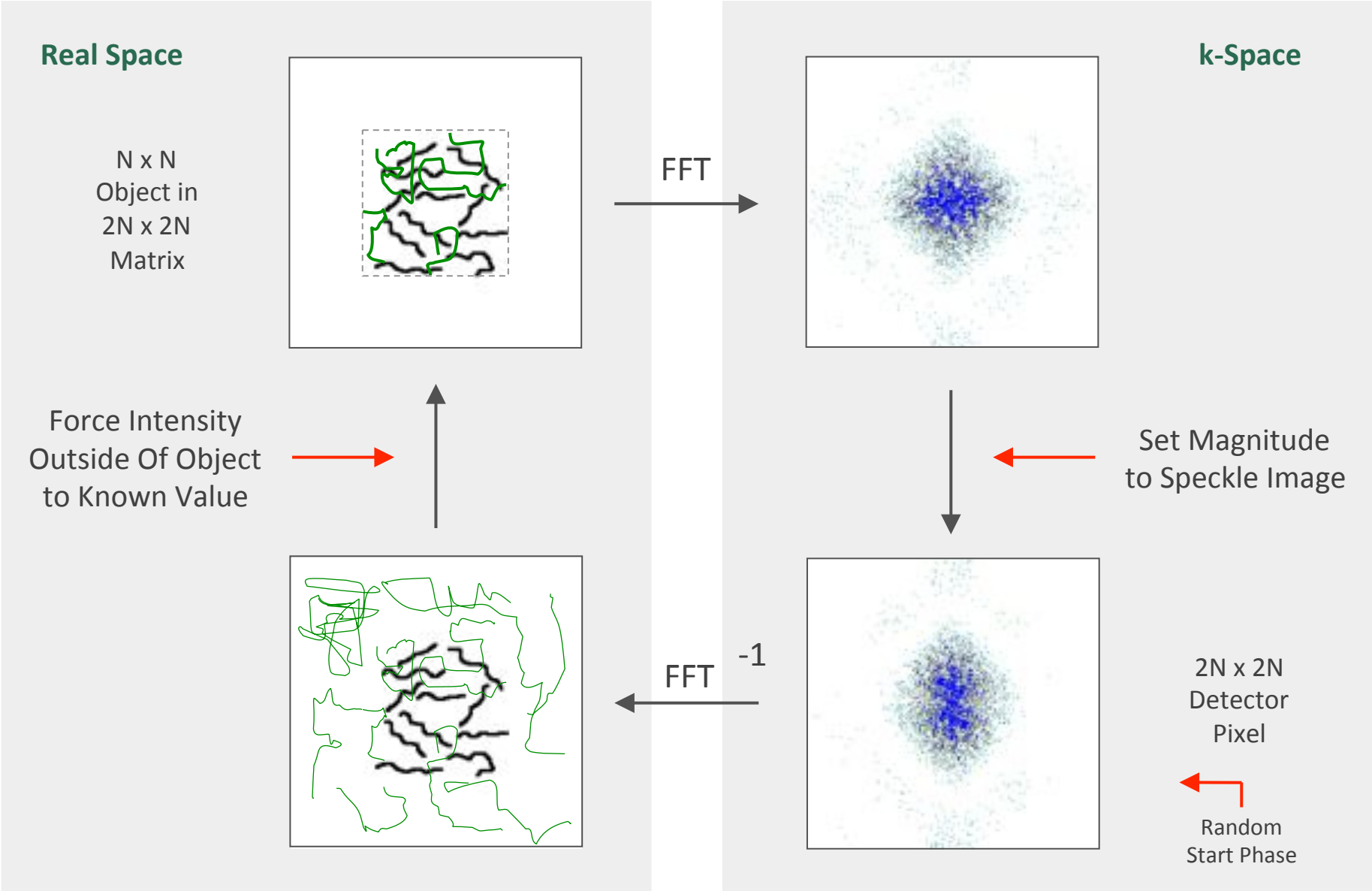

R. Gerchberg and W. Saxton, *Optik* 35, 237 (1972); J.R. Fienup, *Appl. Opt.* 21, 2758 (1982)

Error reduction algorithm

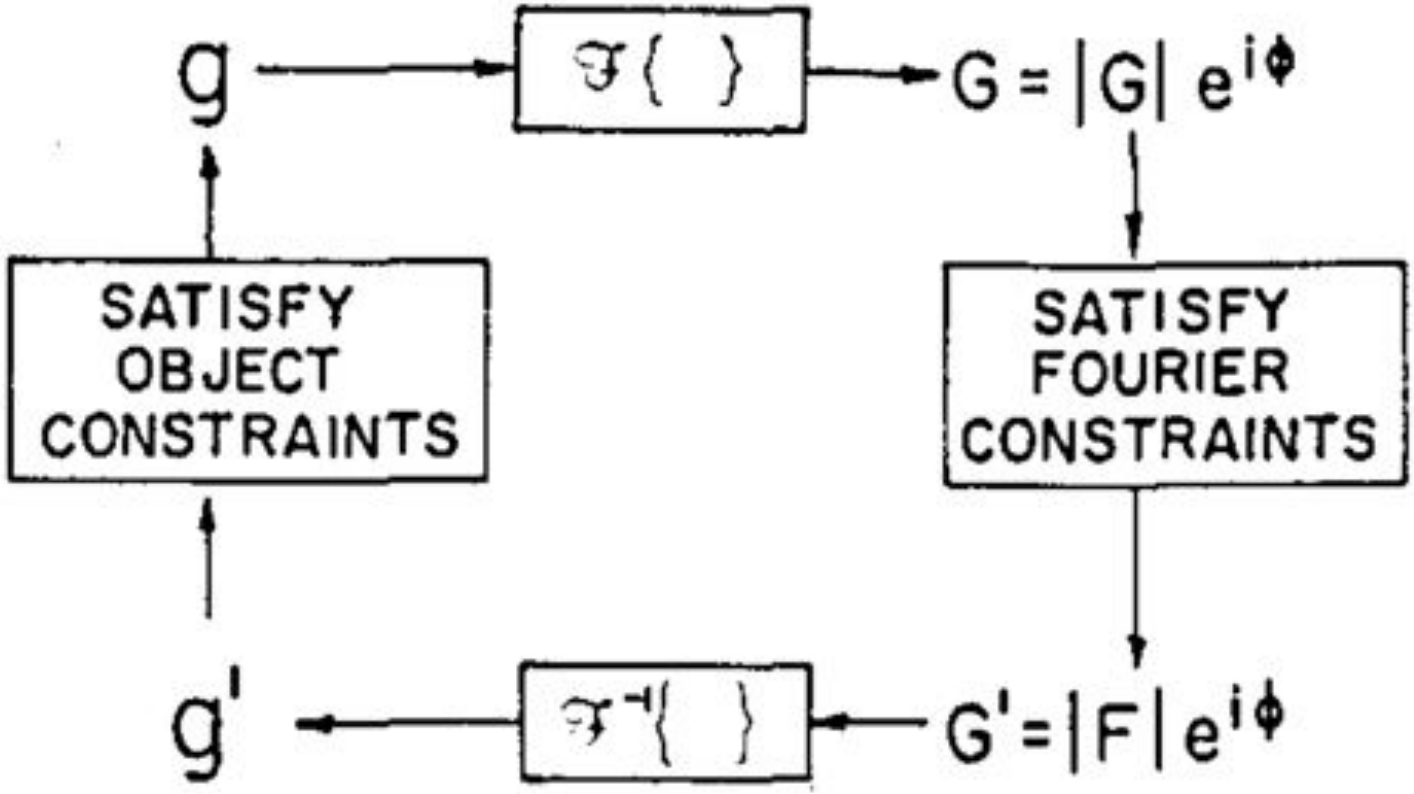

R.W. Gerchberg, W.O. Saxton, Optik 35 237 (1972)
J.R. Fienup, Opt. Lett. 3, 27 (1978)

ER and Hybrid Input-Output algorithms

ER $$g_{n+1} = P_S P_F g_n$$

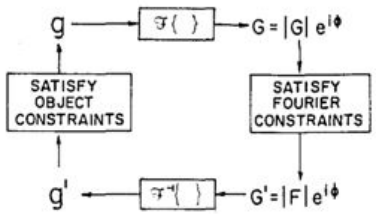

HIO $$g_{n+1} = \begin{cases} P_F g_n(r) & \text{if } r \in \text{ support} \\ g_n(r) - \beta P_F g_n(r) & \text{otherwise} \end{cases}$$

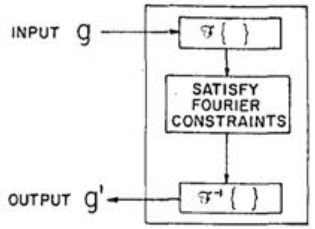

where $G(r) = \mathcal{F}\{g(r)\}$,

$$P_F G(q) = \begin{cases} \sqrt{I(r)}\,\dfrac{G(q)}{|G(q)|} & \text{if } I(r) \text{ is known and } |G(q)| \neq 0 \\ G(q) & \text{otherwise} \end{cases}$$

$$P_S g(r) = \begin{cases} g(r) & \text{if } r \in \text{ support} \\ 0 & \text{otherwise} \end{cases}$$

g_n and g_{n+1} are the nth and (n+1)th iterates,
P_F and P_S are Fourier modulus and support projections,
β is a "feedback" parameter

J.R. Fienup, Appl. Opt. 21, 2758 (1982)

Reconstruction

Real space Magnitude

Real space Phase

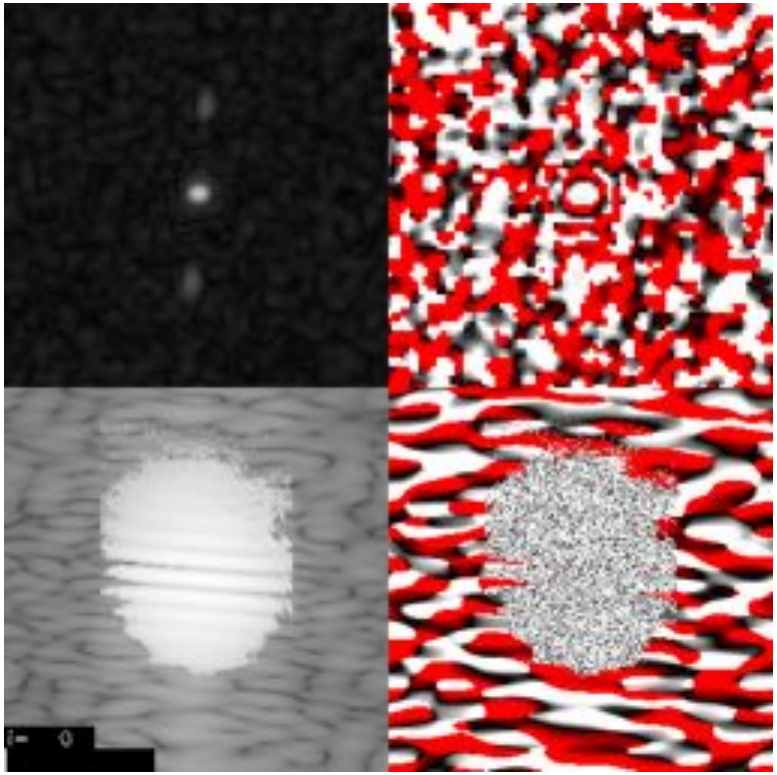

Far field Magnitude

Far field Phase

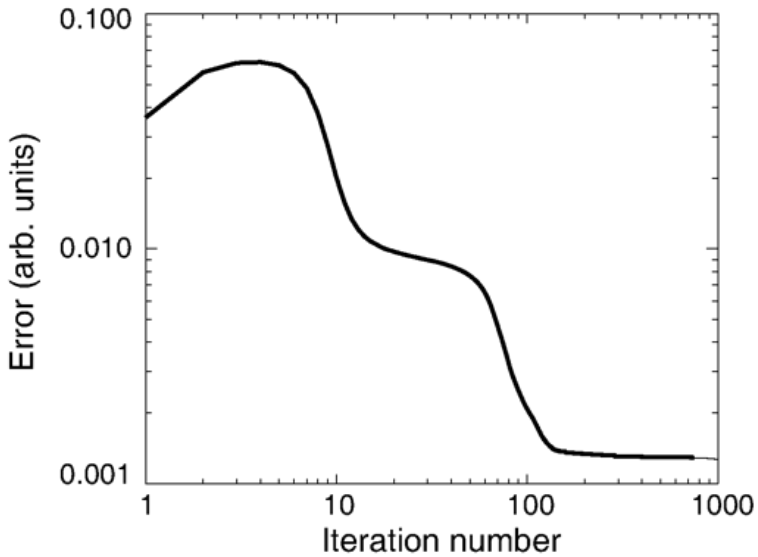

Reconstruction error

Iterative phasing: simple example

High harmonic generation of XUV radiation from femtosecond laser, illuminating two pinholes

Data

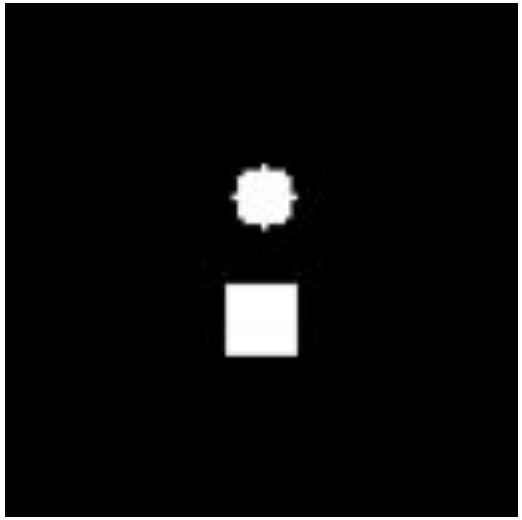

Support constraint (loose)

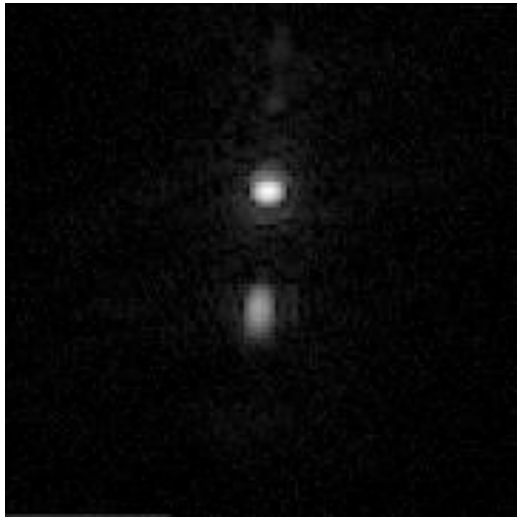

Reconstruction

R. Bartels, Science 297, 376 (2002)

First demonstration with x-rays

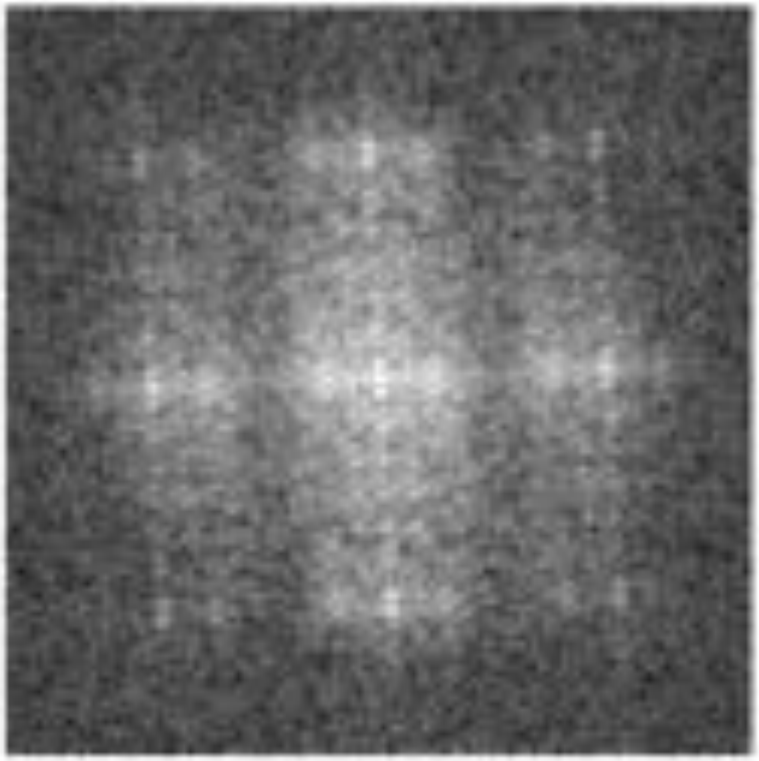

diffraction pattern

reconstruction

J. Miao, Nature 400, 342 (1999)

Difference Map algorithm

The Difference Map is defined by:

$$g_{n+1} = g_n + \beta\left(g_{Fn} - g_{Sn}\right)$$

with *nth* Fourier and support estimates,
$\gamma_s = -\beta^{-1}$ and $\gamma_F = \beta^{-1}$.

$$g_{Fn} = P_F\left[\left(\gamma_S + 1\right)P_S\left(g_n\right) - \gamma_S g_n\right]$$
$$g_{Sn} = P_S\left[\left(\gamma_F + 1\right)P_F\left(g_n\right) - \gamma_F g_n\right]$$

A common choice for DM is $\beta = -1$, giving:
With $\beta = 1$, we get back Fienup's HIO algorithm.

$$g_{Fn} = P_F\left\{2P_S\left(g_n\right) - g_n\right\}$$
$$g_{Sn} = P_S\left(g_n\right)$$

A metric used to monitor convergence is:

$$\varepsilon_n = \left\|g_{n+1} - g_n\right\| = \left\|g_{Fn} - g_{Sn}\right\|$$

V. Elser, JOSA A 20, 40 (2003)
P. Thibault, Acta Cryst. A62, 248 (2006)

Freeze dried yeast cell imaged by CDI

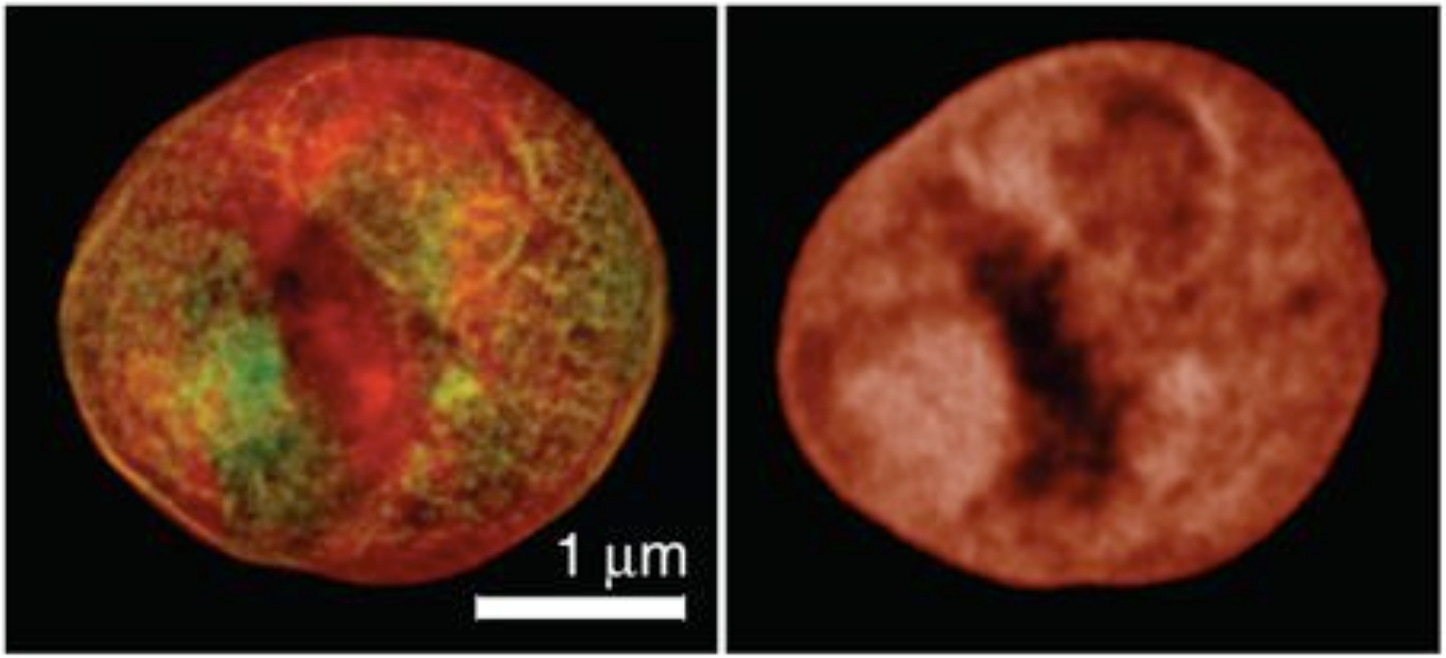

Diffraction reconstruction (data taken at 750 eV; absorption as brightness, phase as hue).

Stony Brook/NSLS STXM image with 45 nm Rayleigh resolution zone plate at 520 eV (absorption as brightness)

D. Shapiro, PNAS 102, 15343 (2005)

CDI setup at APS beamline 2-ID-B (1-4 keV)

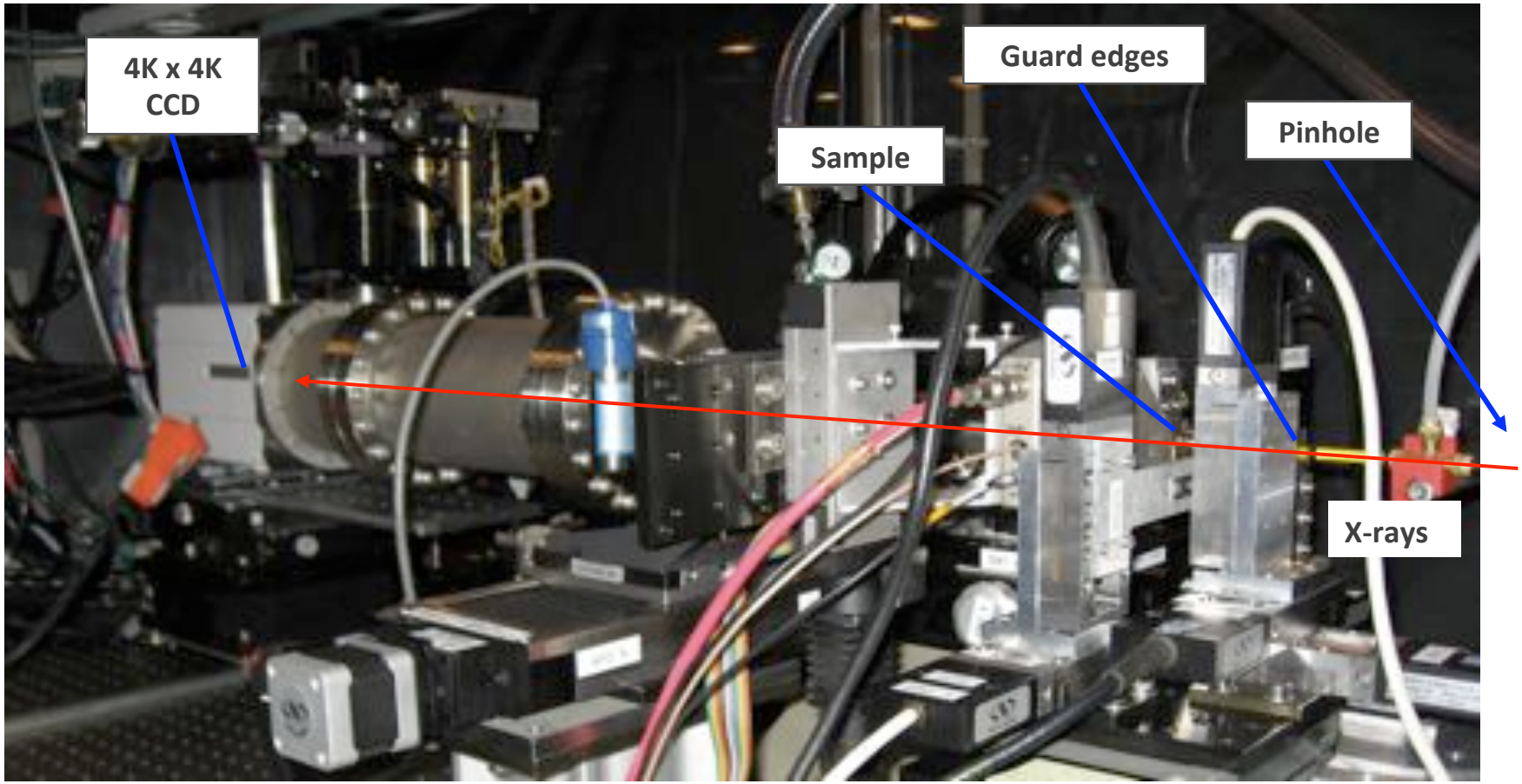

Buried structures can be probed with element specificity

In contrast to weak segregation theory, Bi is locally concentrated in Bi-doped Si crystals

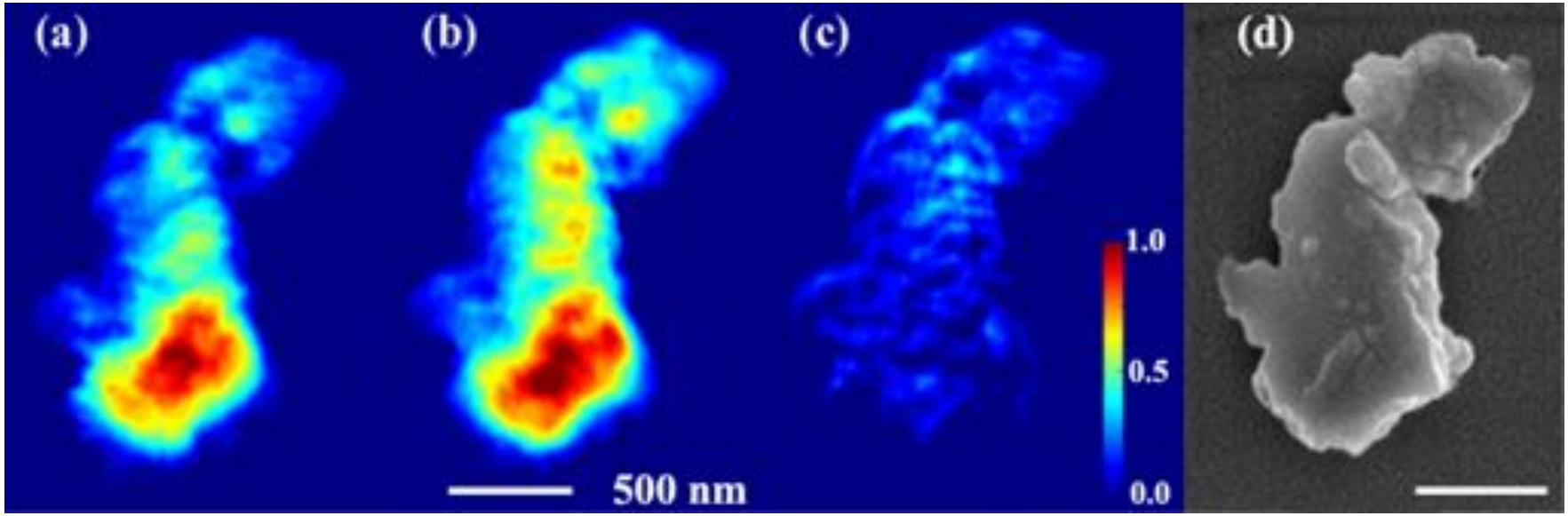

(a) Image below Bi M5 edge (2550 eV)
(b) Image above the Bi M5 edge (2595 eV)
(c) Difference
(d) SEM image

C. Song, PRL 100, 025504 (2008)

Curved object illumination aids unique phase recovery

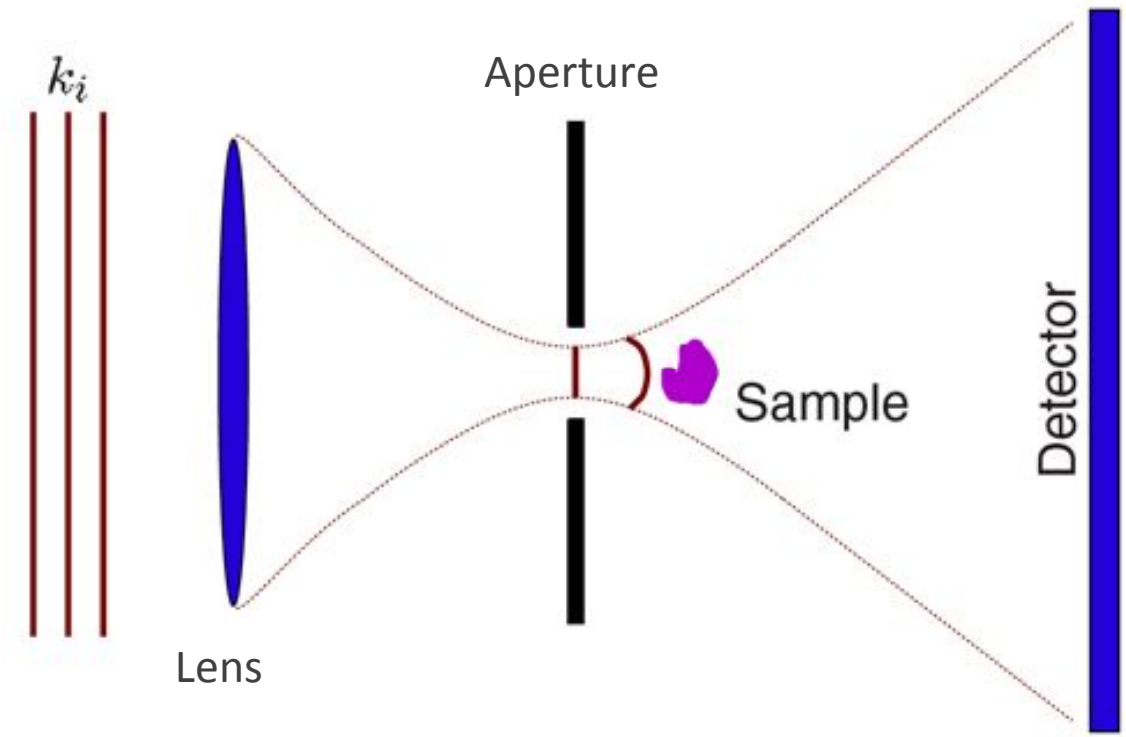

- Lens illuminates object with curved wavefront, defines field of view
- Object illumination is reconstructed by back-propagation, used to retrieve phase of object wave by iterative methods

K. Nugent, PRL 91, 203902 (2003)

Fresnel diffraction

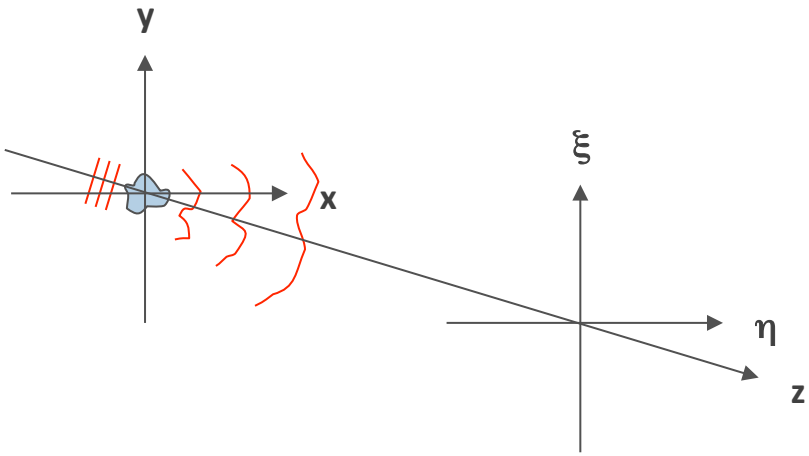

"object wave"

$$a(\xi,\eta) = \frac{e^{ikz}}{i\lambda z}\iint a(x,y)\; e^{\frac{ik}{2z}\left((x-\xi)^2+(y-\eta)^2\right)}\,dxdy$$

$$= \frac{e^{ikz}}{i\lambda z}\; e^{\frac{ik}{2z}\left(\xi^2+\eta^2\right)}\; \mathrm{FT}\left\{ e^{\frac{ik}{2z}\left(x^2+y^2\right)} a(x,y) \right\}$$

… and converges faster

Original

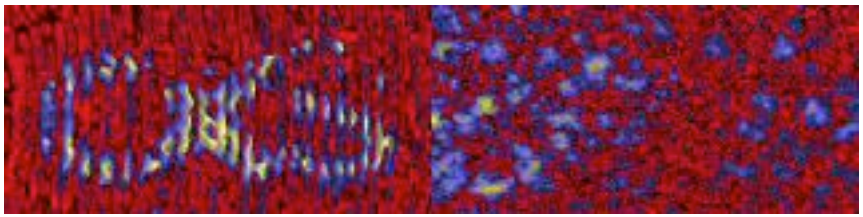

curved beam illumination **plane wave illumination**

Unique solution

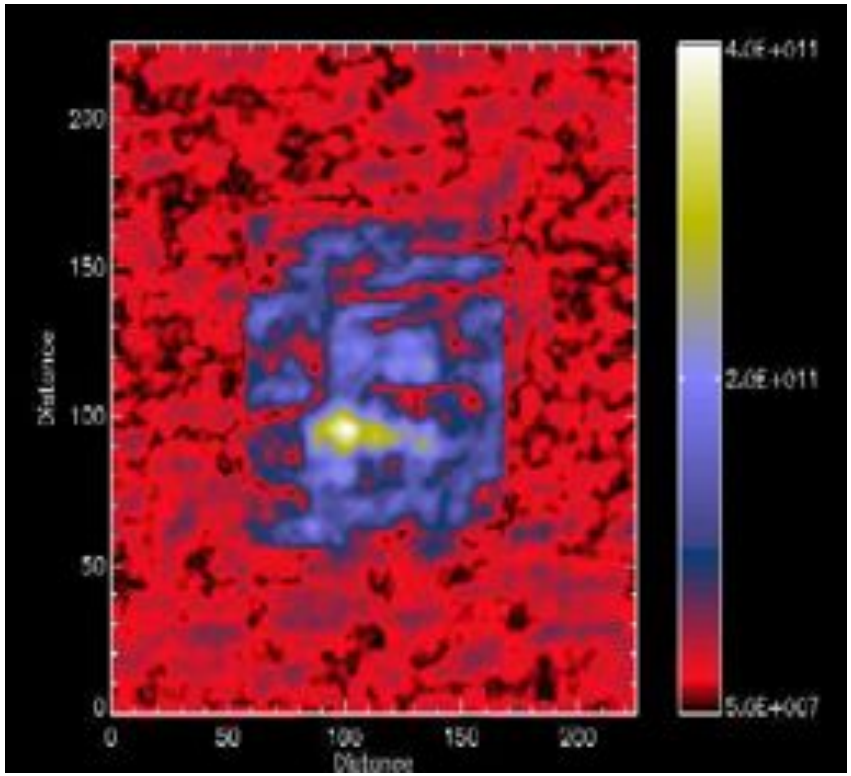

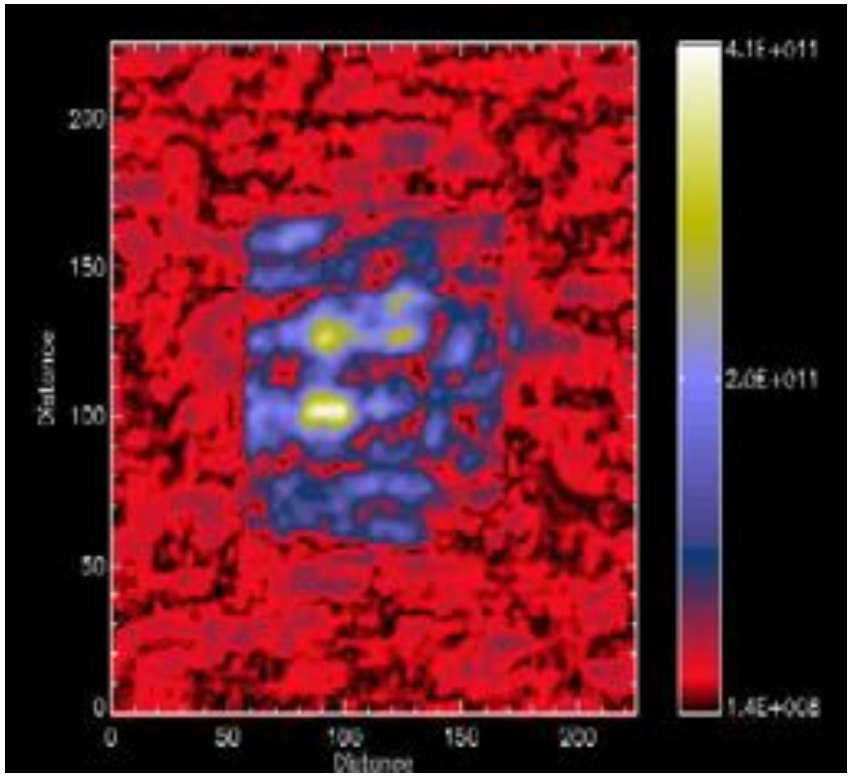

Fresnel coherent diffraction imaging of a gold test pattern

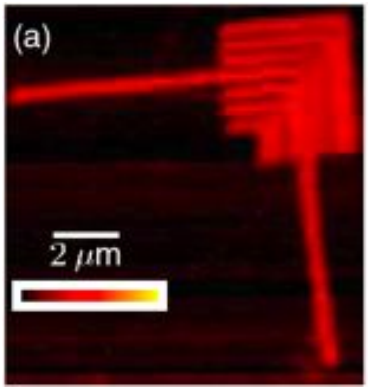

STXM image (1.8 keV)

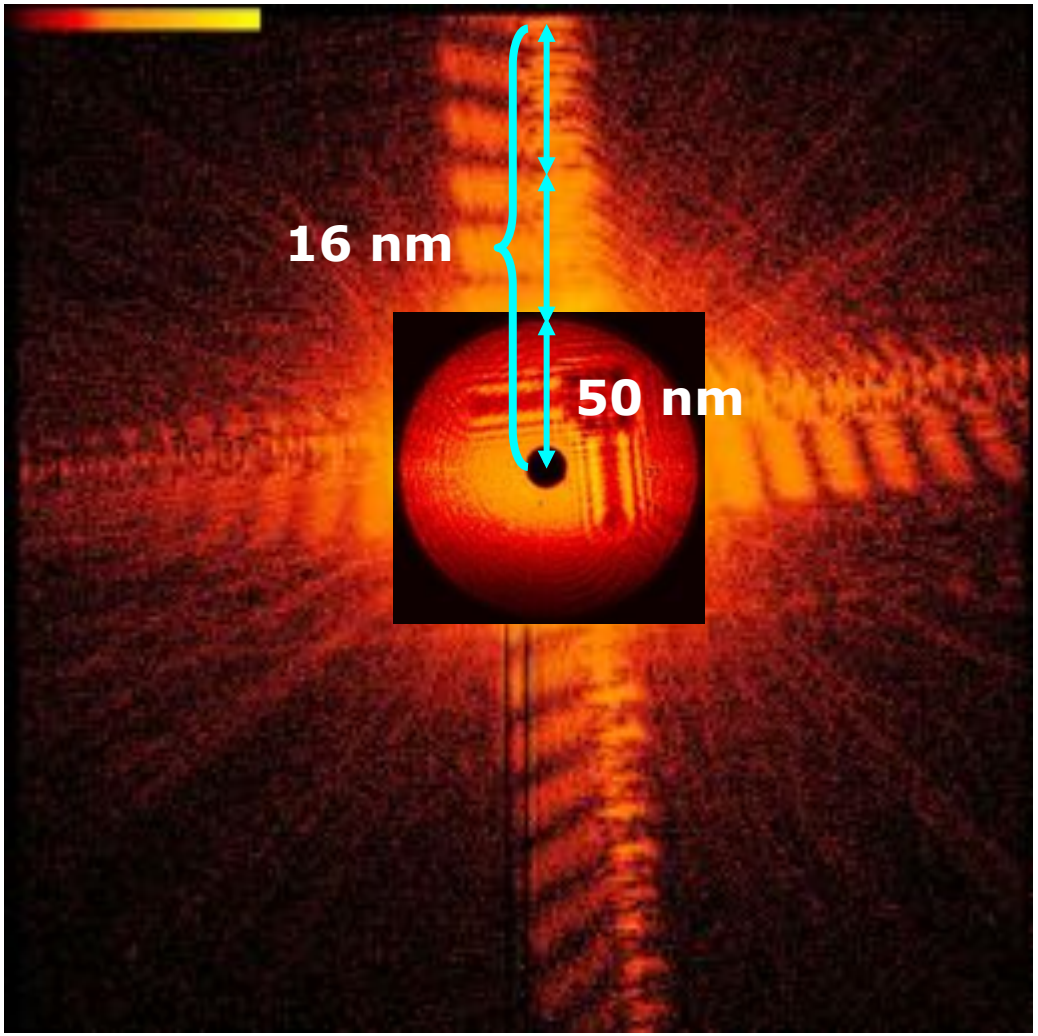

Images reconstructed by FCDI

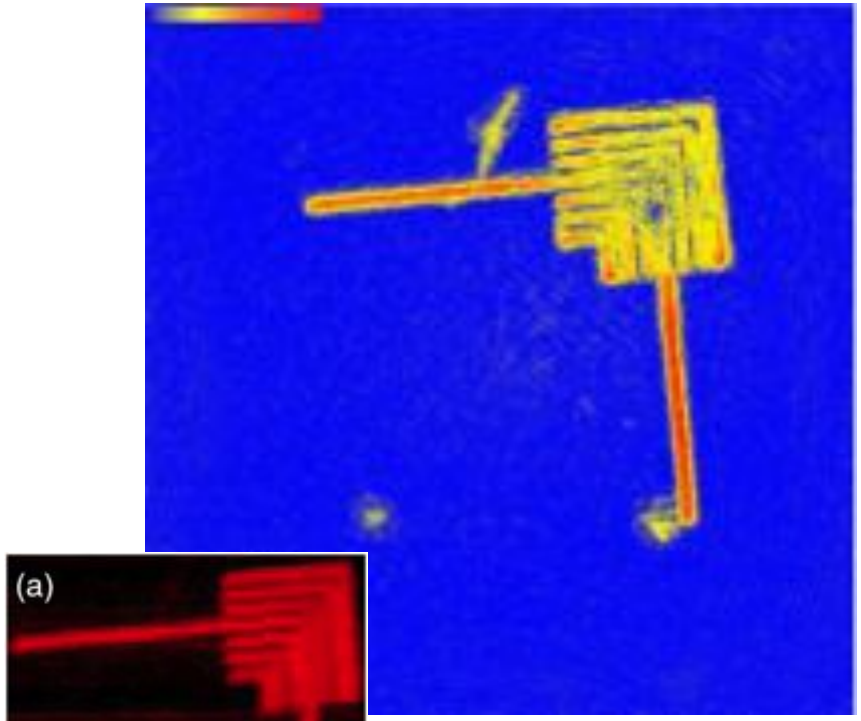

Phase

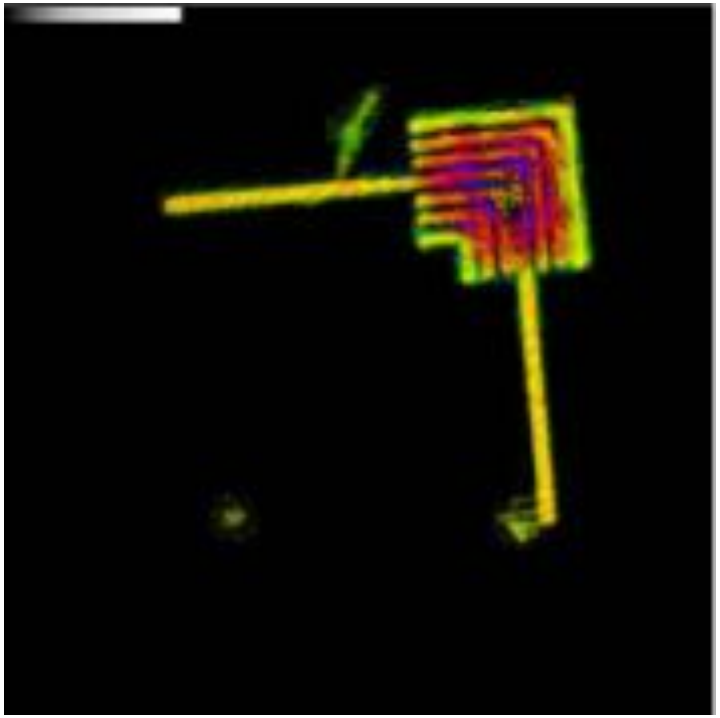

Magnitude with color-encoded phase

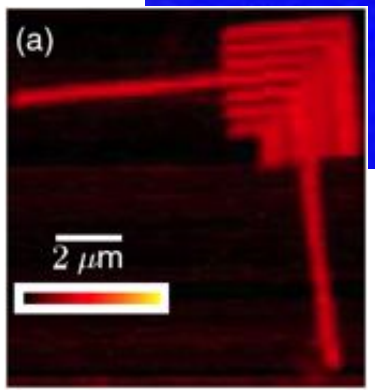

STXM image (1.8 keV)

G. Williams, PRL 97, 022506 (2006)

"Keyhole" FCDI

Use reconstructed illumination profile to determine support in extended sample

H. Quiney,
Nature Physics 2, 101 (2006)

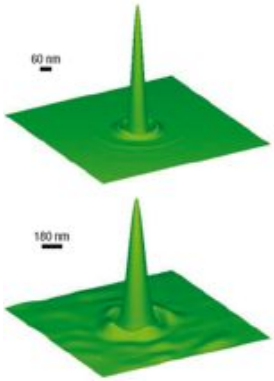

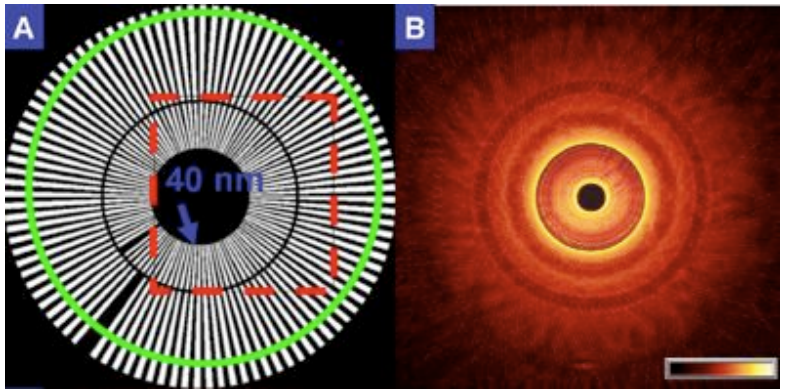

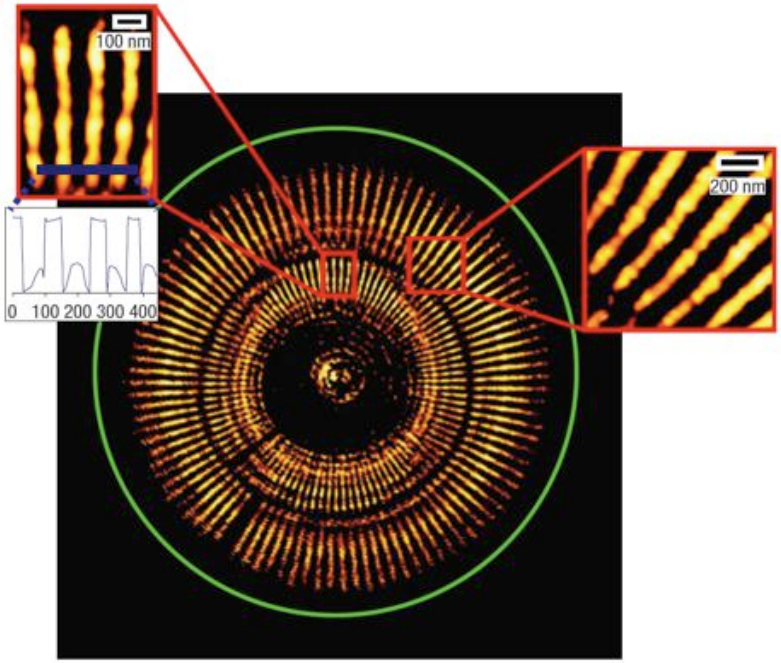

Ability to study extended samples is essential for many real-world problems!

B. Abbey, Nature Physics 4, 394 (2008)

"Fuse bay" structure

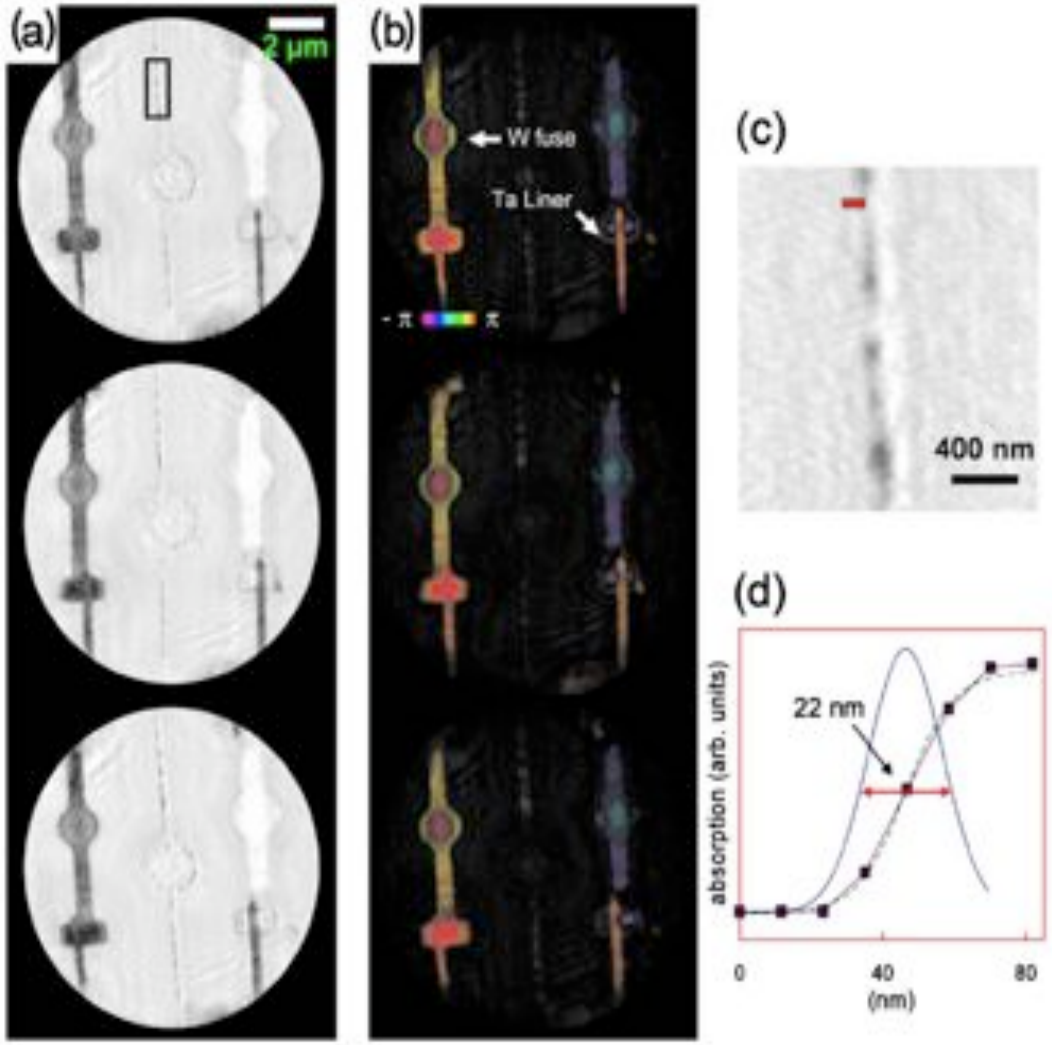

B. Abbey, APL 93, 214101 (2008)

Diffraction microscopy in 3D

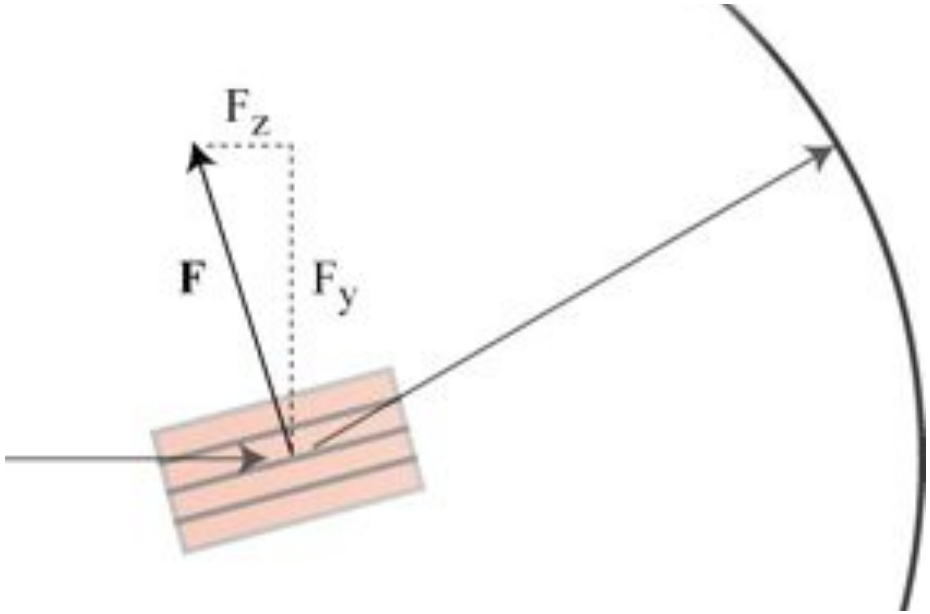

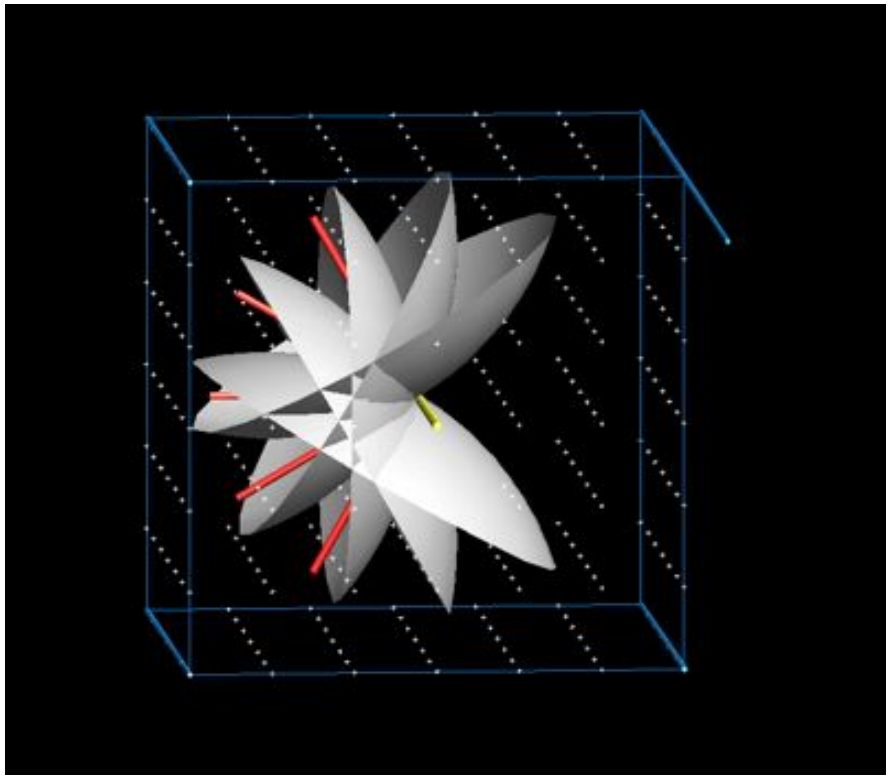

Bragg gratings that diffract to a certain angle represent a specific transverse and longitudinal periodicity (Ewald sphere)

Data collection over a series of rotations about an axis fills in 3D Fourier space for phasing

3D coherent diffraction imaging

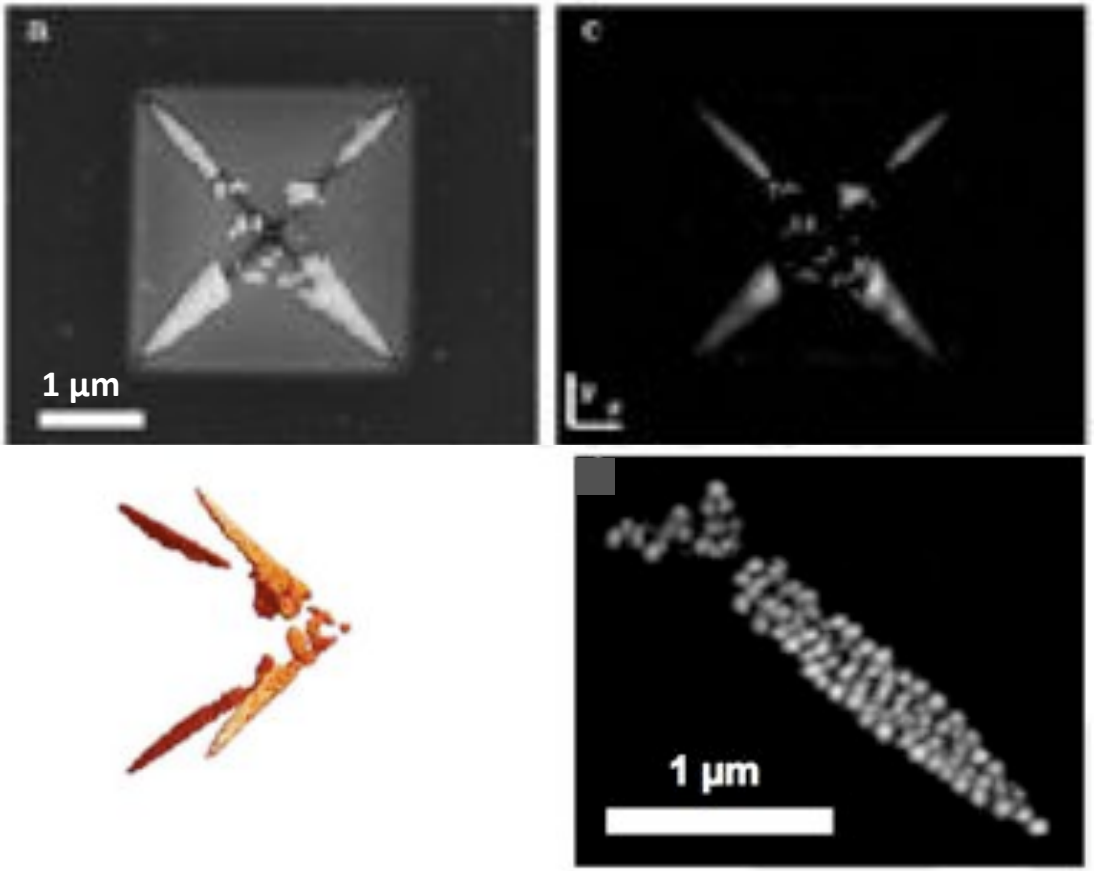

(a) SEM of pyramidal indentation in a 100-nm Si_3N_4 membrane lined with 50-nm Au spheres.
(b) 3D image reconstructed from 123 diffraction projections spanning -57° to +66°, using reality and positivity constraints.
(c) Large DOF projection. (d) Enlarged region of (c).

H. Chapman, JOSA A23, 1179 (2006)

3D CDI of biological specimens is feasible, too

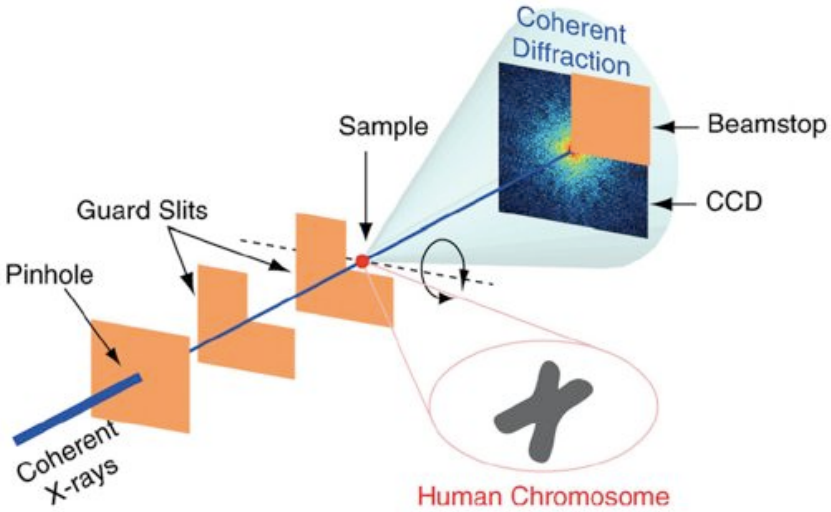

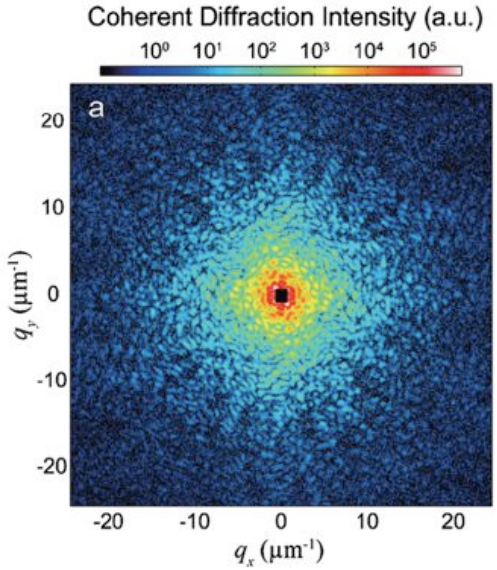

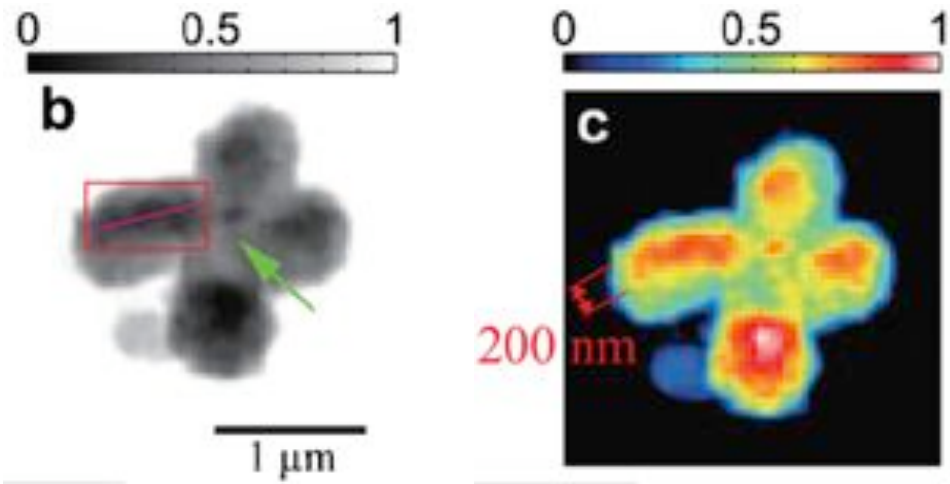

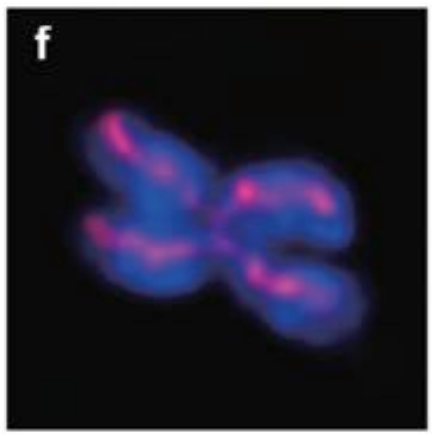

Y. Nishino, PRL 102, 018101 (2009)

Ptychography: scanning approach enables solution to extended object *and* unknown probe

R. Hegerl, Phys. Chemie 74, 1148 (1970)
H. Chapman, Ultramicroscopy 66, 153 (1996)
H. Faulkner and J. Rodenburg, PRL 93, 023903 (2004)
J. Rodenburg, PRL 98, 034801 (2007)

P. Thibault, Science 321, 379 (2008)

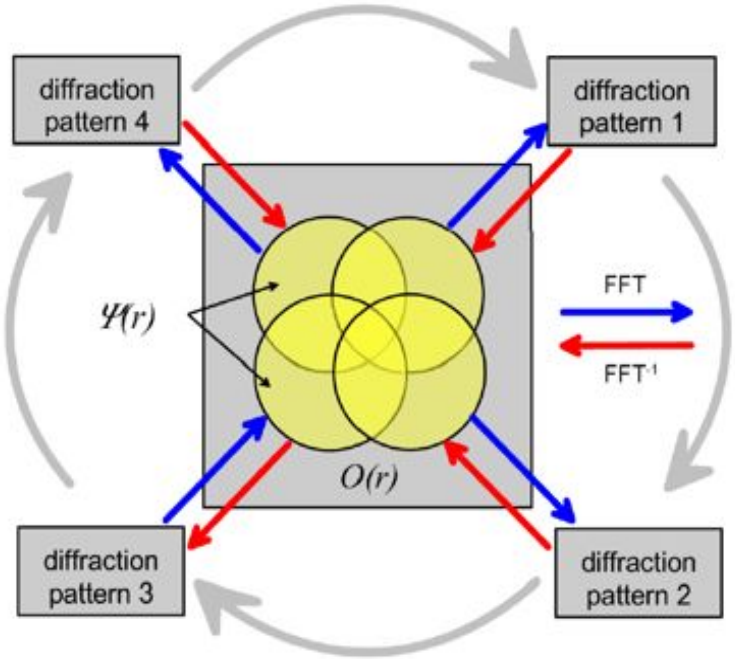

$$\hat{P}_n(\mathbf{r}) = \frac{\sum_j \hat{O}_n^*(\mathbf{r},\mathbf{r}_j)\psi_n(\mathbf{r},\mathbf{r}_j)}{\sum_j |\hat{O}_n(\mathbf{r},\mathbf{r}_j)|^2} = \text{the Probe}$$

$$\hat{O}_n(\mathbf{r}) = \frac{\sum_j \hat{P}_n^*(\mathbf{r},\mathbf{r}_j)\psi_n(\mathbf{r},\mathbf{r}_j)}{\sum_j |\hat{P}_n(\mathbf{r},\mathbf{r}_j)|^2} = \text{the Complex Object}$$

$$\psi_n(\mathbf{r},\mathbf{r}_j) = \hat{O}_n(\mathbf{r})\hat{P}_n(\mathbf{r},\mathbf{r}_j)$$

$$\psi_{n+1}(\mathbf{r},\mathbf{r}_j) = \psi_n(\mathbf{r},\mathbf{r}_j) + p_F[2\hat{P}_n(\mathbf{r},\mathbf{r}_j)\hat{O}_n(\mathbf{r}) - \psi_n(\mathbf{r},\mathbf{r}_j)] - \hat{P}_n(\mathbf{r},\mathbf{r}_j)\hat{O}_n(\mathbf{r})$$

Thibault et al. algorithm

Recipe:

1. Start with guess for $\hat{O}$ and $\hat{P}$, use these guesses to define ψ_0.
2. Update ψ_{n+1} for all j probe positions, holding $\hat{O}$ and $\hat{P}$ constant.
3. Update $\hat{O}$ using sum on previous page, using current $\hat{P}$ and ψ_n.
4. Update $\hat{P}$ using sum on previous page, using current $\hat{O}$ and ψ_n.
5. Back to step 1, repeat.

Good convergence in 10s of iterations

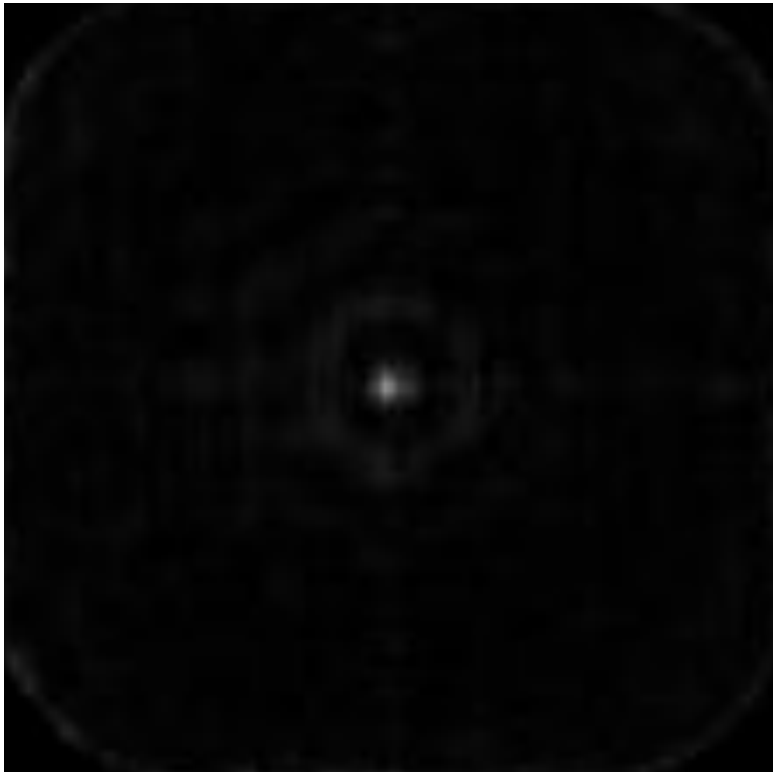

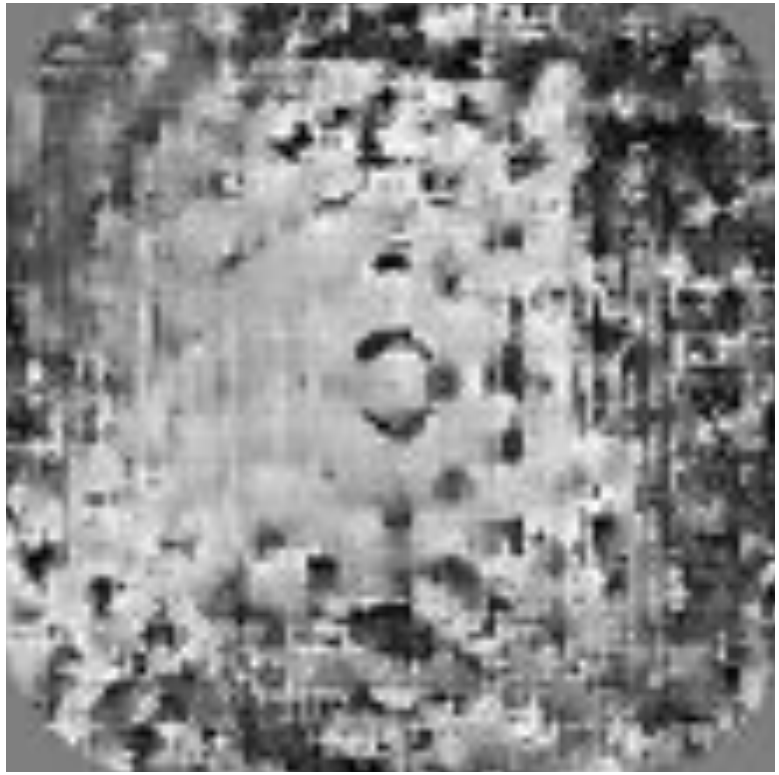

Magnetic multilayers: model magnetic storage media

- Fabricated by sputtering; can be nano-patterned lithographically
- Perpendicular anisotropy spontaneously forms "worm" domains with antiparallel out-of-plane magnetization
- Artificial ferrimagnets with strong coupling at domain interfaces

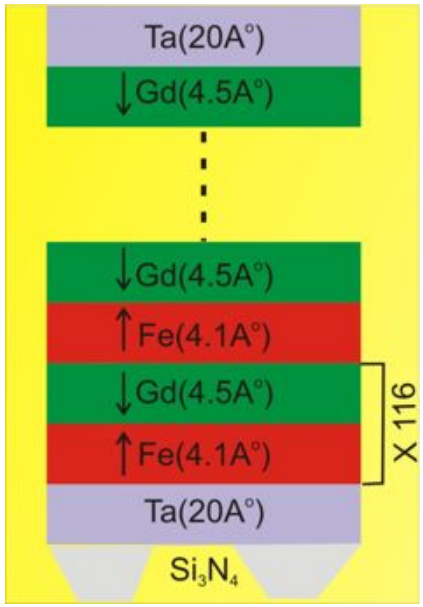

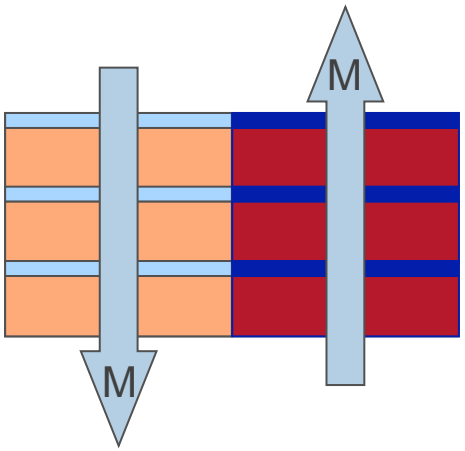

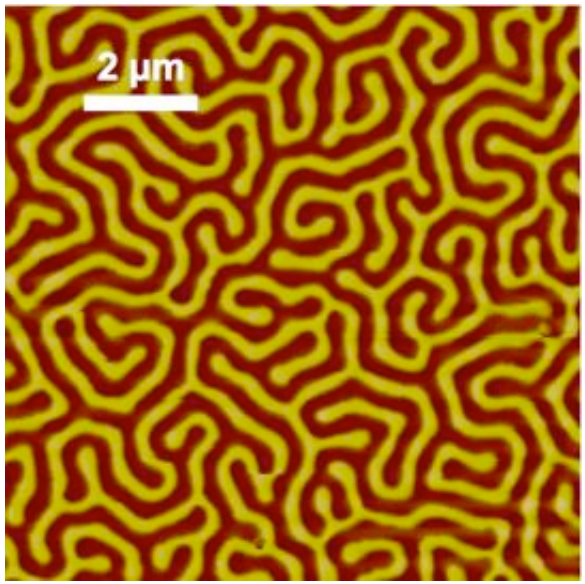

Magnetic force micrograph of 200 nm thick GdFe multilayer (courtesy E. Fullerton, UCSD)

Resonant x-ray scattering

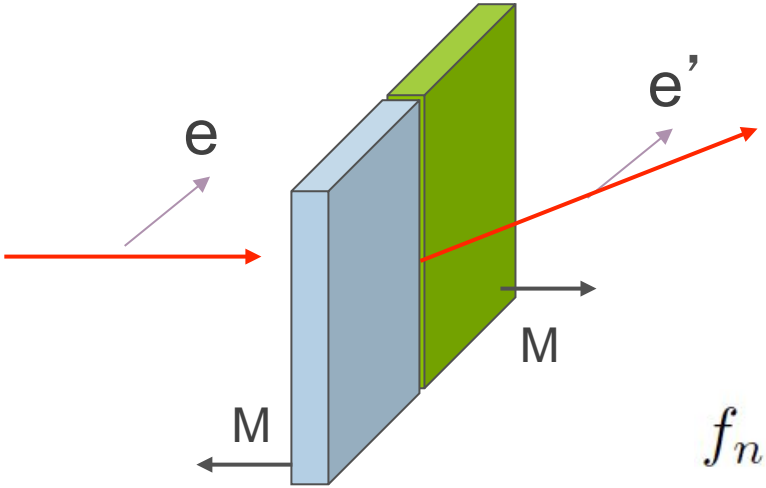

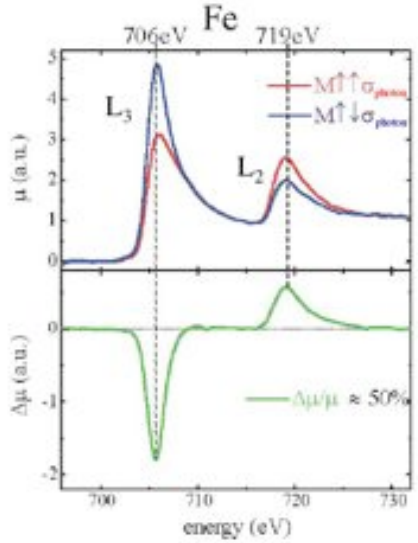

$$f_n \approx f^0_{nonres} + f^{magn}_{nonres} + f' + i f''$$

~0 in this geometry

charge magnetic circular magnetic linear

$$f_{res} = \mathbf{e}' \cdot \mathbf{e}\, F_n^c - i\,(\mathbf{e}' \times \mathbf{e}) \cdot \mathbf{M}_n\, F_n^{m1} + (\mathbf{e}' \cdot \mathbf{M}_n)(\mathbf{e} \cdot \mathbf{M}_n)\, F_n^{m2}$$

$$I \propto \left| \sum_n \exp(i\mathbf{q} \cdot \mathbf{r}_n) f_n \right|^2$$

J.P. Hannon, PRL 61, 1245 (1988)

Magnetic domain structure can be visualized in-situ by resonant x-ray ptychography

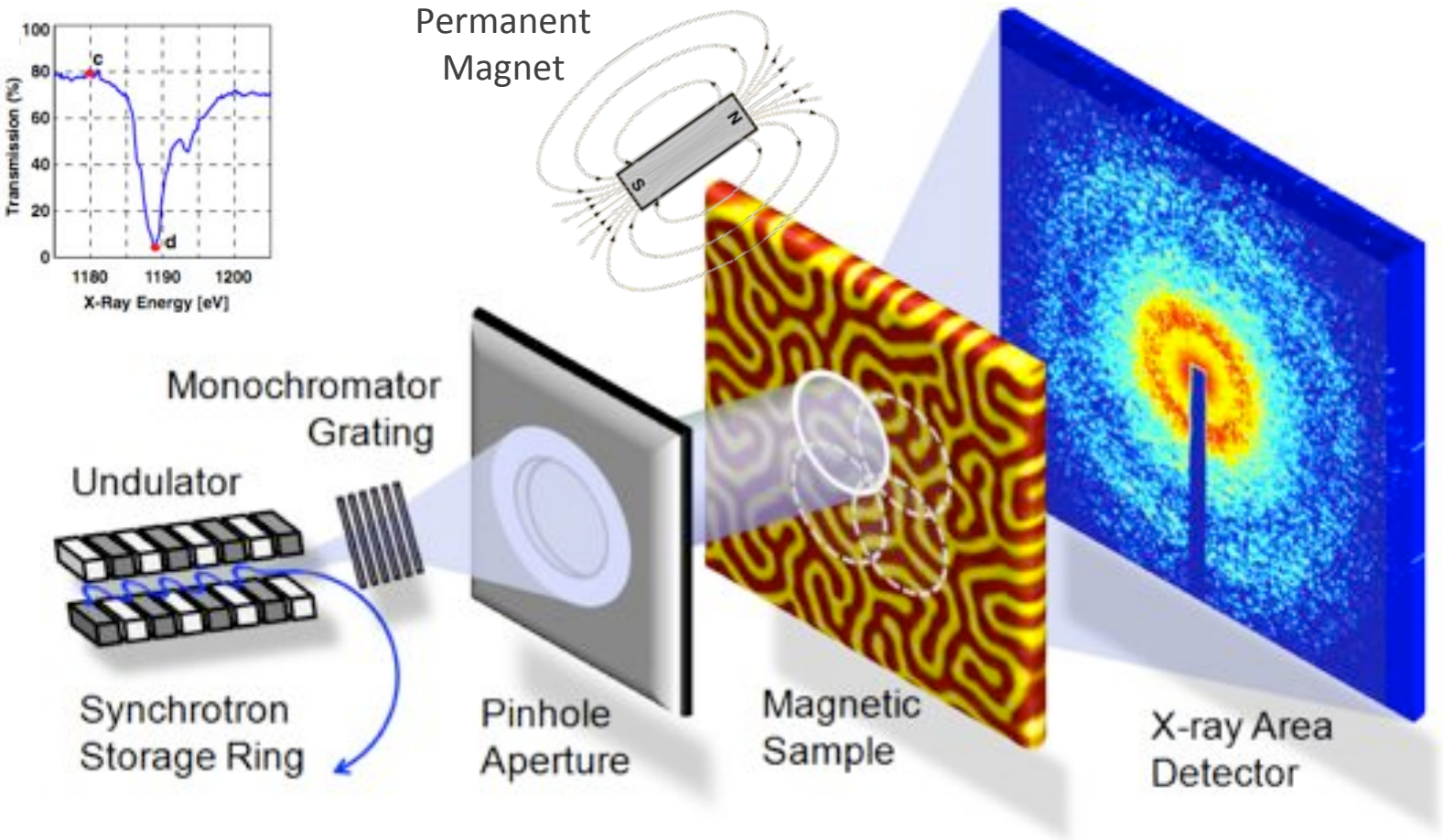

Resonant scattering vs. photon energy

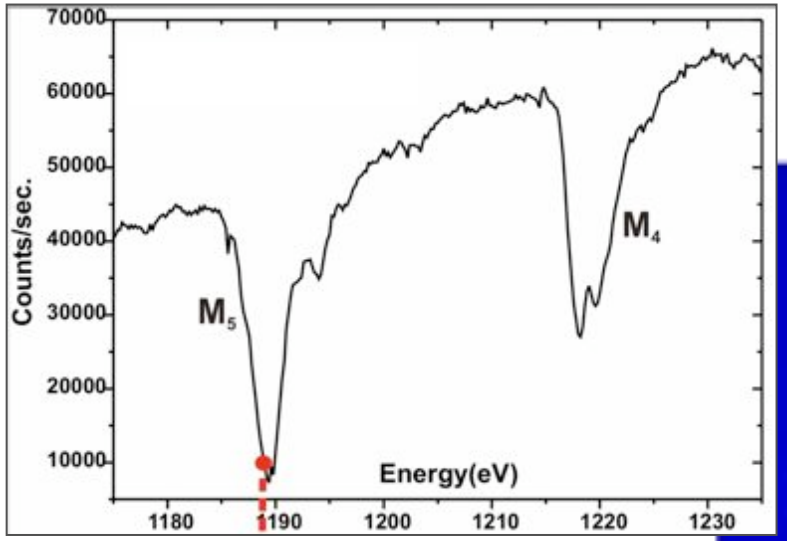

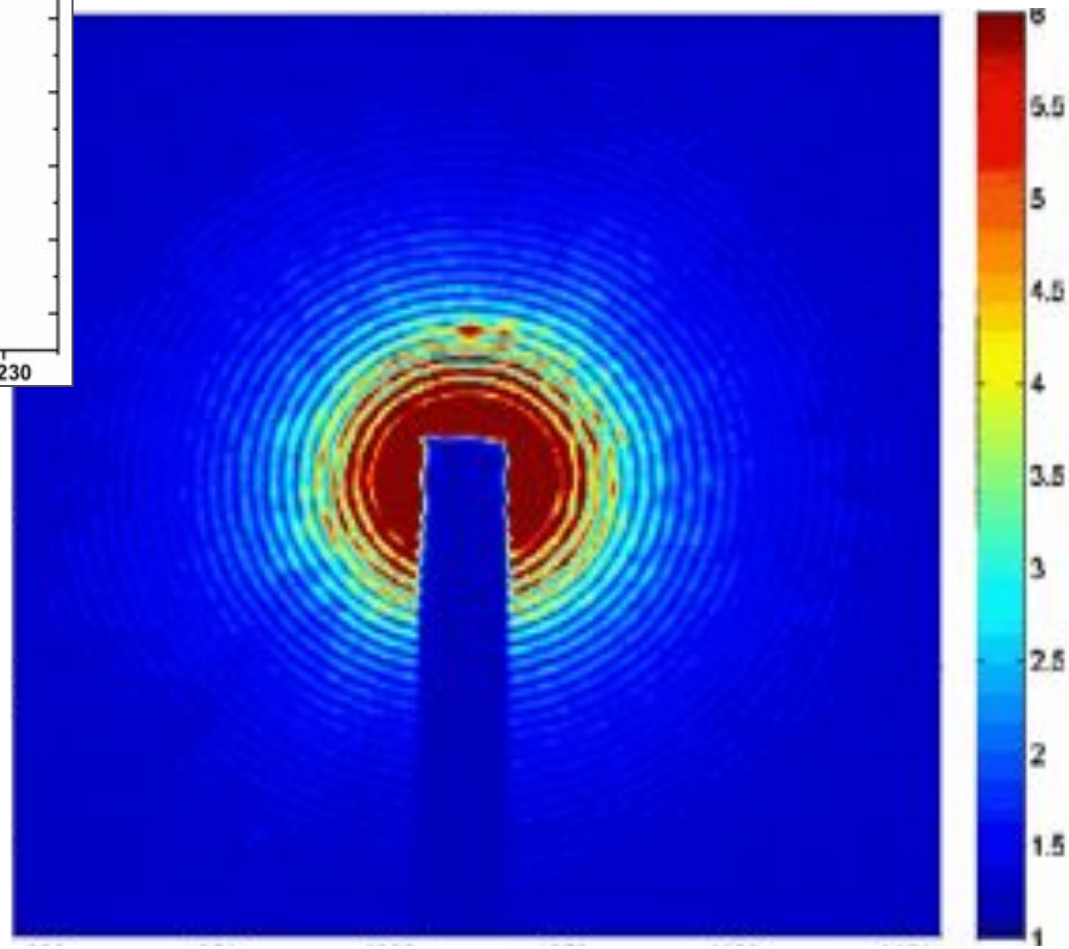

Reconstructed domain structure and probe function

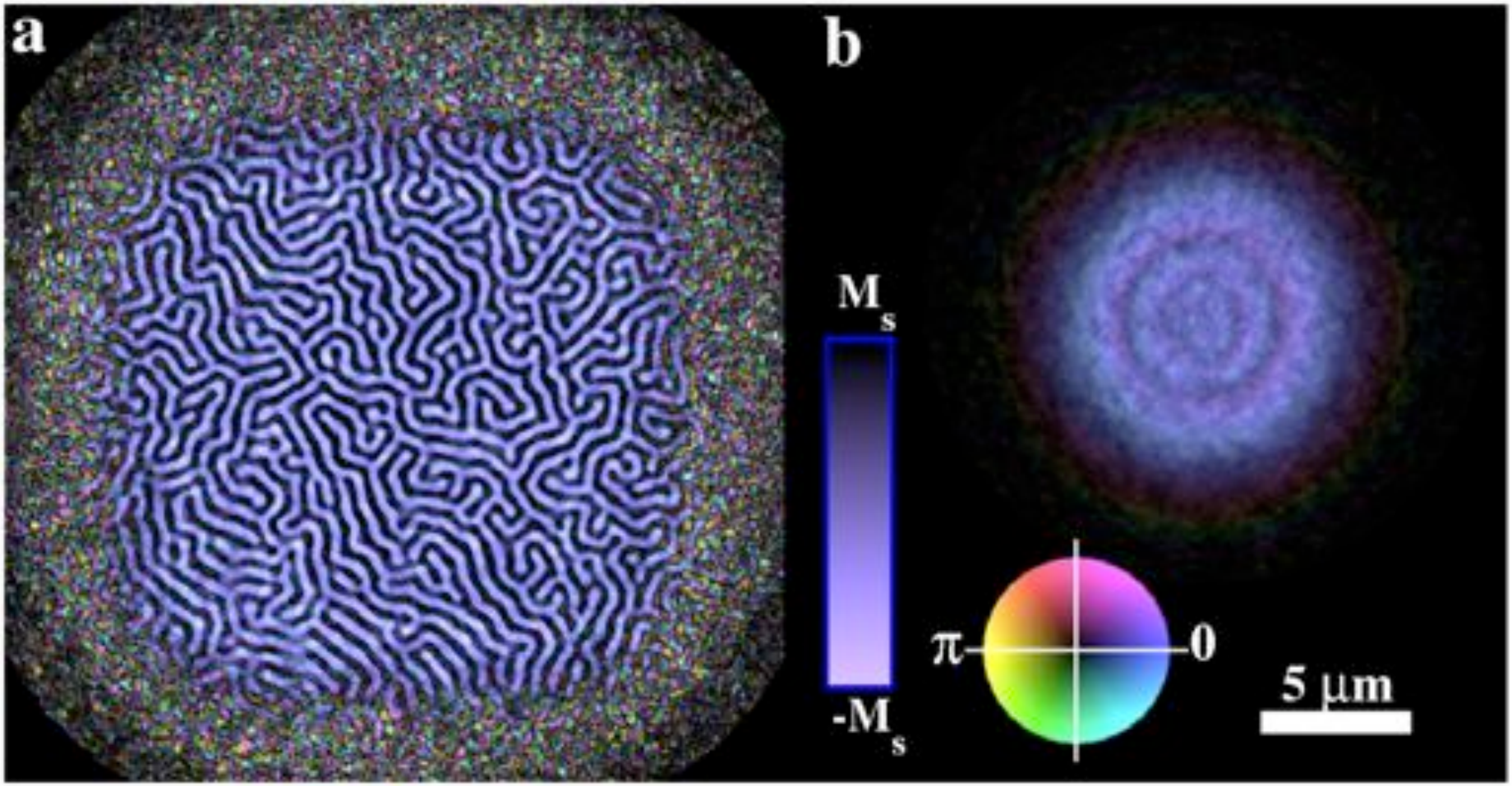

Sample scan: $(14 \times 3\ \mu m)^2 \times (40 \times 1\ s)$ exposures

Magnetic domain evolution with increasing field

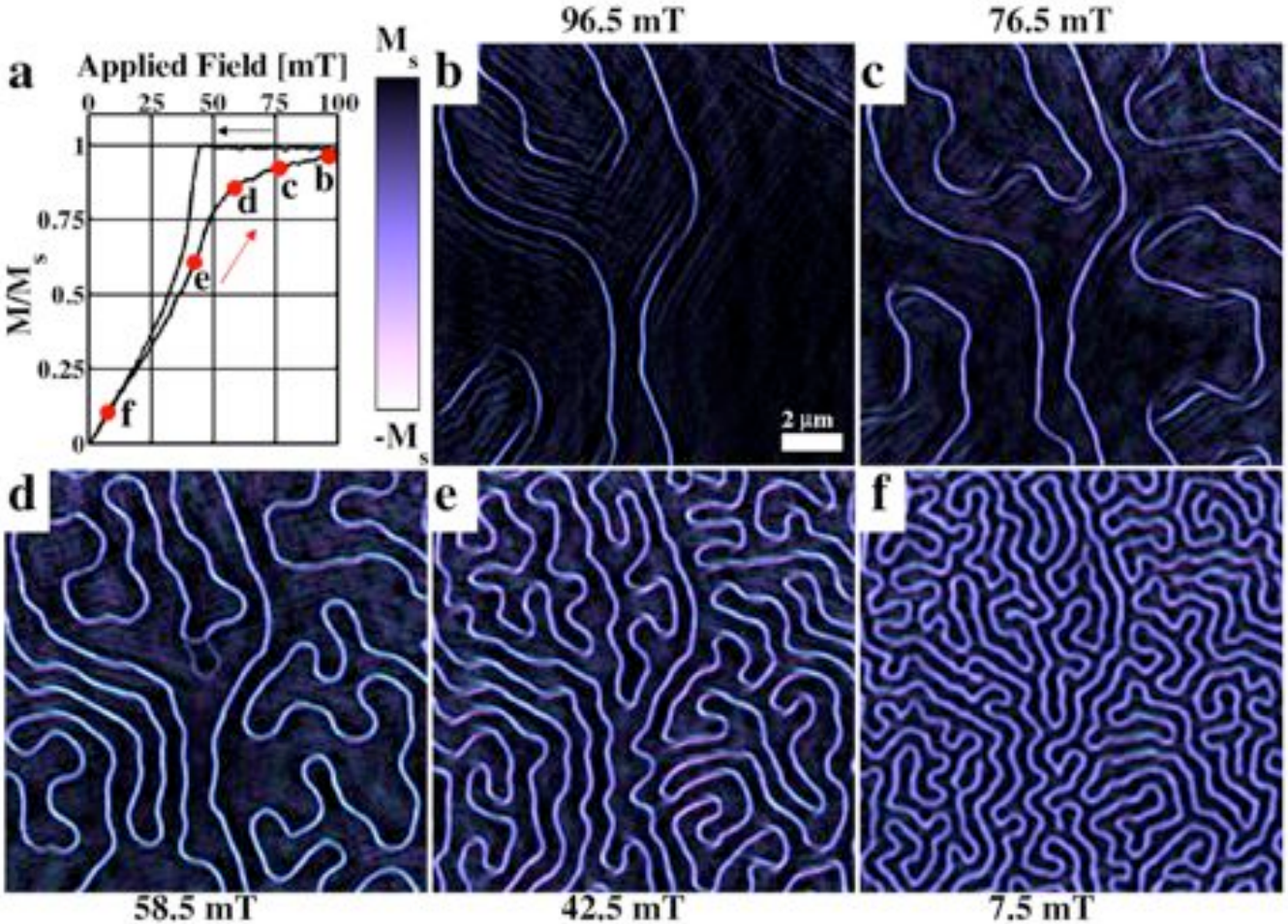

Hysteresis loop of sample magnetization as a function of magnetic field applied normal to the film surface. (b-f) Reconstructions from a series of diffraction patterns taken at indicated points in hysteresis curve. Bright domains are anti-parallel to the applied magnetic field.

Decreasing field

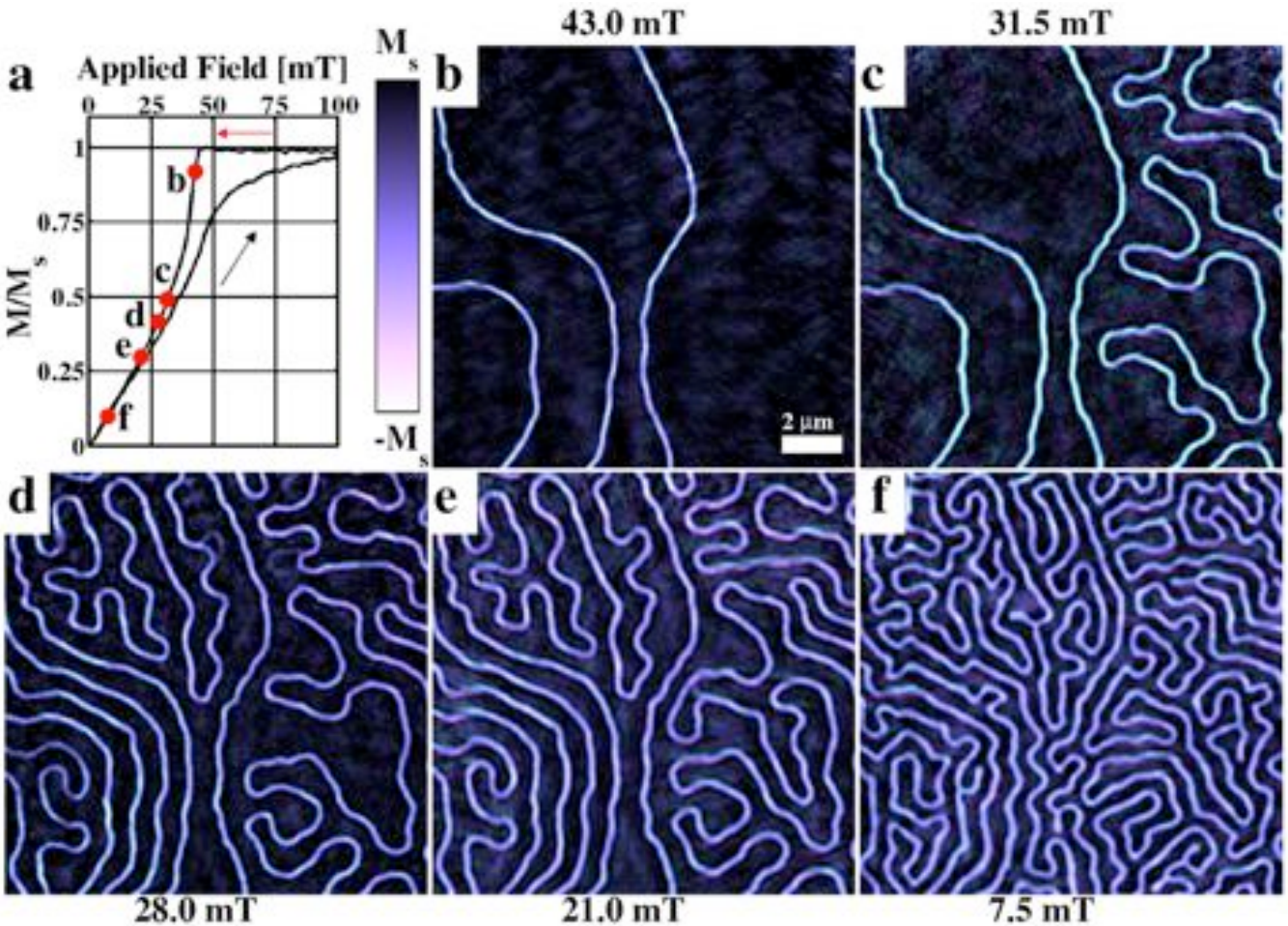

Domain evolution as the magnetic field was *decreased* from saturation towards zero. (a) Sample hysteresis loop as a function of applied field; (b-f) reconstructions from series of scanned diffraction patterns taken at various points in (a).

A. Tripathi, PNAS 108, 13393 (2011)

Bragg diffraction from crystals

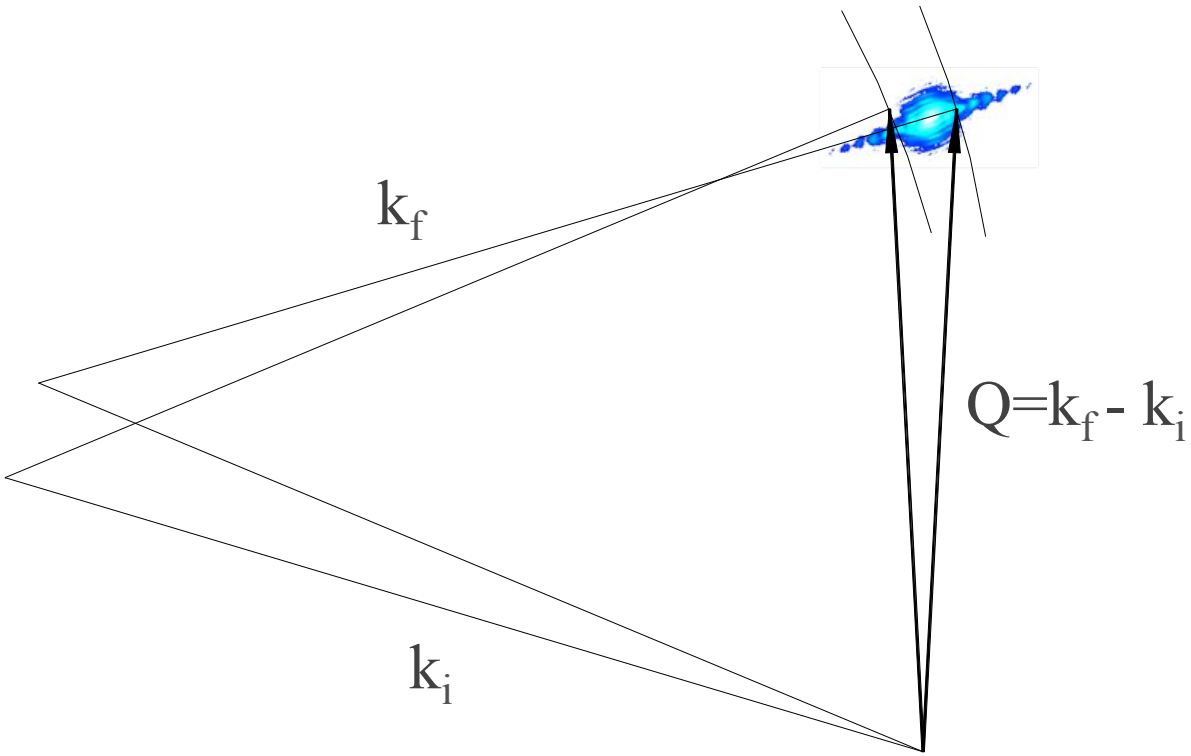

Coherent diffraction from crystals

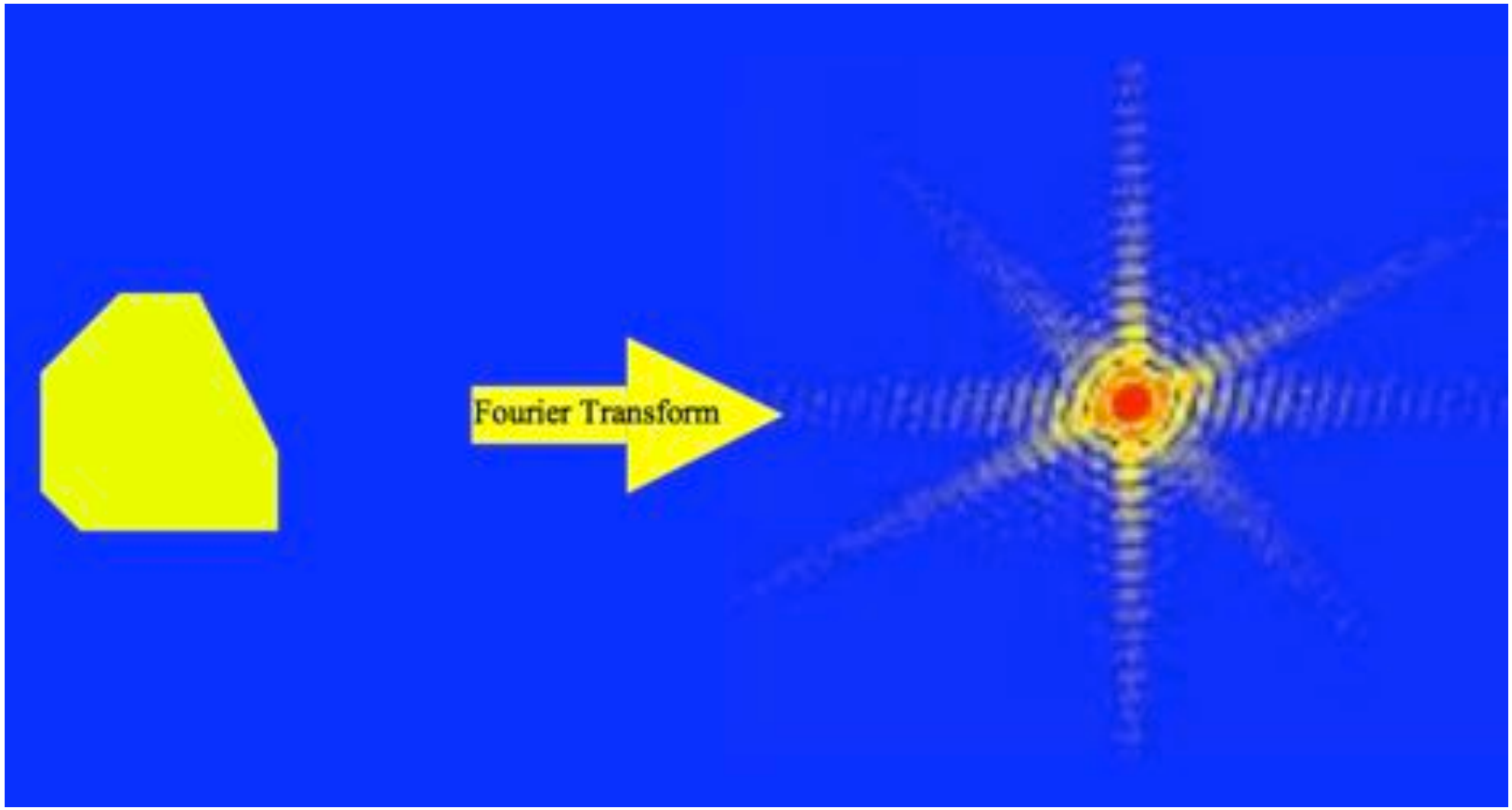

Each Bragg spot contains the shape information

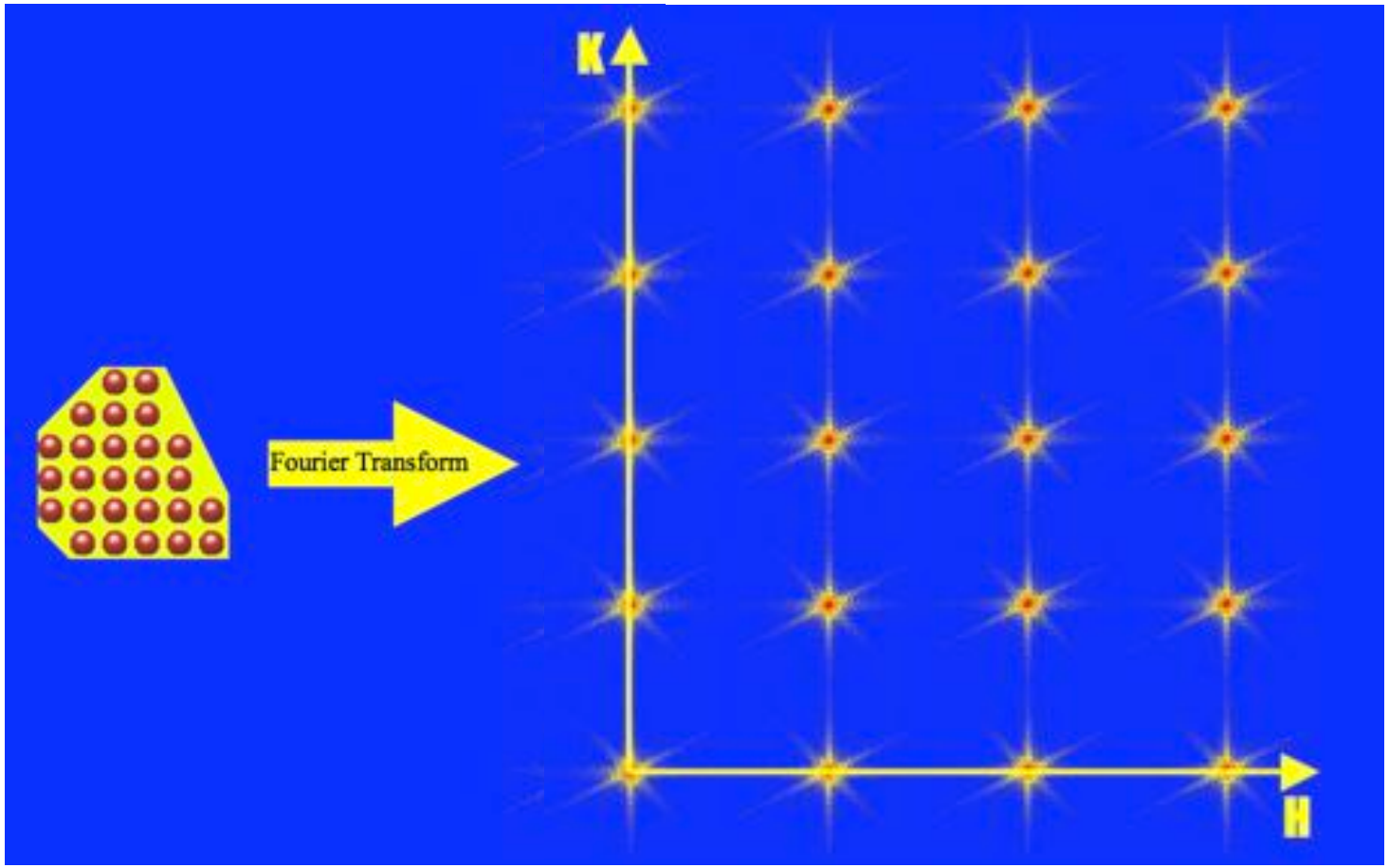

Bragg coherent diffractive imaging

- Bragg CDI is uniquely sensitive to crystalline order and lattice strain
- The Ewald sphere can be tiled by rocking the crystal to get 3D information

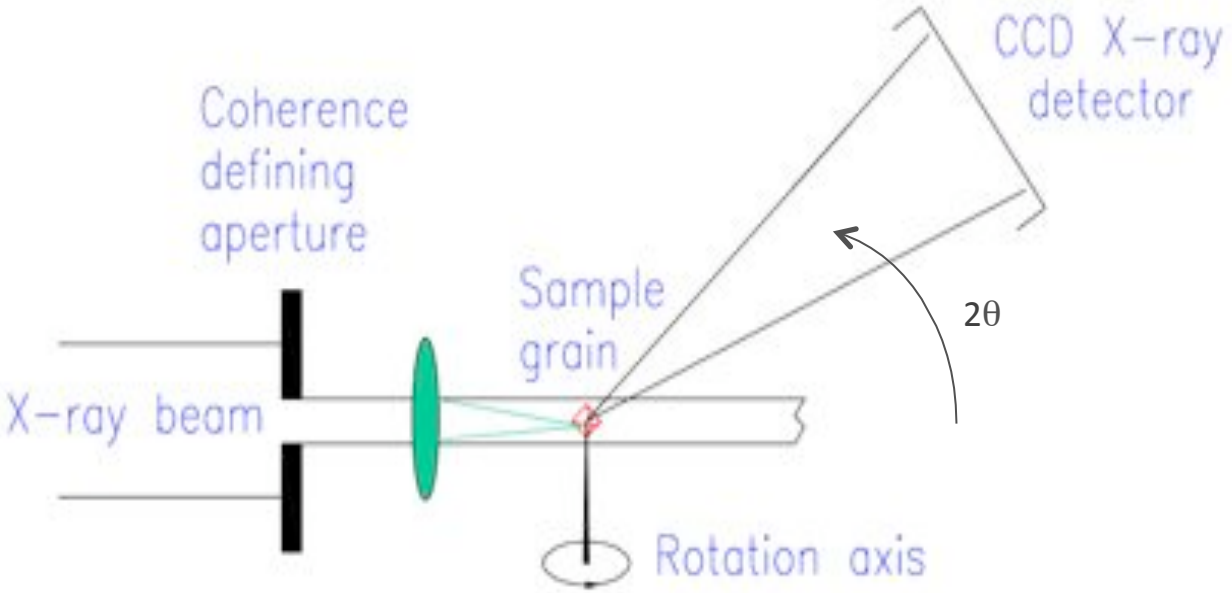

I. Robinson and R. Harder, Nature Mater. 8, 291 (2009)

Three-dimensional Bragg method

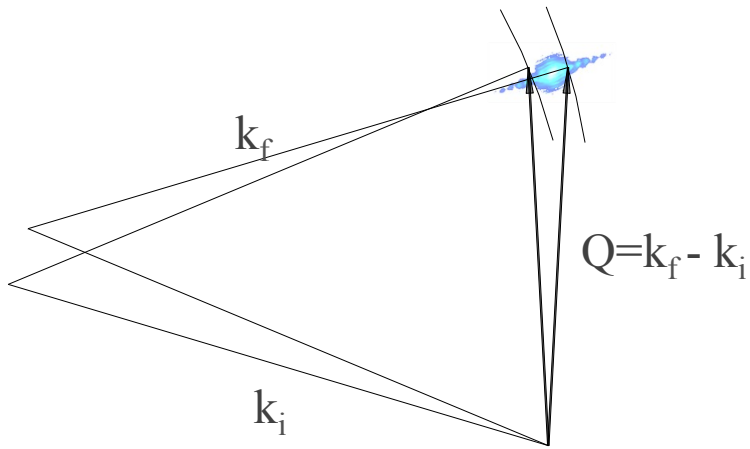

- Select coherent part of hard x-ray beam with double crystal monochromator and precision slits
- Locate sample in beam and Bragg peaks (ideally, 3 to get complete strain tensor)
- Rock sample around Bragg peaks to record diffraction vs. angle
- Assemble 3D XYθ data set, align to central peak
- Reconstruct via iterative phase retrieval, using constraint applied in pixel coordinates

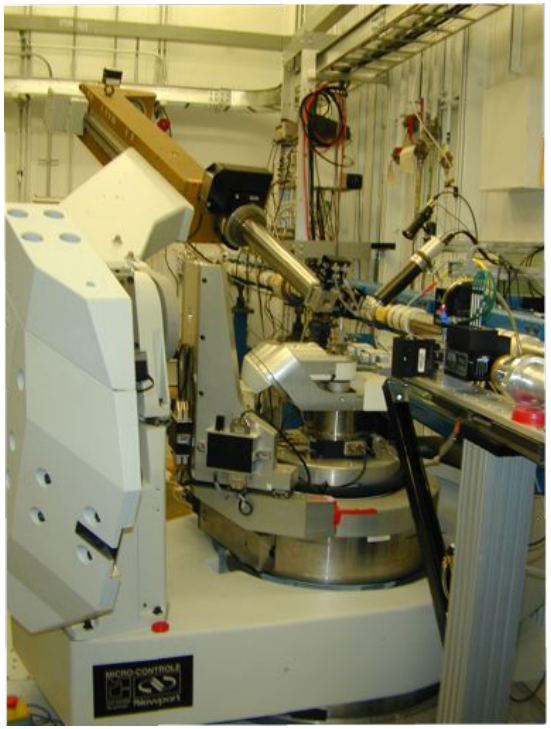

Setup at APS 34-ID-C beamline

Diffractometer and cryo setup at 34-ID-C

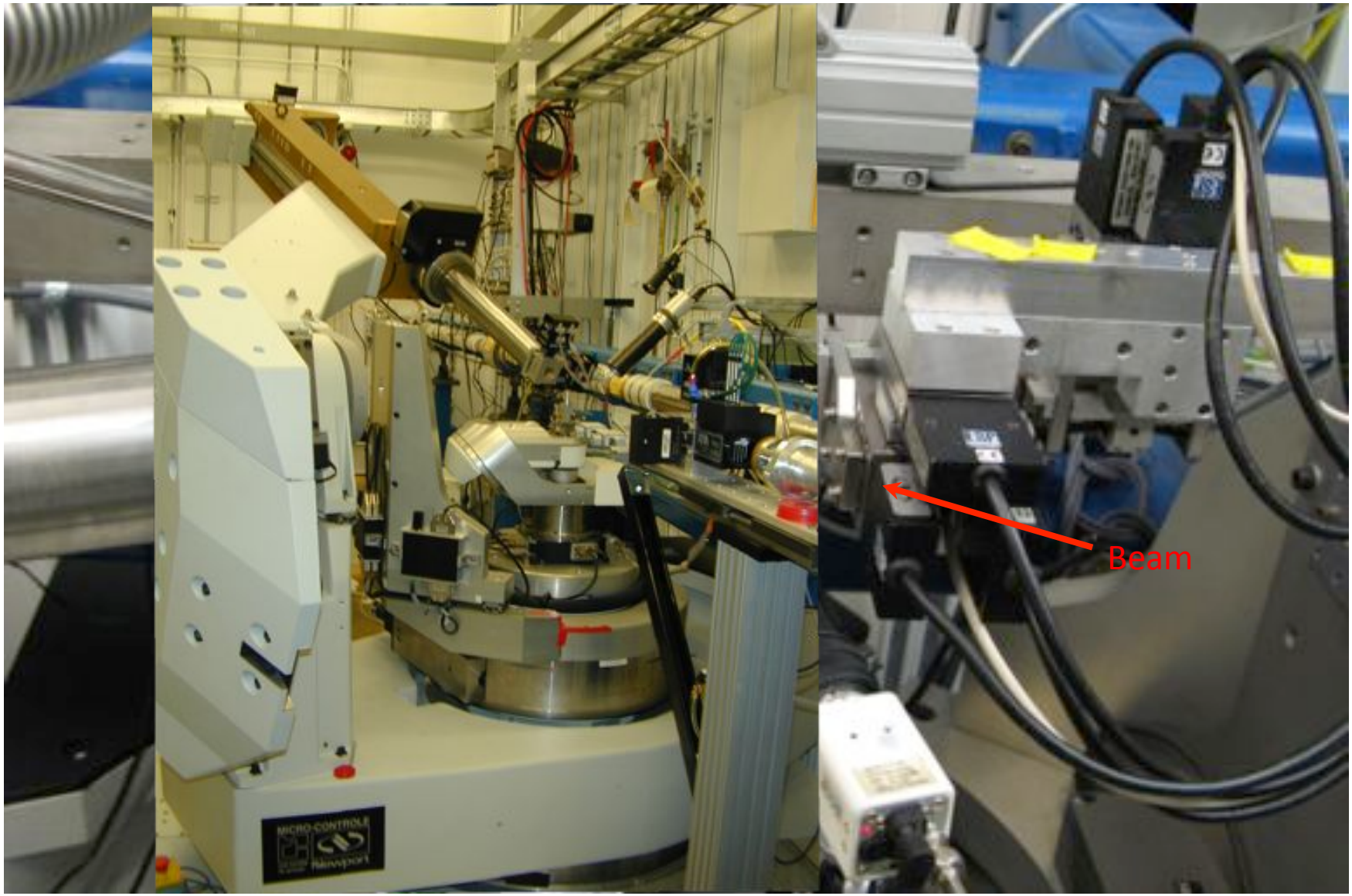

Mapping crystal strain in 3D by CDI

0.5 µm Pb crystal grown on SiO_2 substrate

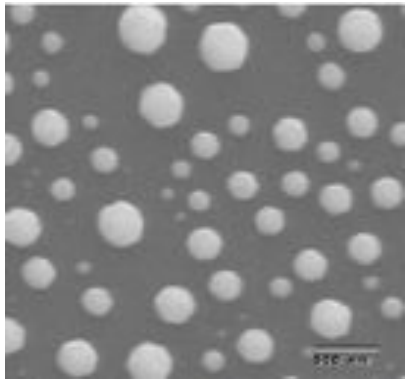

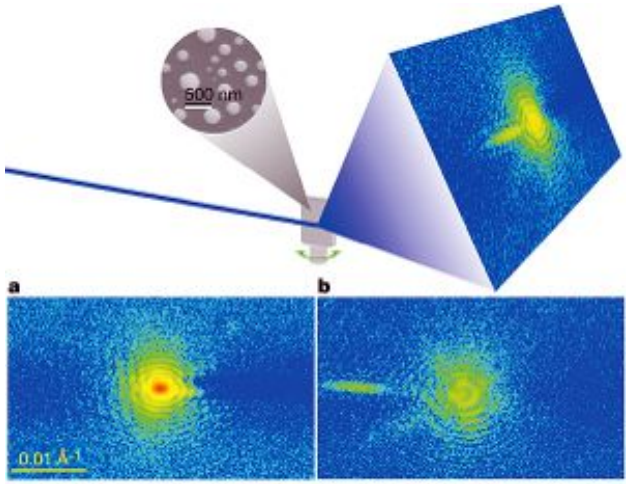

Map series of diffraction patterns about (111) Bragg peak

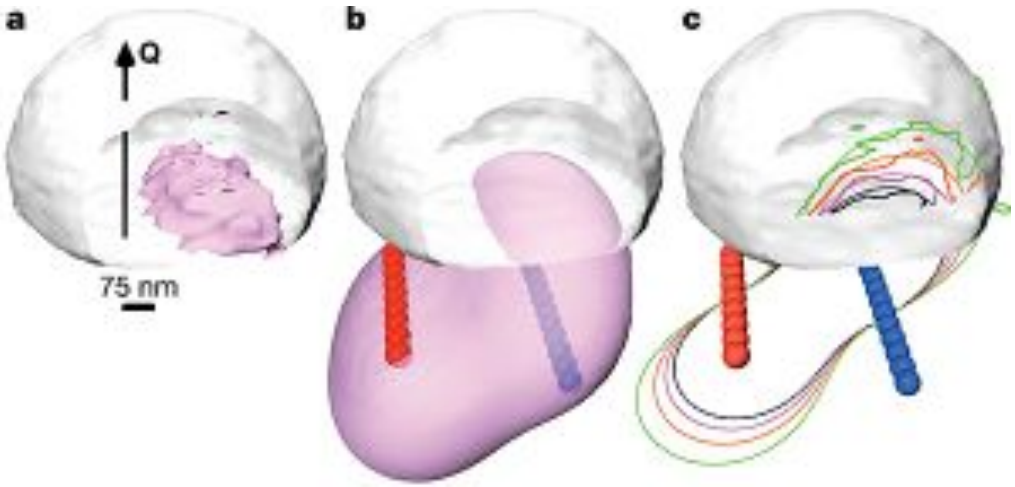

Reconstructed diffraction data

M. Pfeifer, Nature 442, 63 (2006)

Asymmetries in the Bragg spots arise from lattice strain

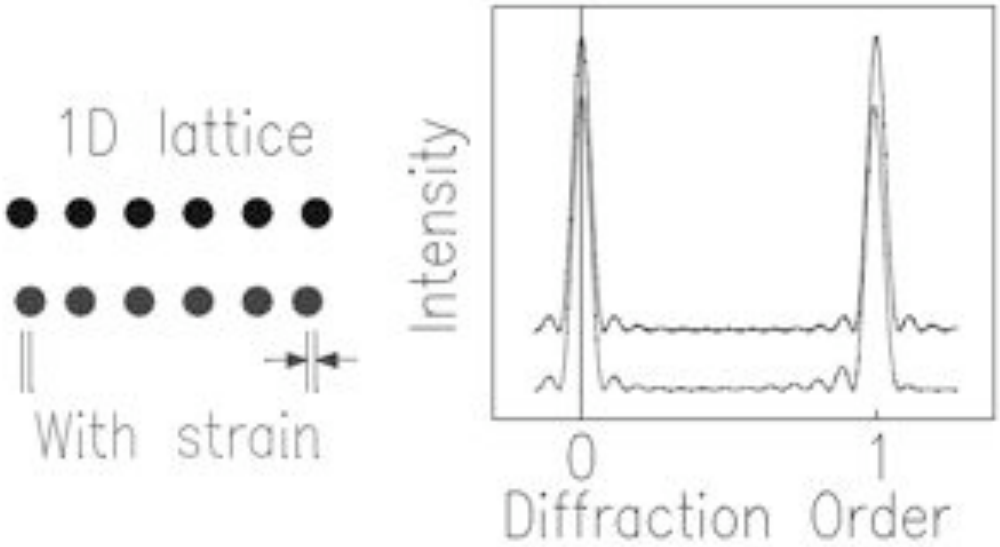

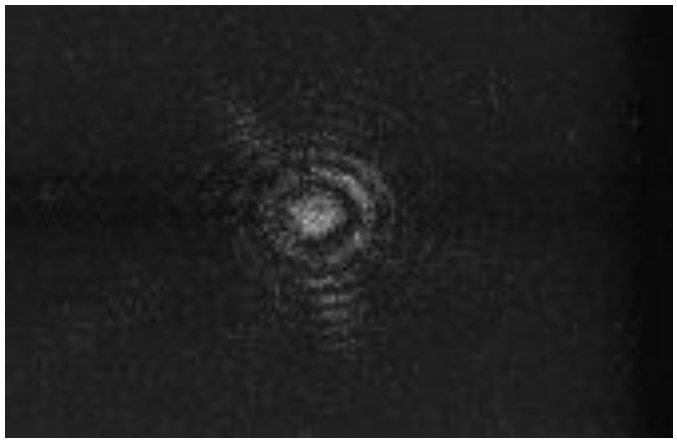

I. Robinson and R. Harder, Nature Mater. 8, 291 (2009)

3D strain is expressed as a tensor

$$\varepsilon_{ij} = \begin{bmatrix} \varepsilon_{xx} & \gamma_{xy} & \gamma_{xz} \\ \gamma_{xx} & \varepsilon_{yy} & \gamma_{yz} \\ \gamma_{xx} & \gamma_{yz} & \varepsilon_{zz} \end{bmatrix}$$

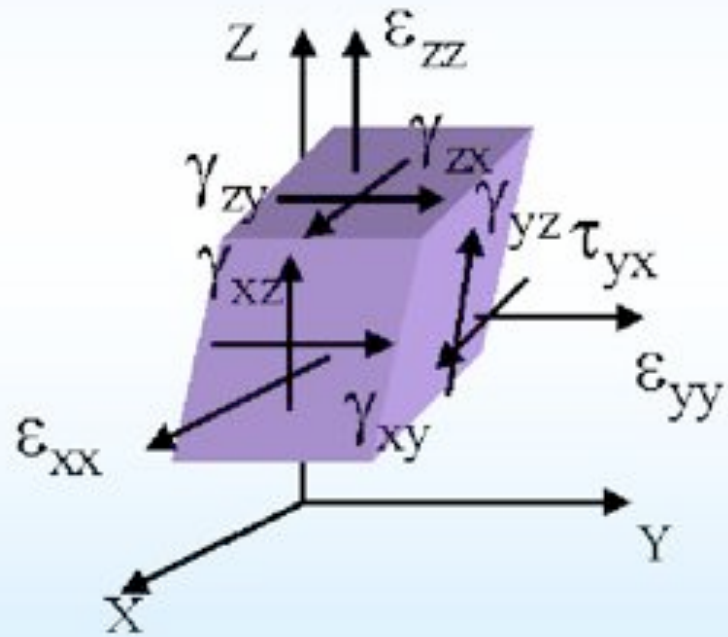

$$\varepsilon_x = \frac{\partial u_x}{\partial x} \qquad \varepsilon_y = \frac{\partial u_y}{\partial y} \quad , \qquad \varepsilon_z = \frac{\partial u_z}{\partial z}$$

$$\gamma_{yz} = \gamma_{zy} = \frac{\partial u_y}{\partial z} + \frac{\partial u_z}{\partial y} \quad , \qquad \gamma_{zx} = \gamma_{xz} = \frac{\partial u_z}{\partial x} + \frac{\partial u_x}{\partial z}$$

Vector displacement field around a lattice defect (Au crystal)

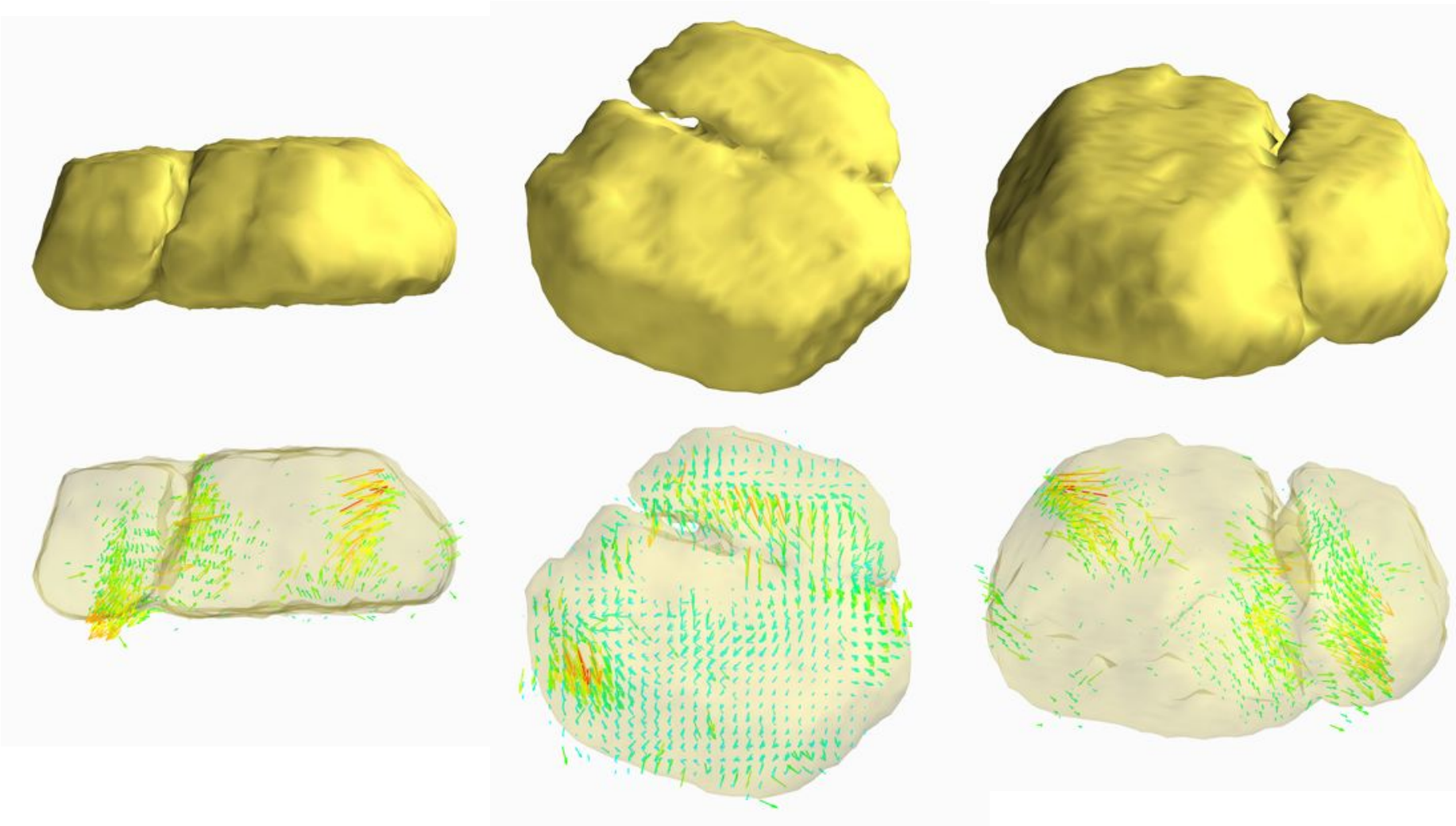

Produced by combining reconstructions from (11-1), (020), and (-111) reflections

3D strain map in ZnO nanorods

Nanoscale structures can be highly strained because of confinement effects, resulting in dramatically different electronic, magnetic and optical properties

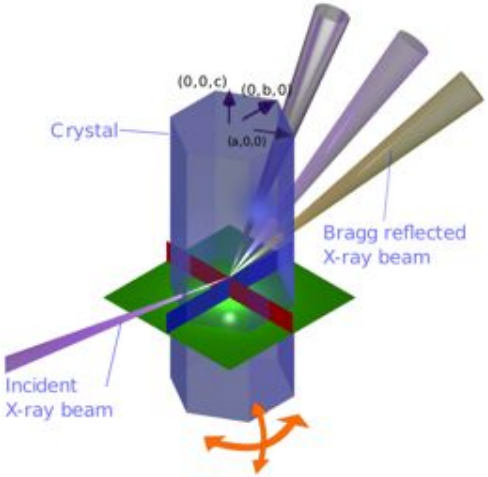

$$\epsilon_{ij} = \frac{1}{2}\left(\frac{\partial u_j}{\partial x_i} + \frac{\partial u_i}{\partial x_j}\right), \qquad \tau_{ij} = \left(\frac{\partial u_j}{\partial x_i} - \frac{\partial u_i}{\partial x_j}\right)$$

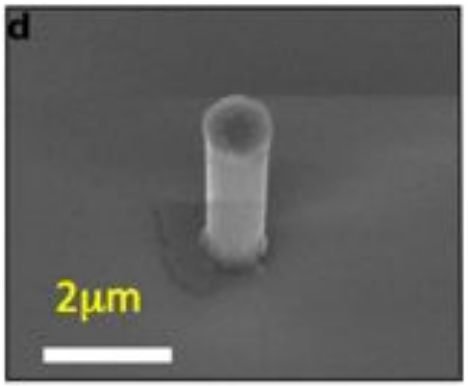

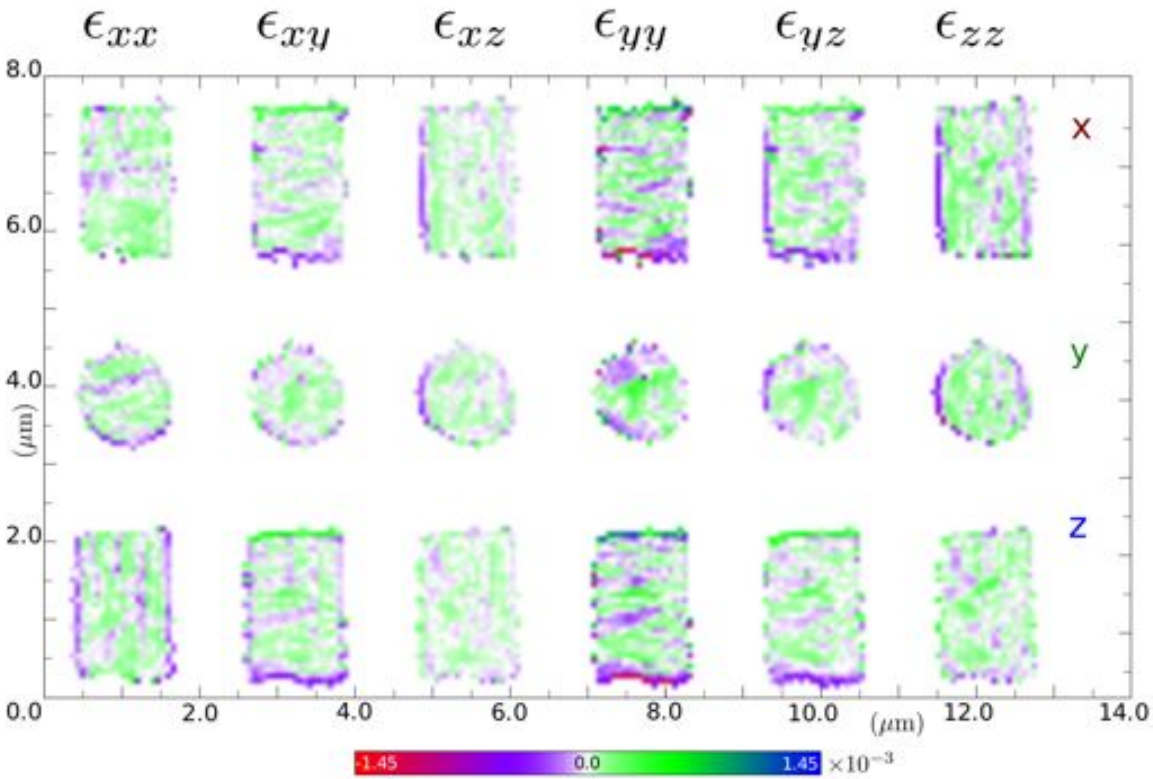

M. Newton, Nature Mater. 9, 120 (2010)

Unusual internal core-shell strain in zeolite crystals

Calcination of ZSM-5 zeolite crystals results in a surprising triangular strain distribution.

Nano-engineering of local strain by organic templating could be used to develop new catalysts.

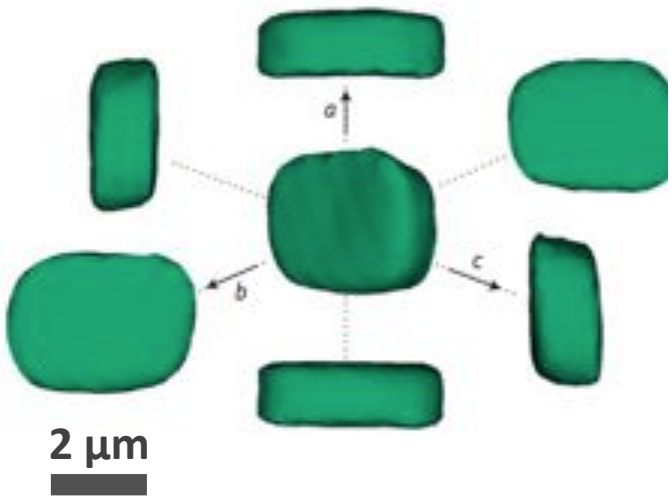

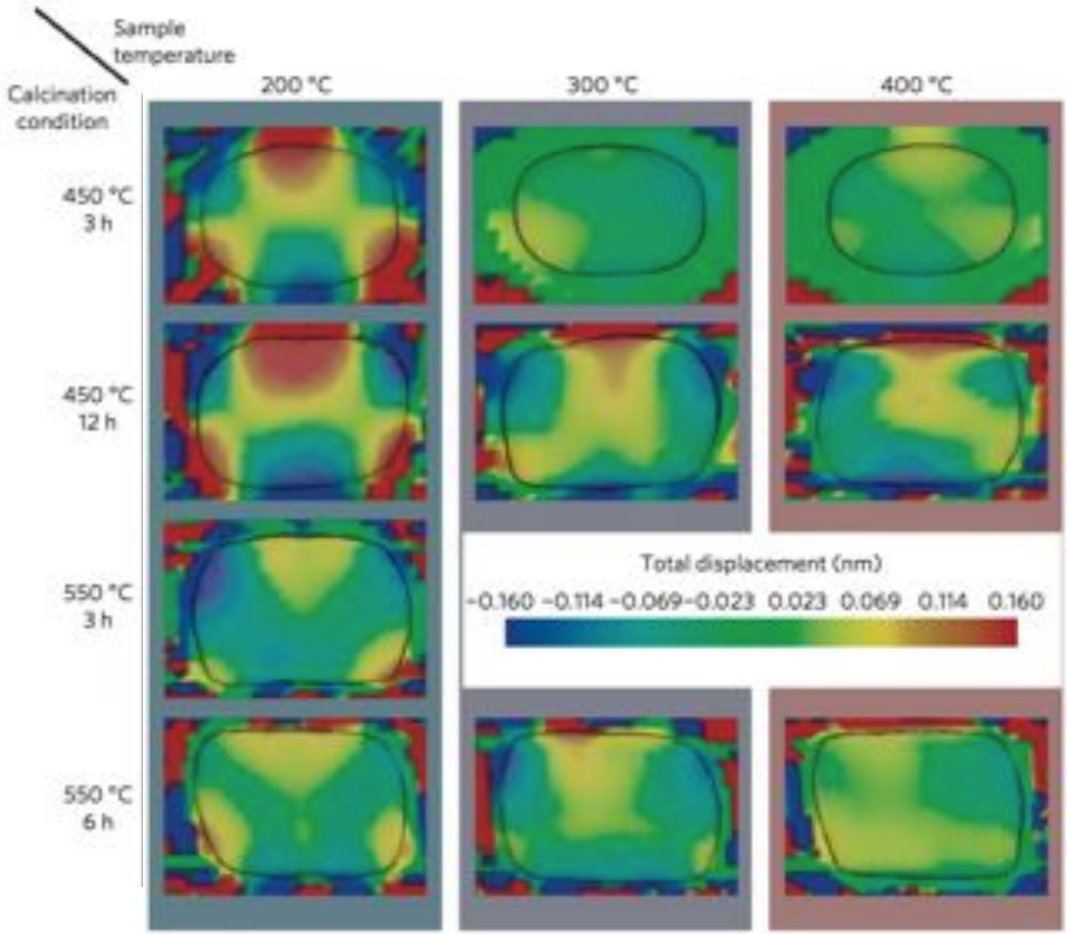

Internal strain distribution undergoes phase transition at ~200 C, as seen by Bragg CDI.

W. Cha, Nature Materials 12, 729 (2013)

X-ray Bragg ptychography

- Extension of scanning small-angle CDI methods to the Bragg regime.
- Algorithm enables reconstruction of both unknown probe and object wave
- ***More robust reconstruction than single-view; Bragg gives crystal strain as well as structure***
- First experiments on ferroelectric materials are yielding structure at ~6 nm resolution and strain at the 10^{-5} $\Delta c/c$ scale

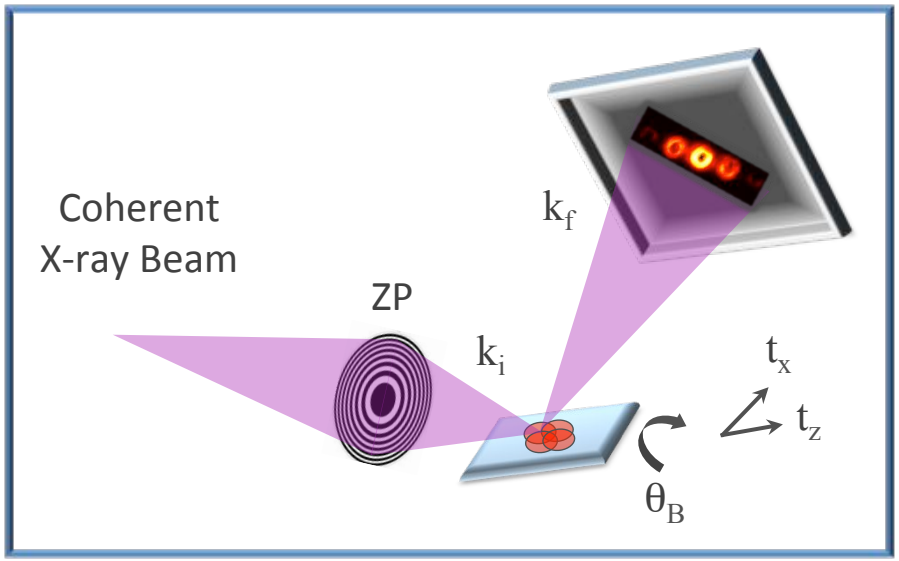

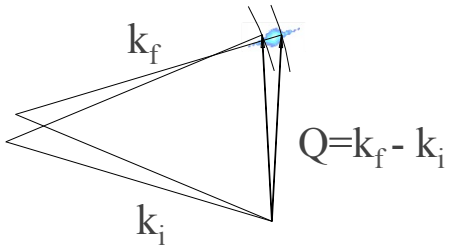

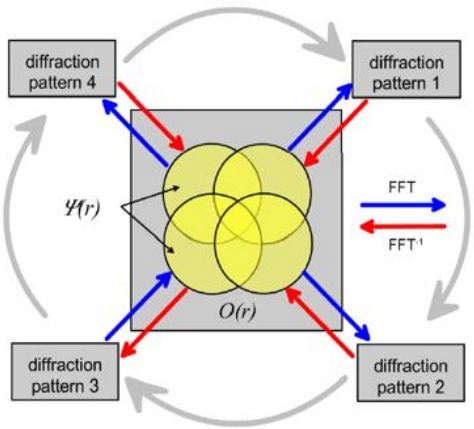

Initial experiments

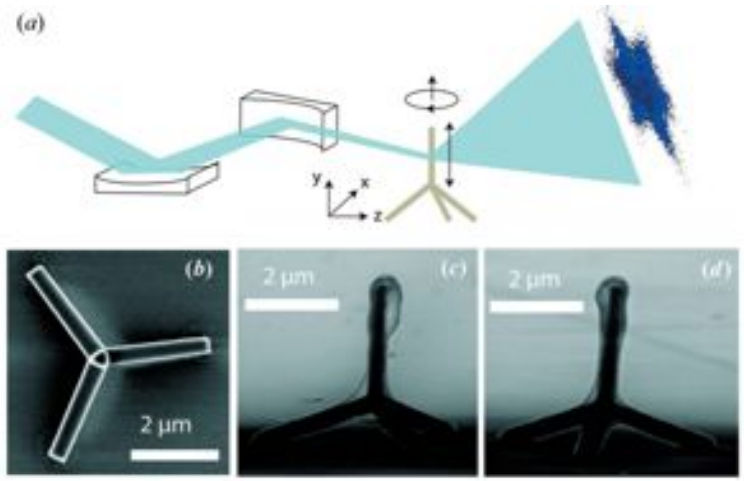

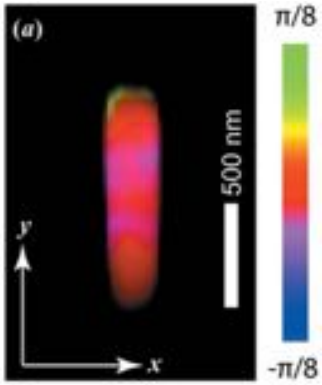

Scan along vertical arm of ZnO tetrapod
- 11.5 keV x-rays, ~1.3 µm focus, < 0.5 µm steps
- Collect 3D diffraction pattern (rock) at each scan position
- Reconstructed real-space voxels: 14x19x14 nm

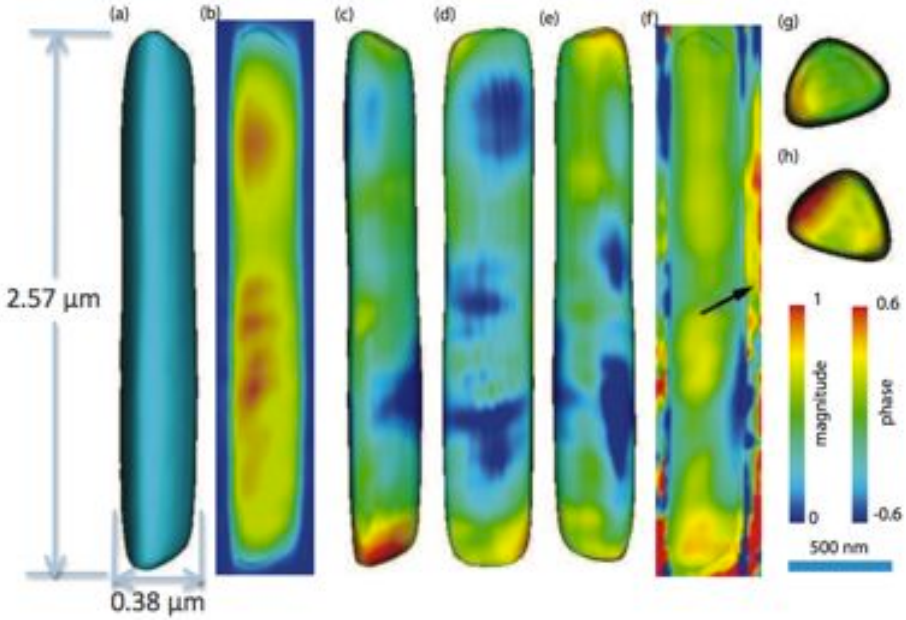

X. Huang, JAC 45, 778 (2012)

Local polarization in ferroelectric thin films

Critical phenomena such as domain fluctuations and order parameter pinning can lead to unexpected behavior at the nanoscale

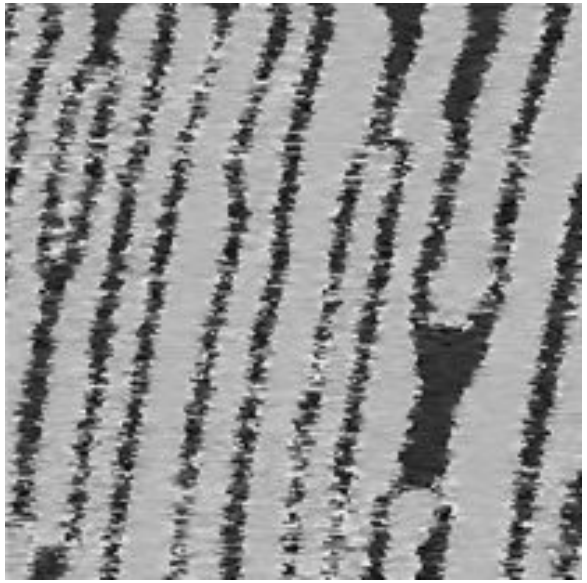

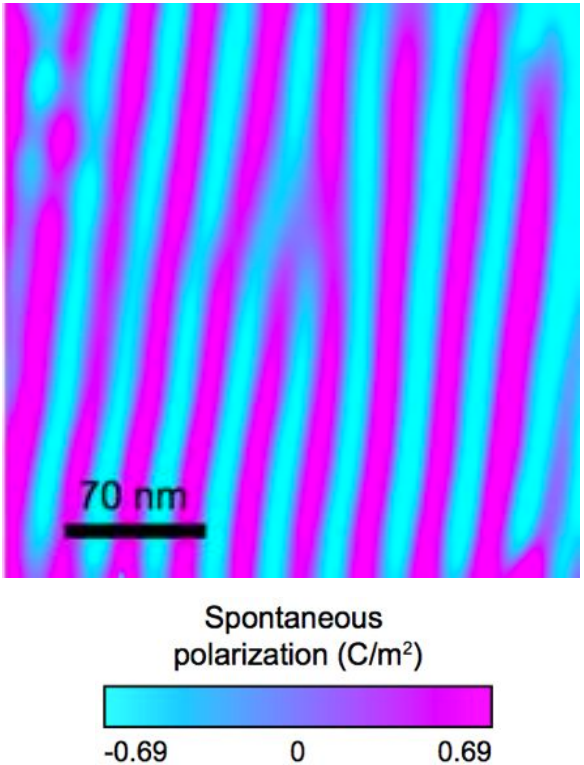

(left) Ferroelectric polarization domains in thin-film $PbTiO_3$ mapped by piezoresponse force microscopy.
(right) Domains imaged by x-ray Bragg ptychography to 5.7 nm.

S. Hruszkewycz, PRL 110, 177601 (2013)

Holography

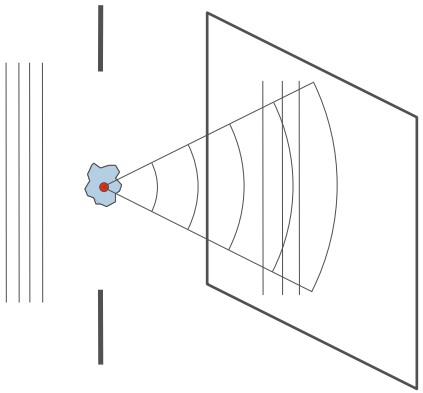

Gabor

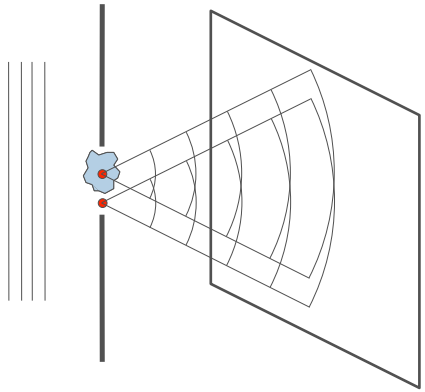

Fourier transform

Record hologram

$$I = |a+b|^2 = |a|^2 + |b|^2 + a^* b + a b^*$$

Reconstruct

$$\begin{aligned} bI &= b|a|^2 + b|b|^2 + a^* bb + abb^* \\ &= aI_b + b(I_a + I_b) + \text{background} \end{aligned}$$

- Reference wave encodes magnitude and phase of object wave
  - Reconstruct object wave by "re-illuminating" hologram with reference wave (or its C.C.)

Gabor holography

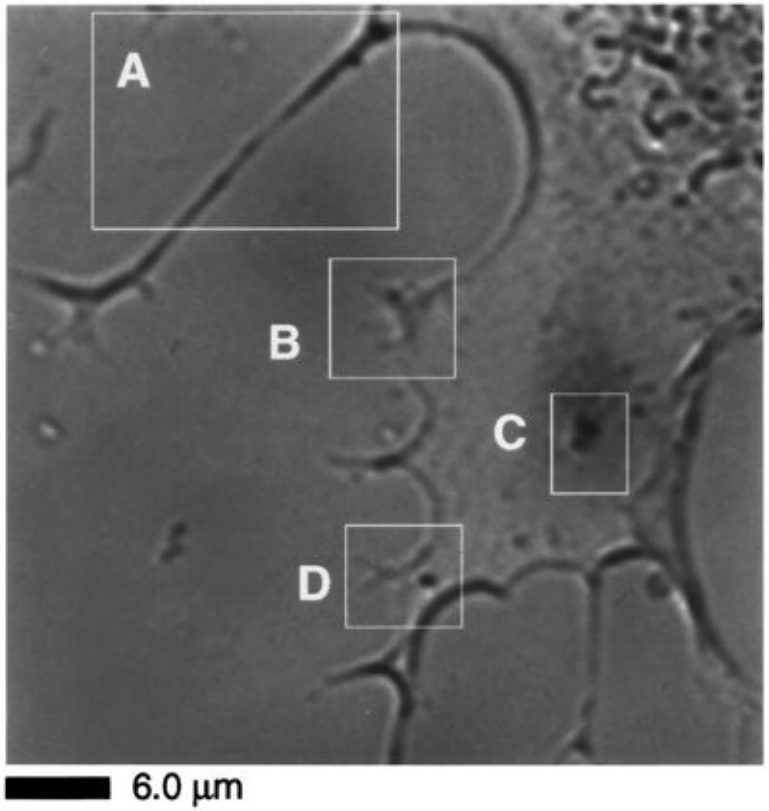

Visible light

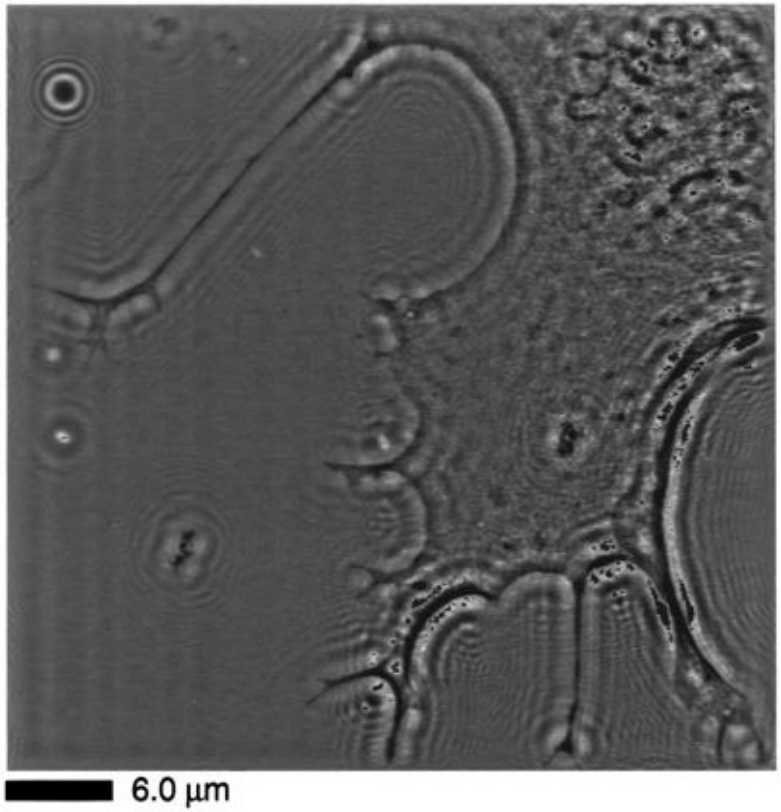

X-ray

Reconstructed hologram (right) of a NIL8 hamster neural fibroblast recorded with 656 eV x-rays. Estimated dose was 7.5 x105 Gy

S. Lindaas, JOSA A13, 1788 (1996)

FT hologram formation

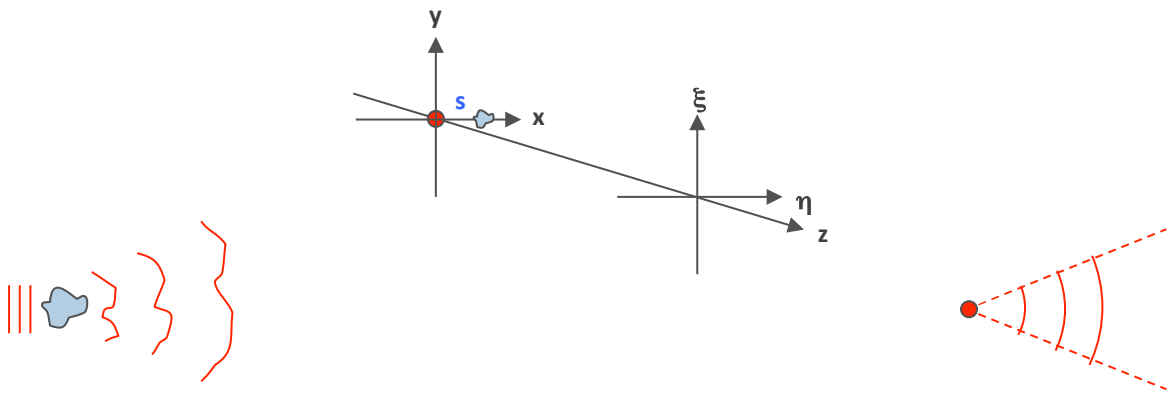

$$a(\xi,\eta) = \frac{e^{ikz}}{i\lambda z}\iint a(x-s,y)\; e^{\frac{ik}{2z}\left((x-\xi)^2+(y-\eta)^2\right)}\,dxdy$$

object wave

$$b(\xi,\eta) = \frac{e^{ikz}}{i\lambda z} b_0 e^{\frac{ik}{2z}\left(\xi^2+\eta^2\right)}$$

reference wave

$$I = |a+b|^2 = |a|^2 + |b|^2 + a^* b + a b^*$$

hologram intensity

Reconstruction

- Numerically take FT of hologram intensity to reconstruct
- Spatially separated primary, conjugate object waves result
- Weak curvature f(x,y) on object wave can be ignored

Image terms: $$a^*b+ab^* = \varphi(s\xi)F(\xi,\eta)+\varphi(s\xi)^*F(\xi,\eta)^*$$

where: $$F(\xi,\eta) = \frac{e^{ikz}}{i\lambda z} f(\xi,\eta)\iint a(x,y)f(x,y)e^{-\frac{ik}{z}(x\xi+y\eta)}\,dxdy \quad ,$$

$$\varphi(s,\xi) = e^{-\frac{ik}{z}s\xi} \quad \text{and} \quad f(\xi,\eta) = e^{\frac{ik}{2z}(\xi^2+\eta^2)}$$

$$FT^{-1}\left\{a^*b+ab^*\right\} = \boxed{f(x-s,y)\,a(x-s,y)} + f(-(x-s),-y)^*\,a(-(x-s),-y)^*$$

UE56-SGM beamline and ALICE

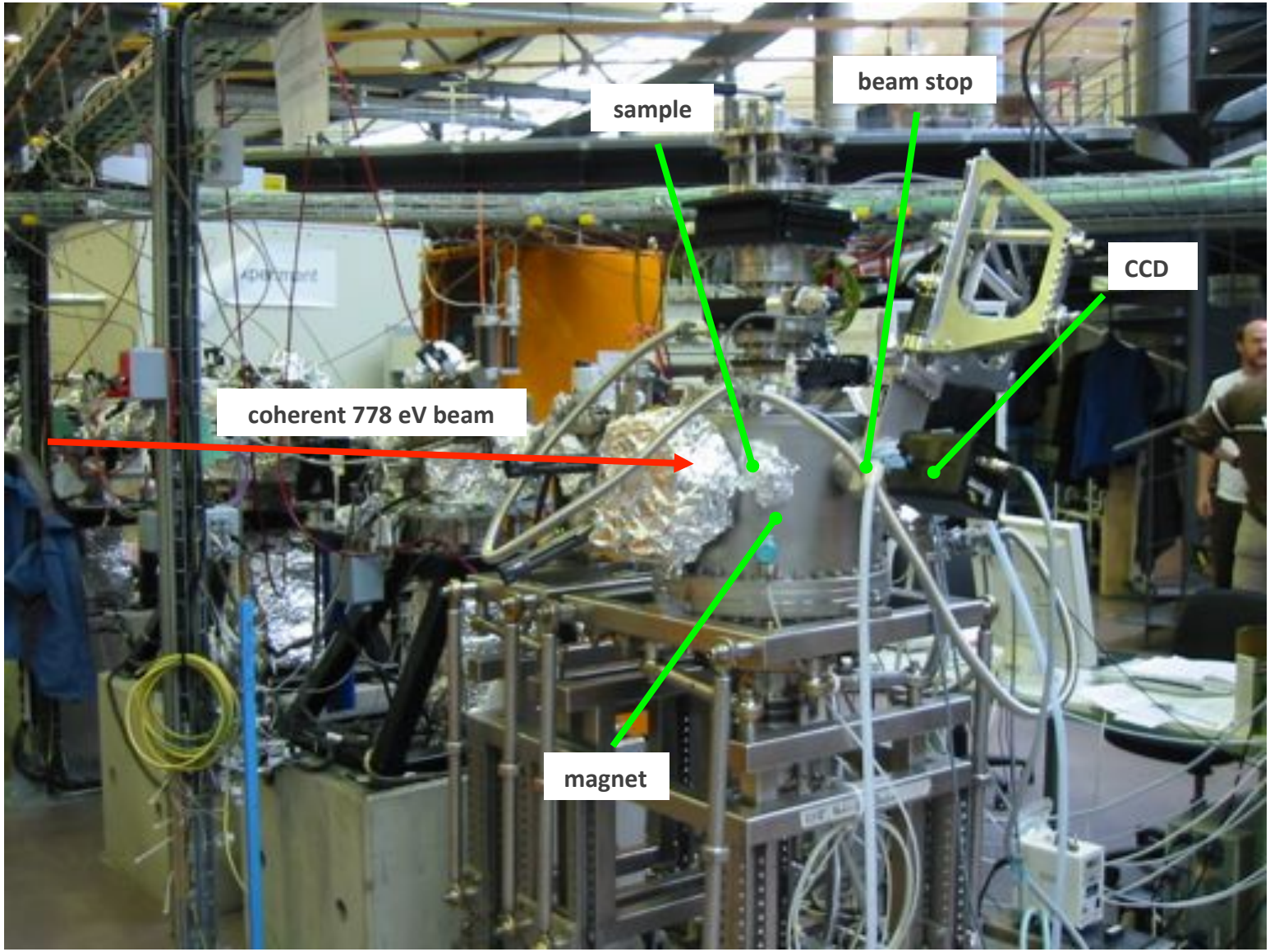

Fourier transform holography with a pinhole mask

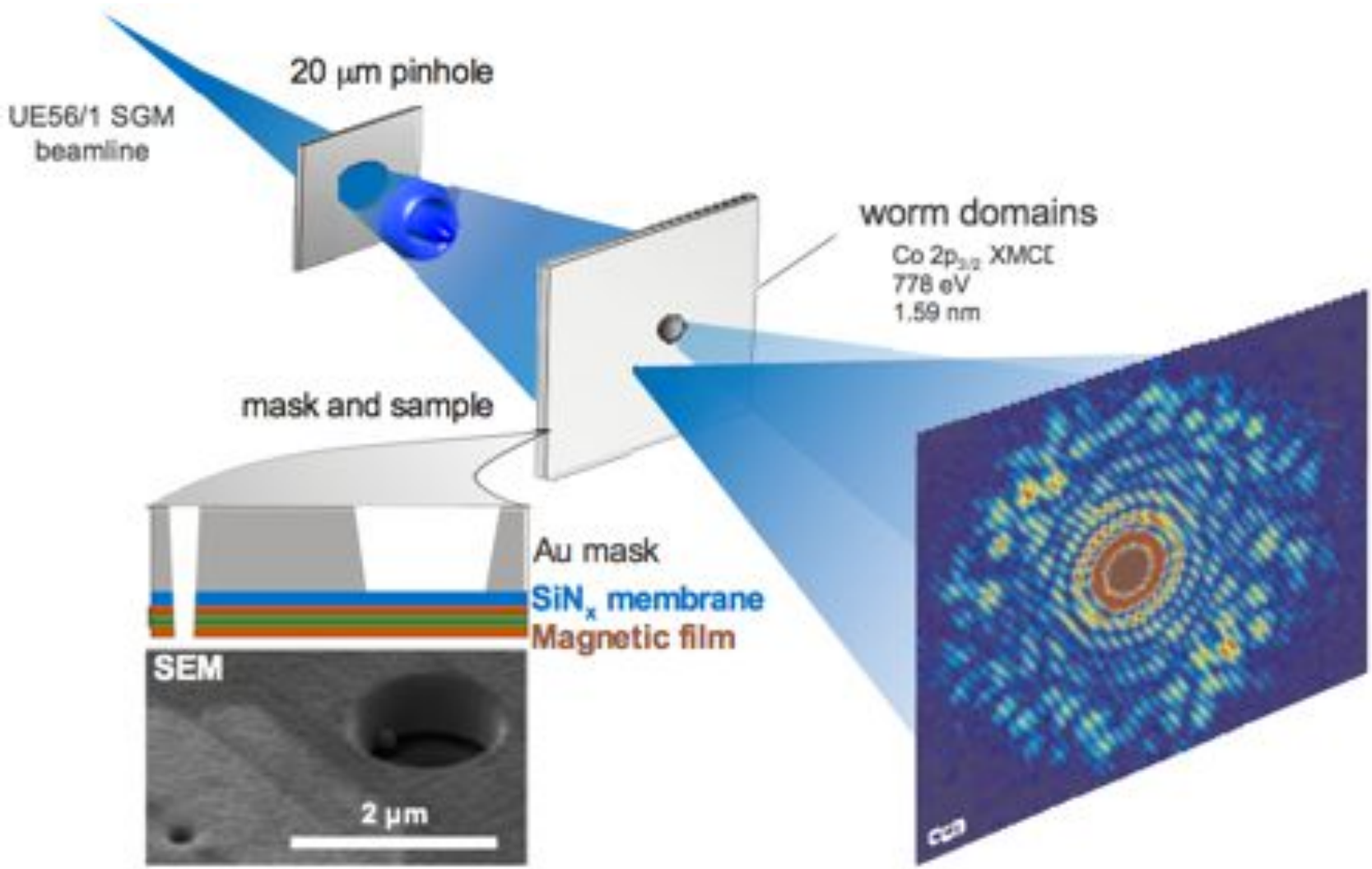

S. Eisebitt, Nature 432, 885 (2004)

FTH

STXM

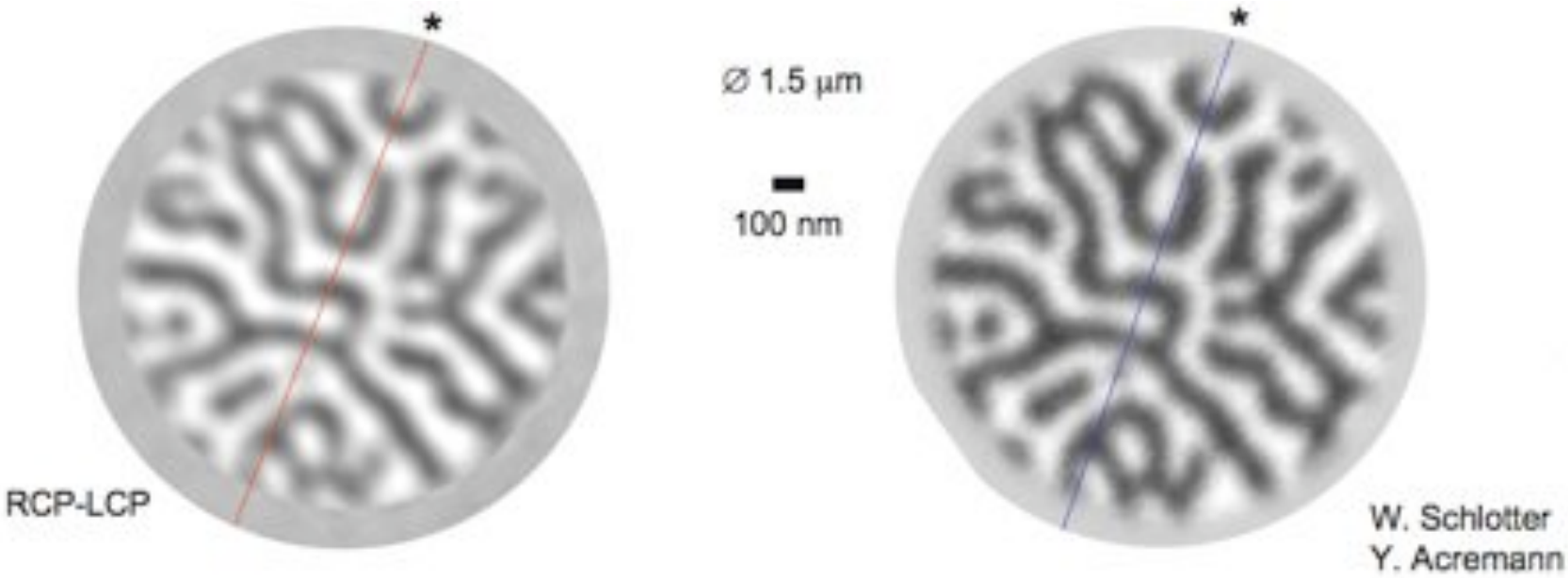

Reconstructed resolution ~50 nm

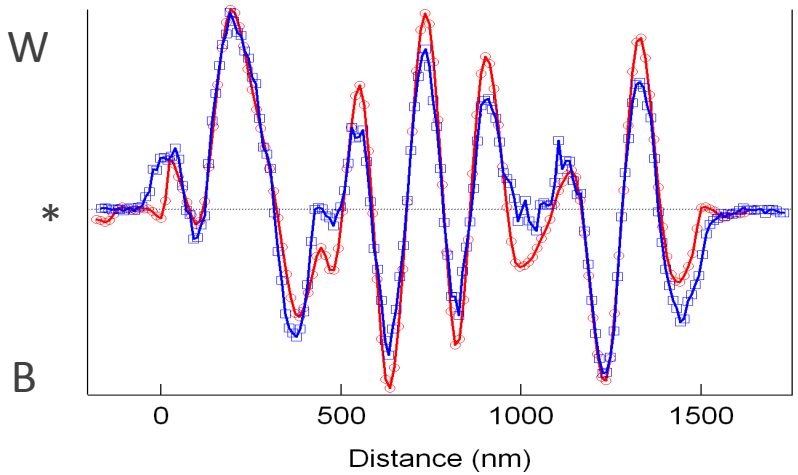

Resolution ~35 nm

S. Eisebitt,
Nature 432, 885 (2004)

Single-shot compatible

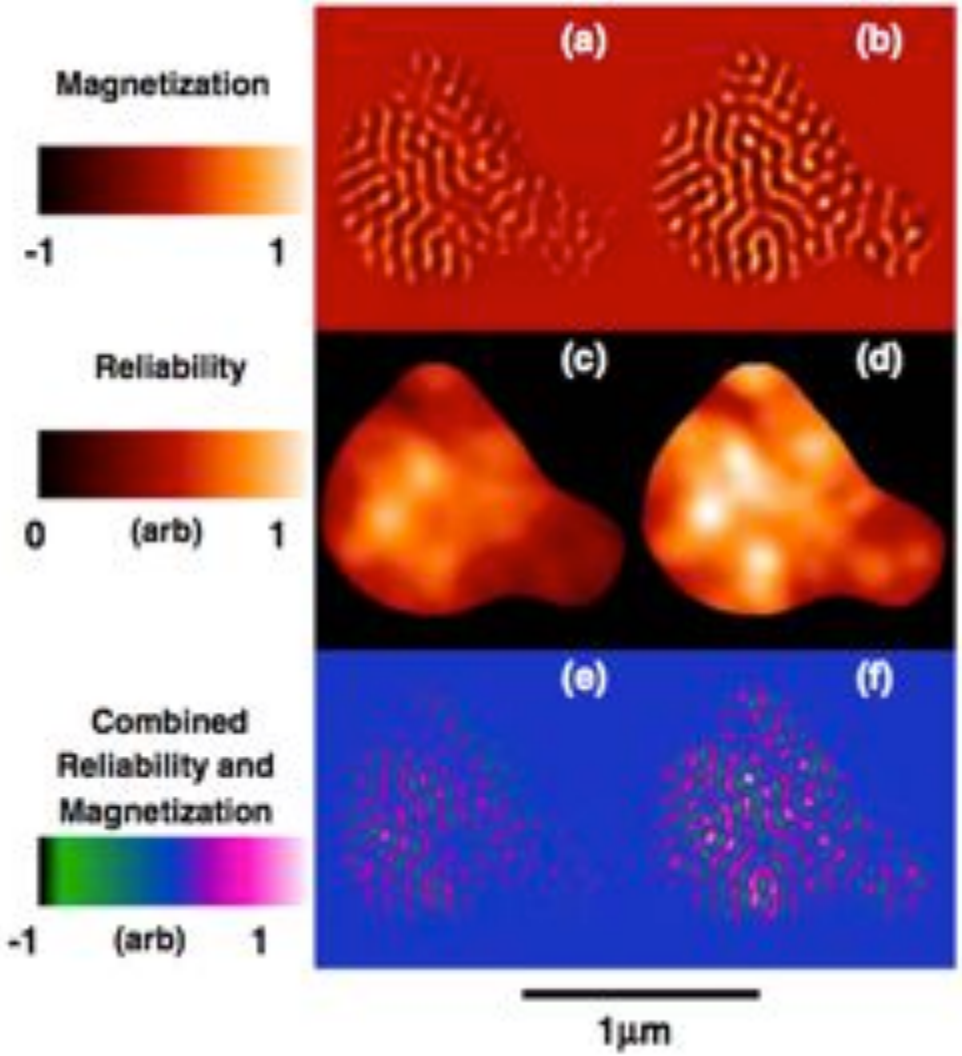

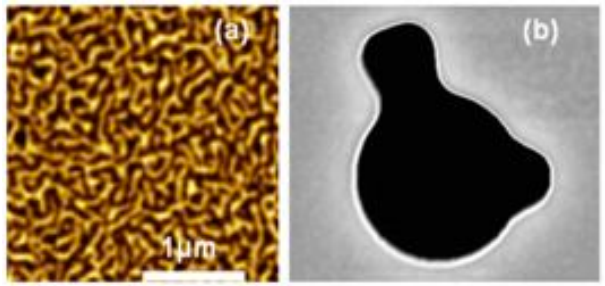

Sample: [0.7 nm Pt/1.2 nm Co]$_{x50}$ multilayer on Si_3N_4 membrane

(a) MFM image

(b) Gold proximity mask

S. Flewett, PRL 108, 223902 (2012)

CDI can be done on a tabletop!

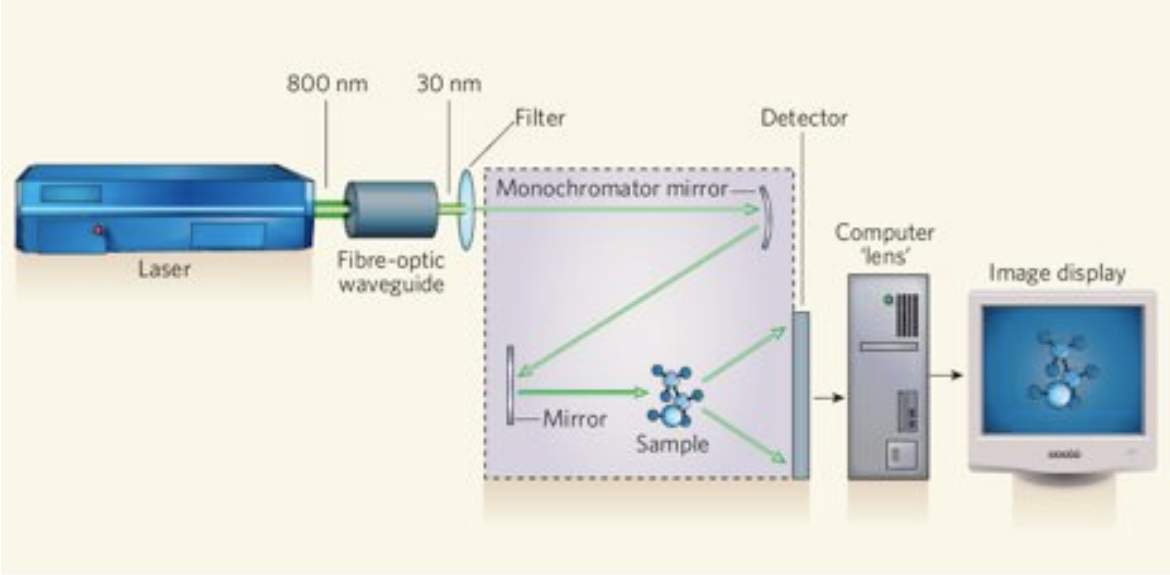

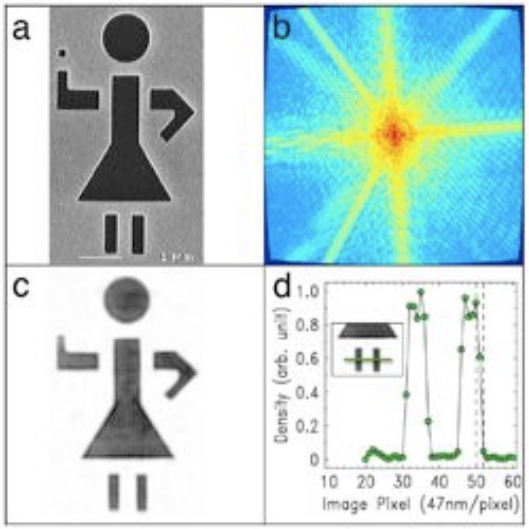

R. Sandberg, PRL 99, 098103 (2007)

R. Sandberg, PNAS 105, 24 (2008)

First ultrafast CDI of a virus with an x-ray laser

Linac Coherent Light Source at Stanford University, CA

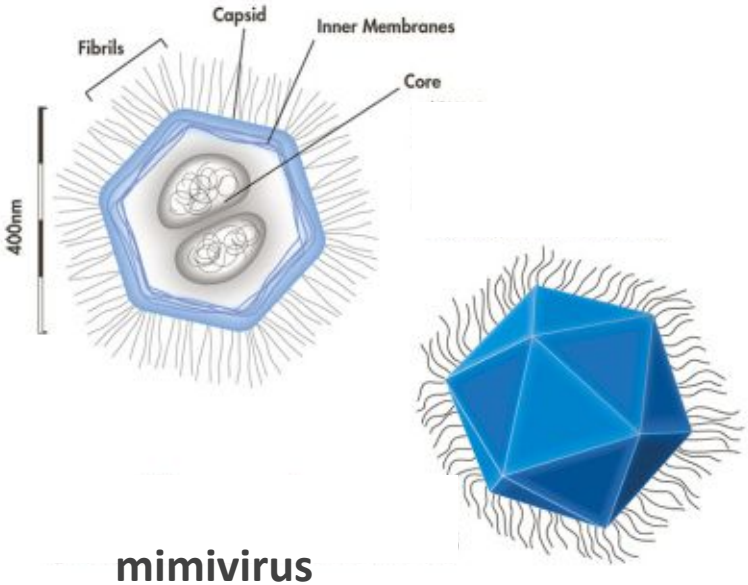

mimivirus

1.8 keV x-rays,
70 fs exposure !

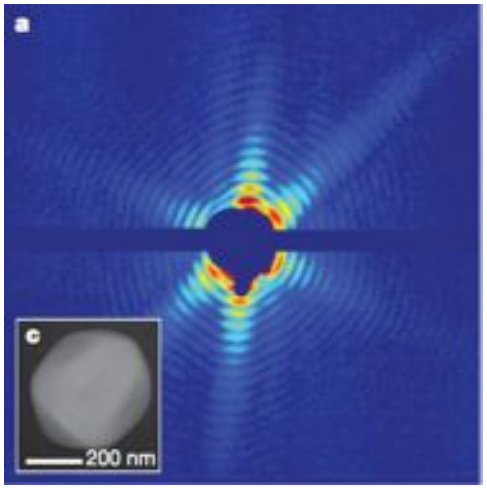

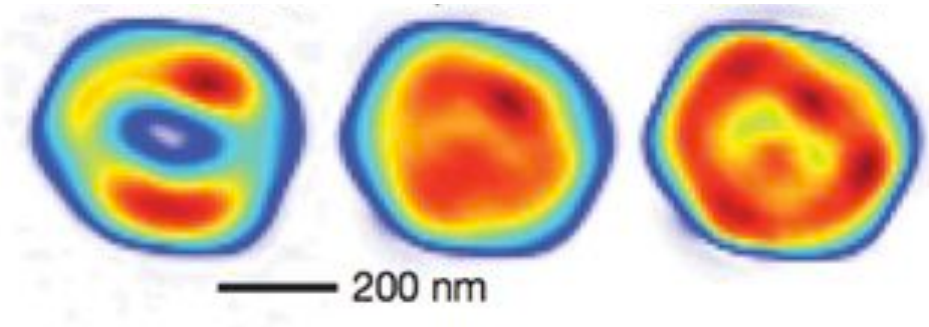

M. Seibert, Nature 470, 78 (2011)

Imaging lattice dynamics: Laser pump - CDI probe

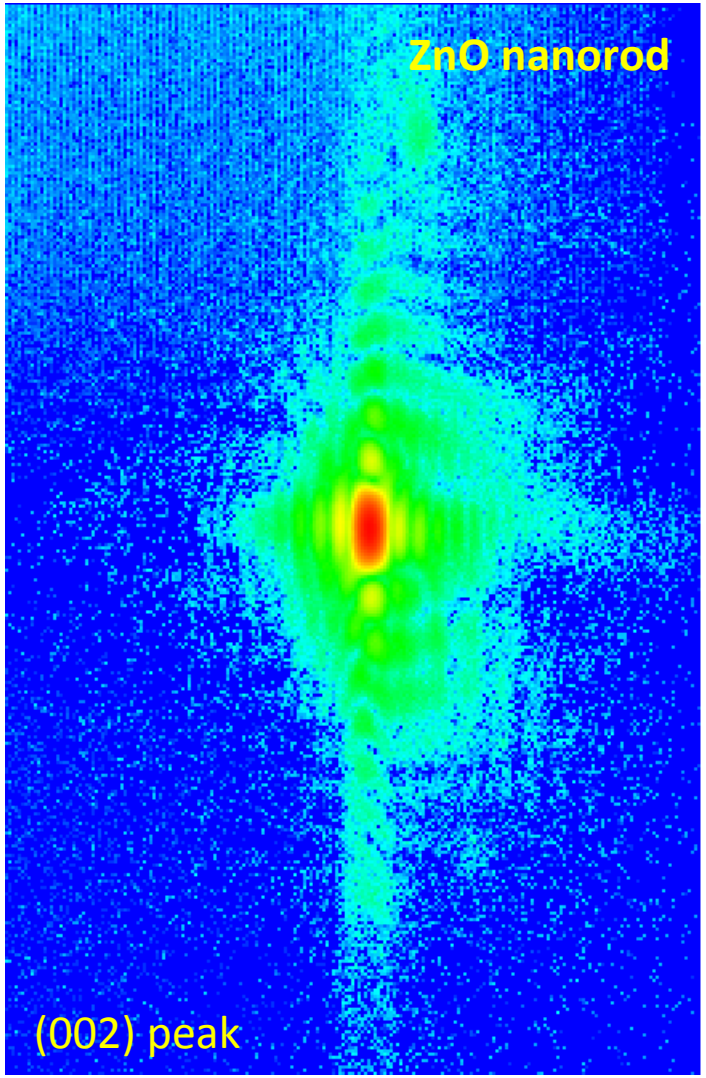

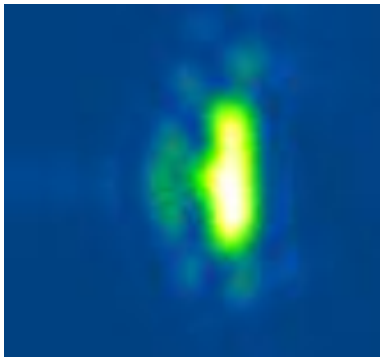

Diffraction pattern as a function of laser delay.
fast period = 400ps
slow period = 5.56ns

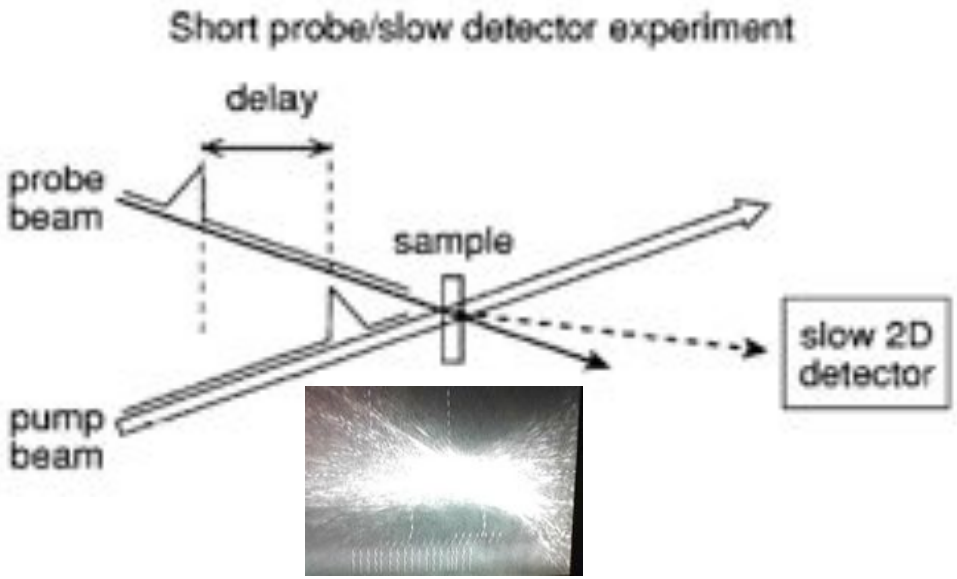

E. Dufresne, Nucl. Instrum. Meth A 649, 191 (2011)

Imaging lattice dynamics: Laser pump - CXD probe

$$DifferenceMap = FT[(A_1^{Exp} - A_2^{Exp})\exp(i\phi_1^{recon})]$$

A_1^{Exp} - Measured Amplitudes of the reference structure (no laser)
ϕ_1^{recon} – Phases retrieved for the reference data.
A_2^{Exp} – Measured Amplitudes of modified structure (laser fixed time offset)

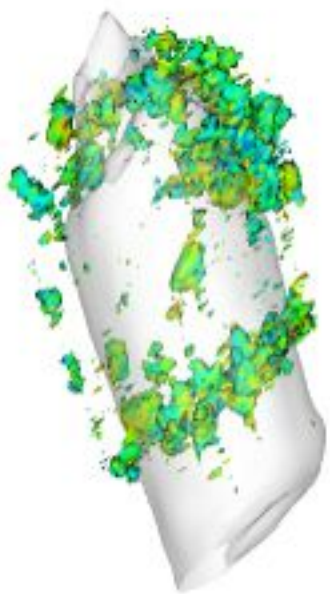

Time zero

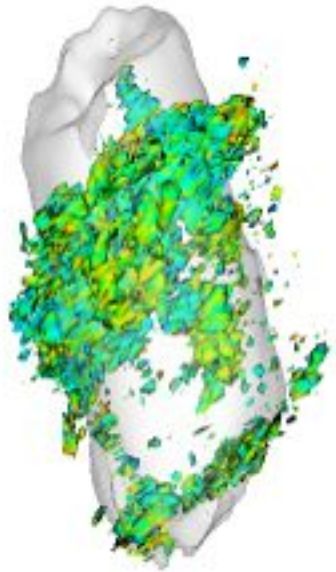

Time +50ps

Phonon modes in a laser-shocked gold nanocrystal

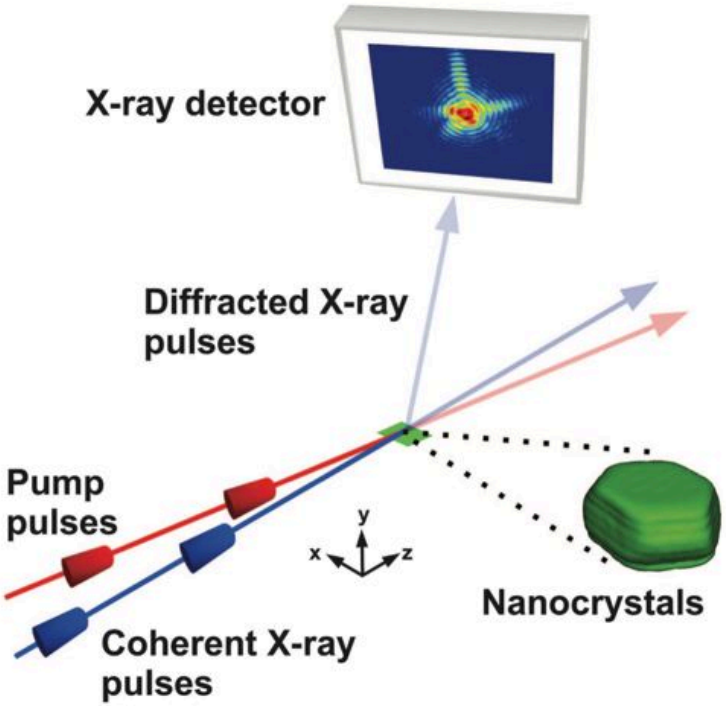

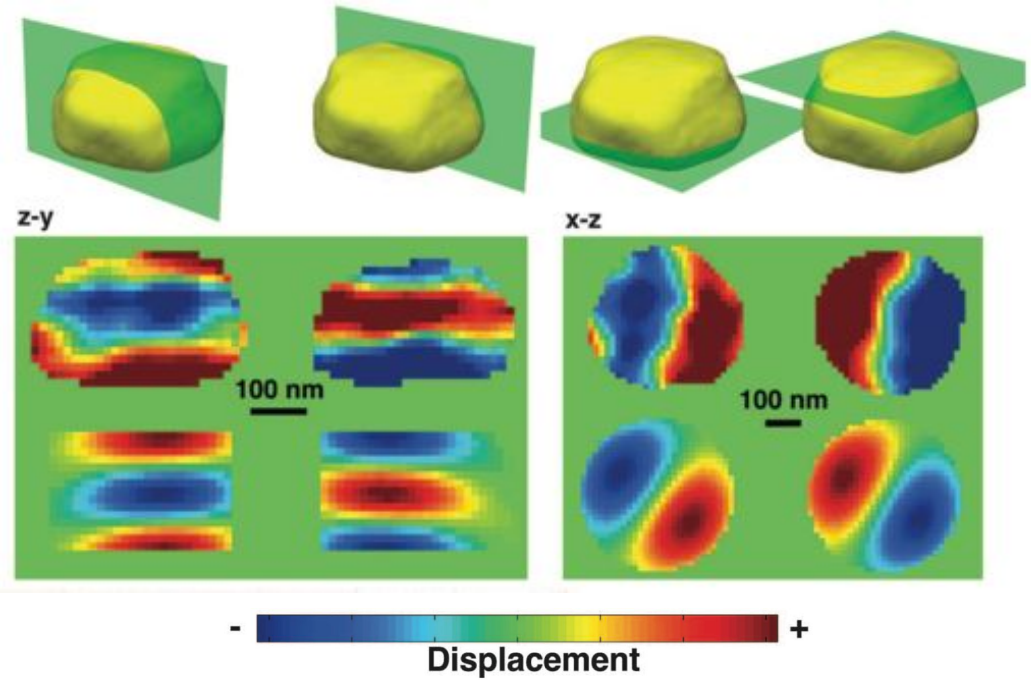

(top) Orthogonal slices taken either side of the center of a gold nanocrystal.
(middle) Projected displacement obtained from experiment.
(bottom) Simulated (1, 1) mode for a cylinder.

Comparison is for a delay time of +110 ps for a separation of 180 nm between z-y an
120 nm between x-z slices.

J. Clark, Science 341, 56 (2013)

Imaging resolution by x-ray holography

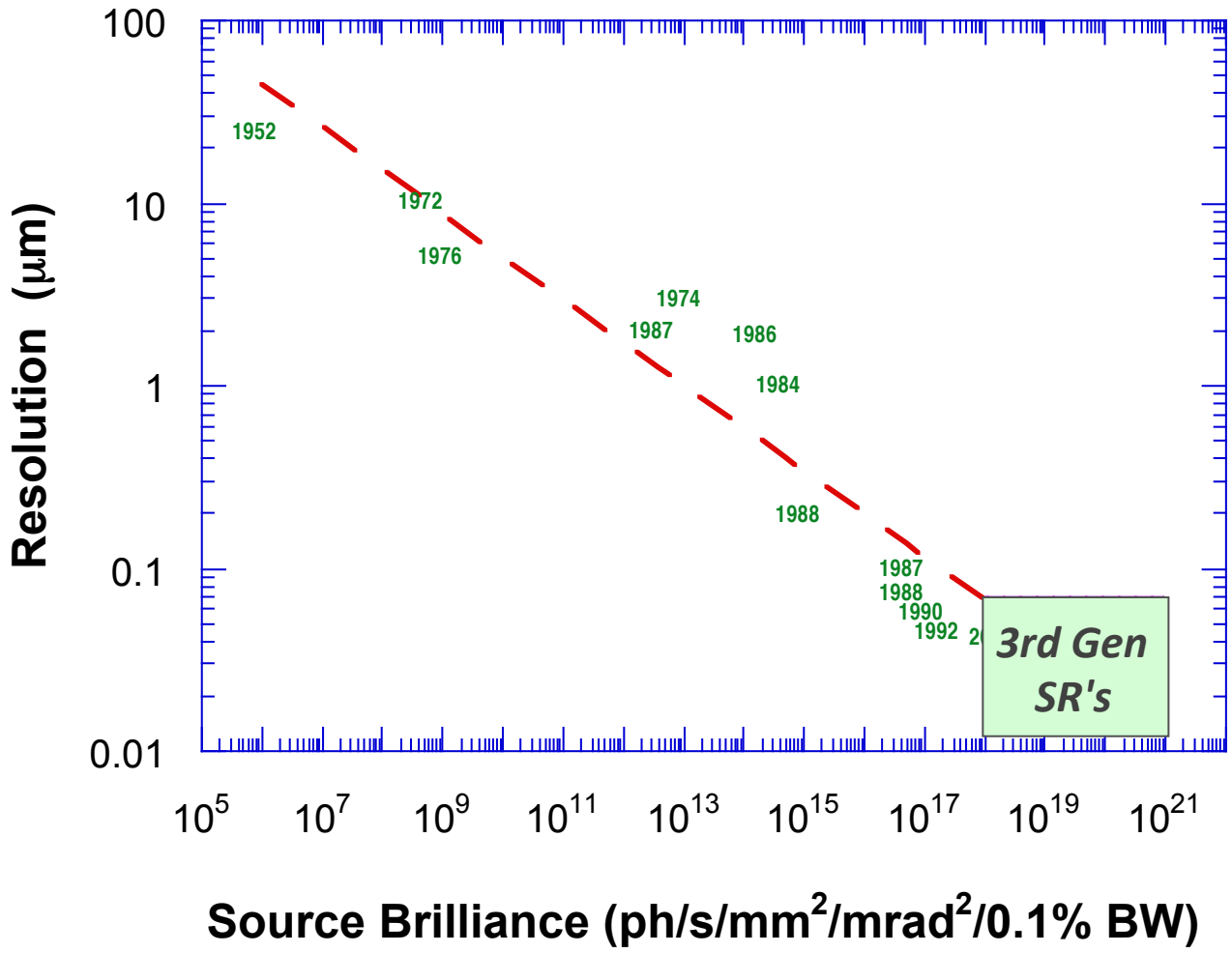

Coherent vs. total flux of SR sources

Flux per spatially coherent mode: $F_c = B\,\lambda^2/4$

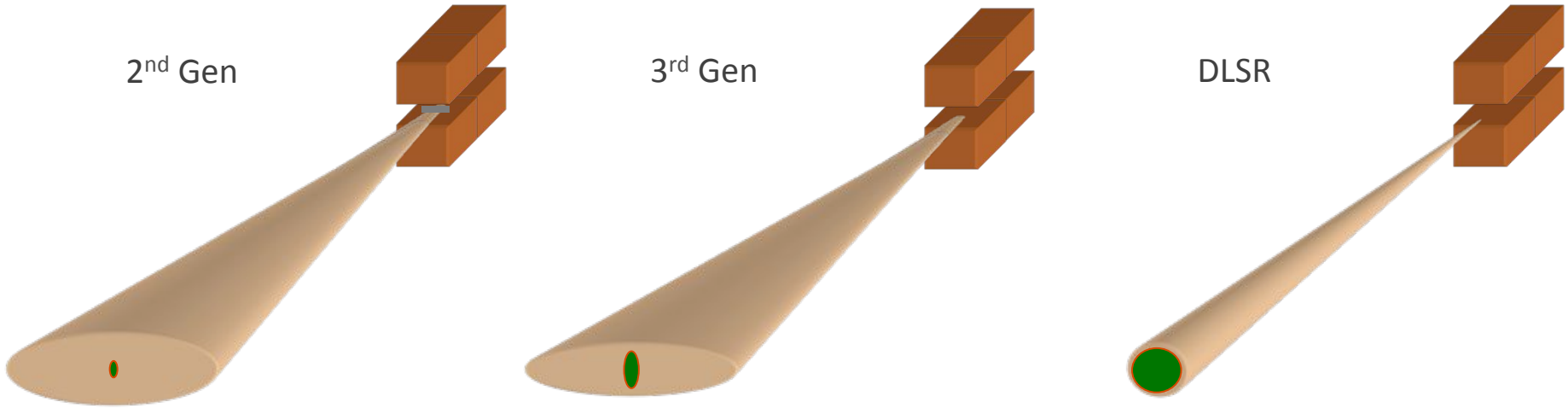

Large emittance, low brilliance,
small coherent fraction and flux

Small emittance, high brilliance,
large coherent fraction and flux

APS source today and proposed "MBA lattice"

Today

Future: 100-fold increase in brightness

- Bunch structure, flux:
  - Pump-probe diffraction/crystallography
  - Pump-probe scattering
  - Imaging
  - CDI
- Brightness:
  - XPCS
  - Imaging
  - CDI
  - IXS

APS brightness with MBA lattice

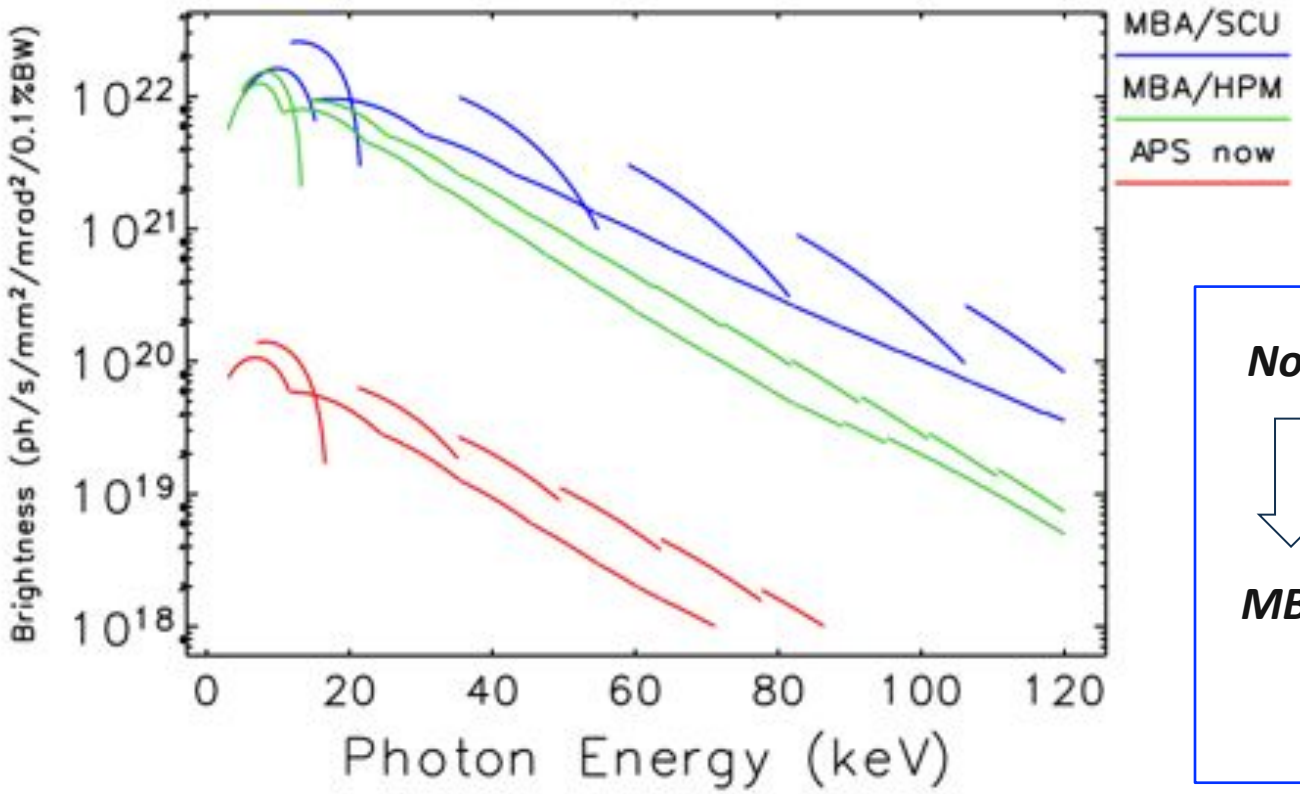

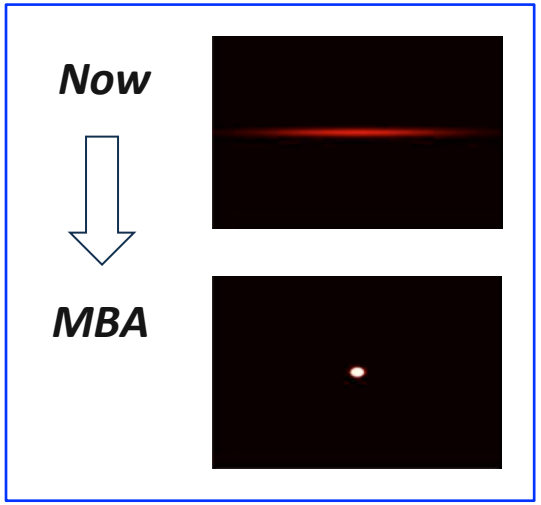

Figure 1: Comparison of brightness from the present APS to selected hybrid-permanent magnet and superconducting undulators in the MBA lattice design described here.

M. Borland (ANL)

Coherent fraction of proposed DLSR's

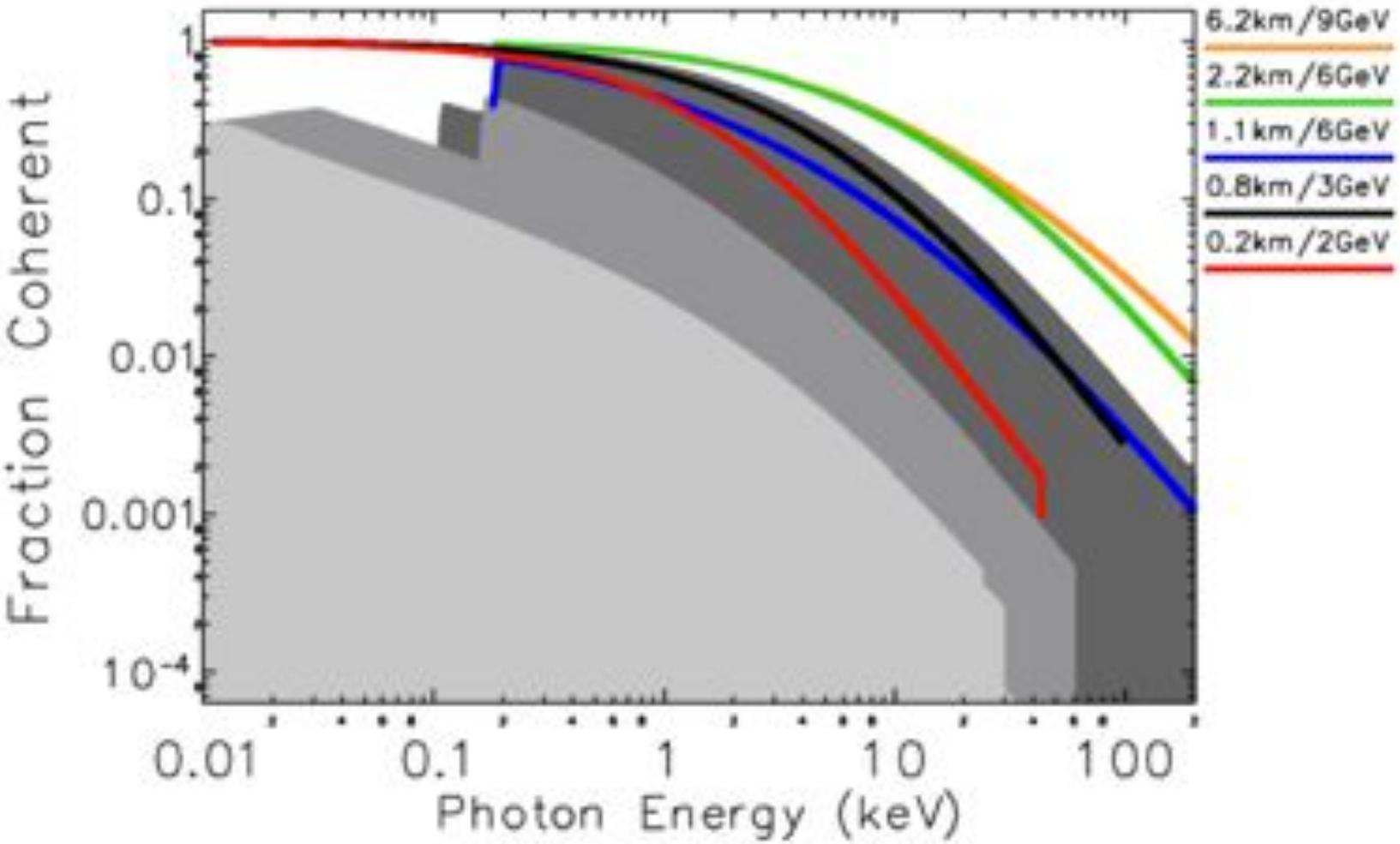

Partial coherent light can be treated as a distribution of coherent modes

$$J(\boldsymbol{r}_1, \boldsymbol{r}_2) = \sum_{n=1}^{N} \mu_n \psi_n(\boldsymbol{r}_1) \psi_n^*(\boldsymbol{r}_2),$$

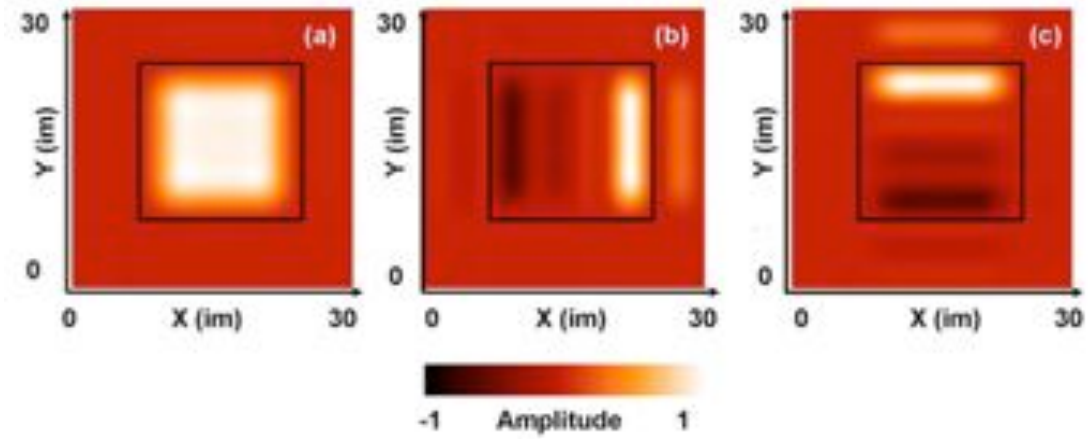

Coherent modes for the lower-coherence set of experimental data. The square delineates the edge of the physical aperture. (a) (0,0) mode, (b) (1,0) mode, (c) (0,1) mode.

S. Flewett, Opt. Lett 34, 2198 (2009)

Diffractive imaging with partially coherent light

- Conventional phase retrieval algorithms that assume full coherence break down with partially coherent light

$$I(\boldsymbol{k}) = \sum_{n=1}^{N} \mu_n I_n(\boldsymbol{k})$$

- If you know (or guess) the modal distribution (i.e. its weighting μ_n), you can fold this into the algorithm to optimize for each mode

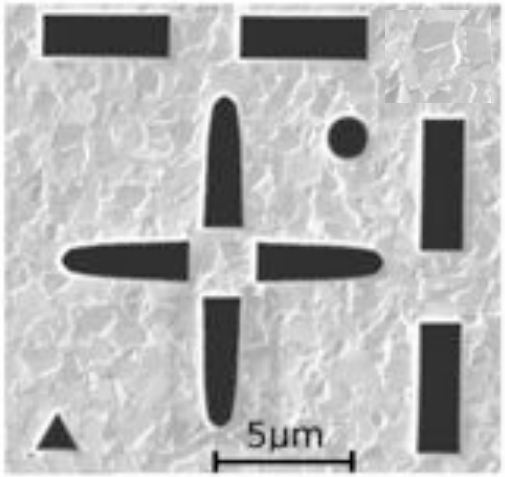

SEM of Au test pattern

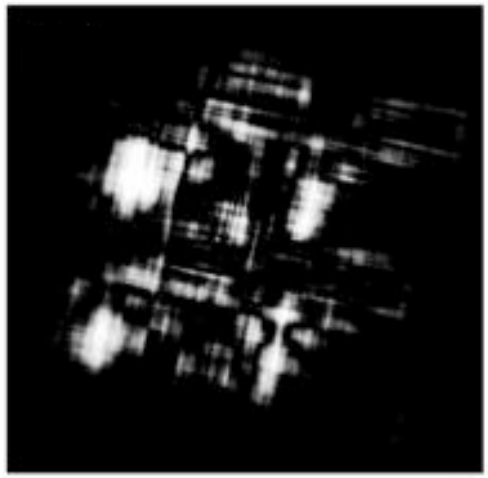

Conventional reconstruction with partial spatial coherence

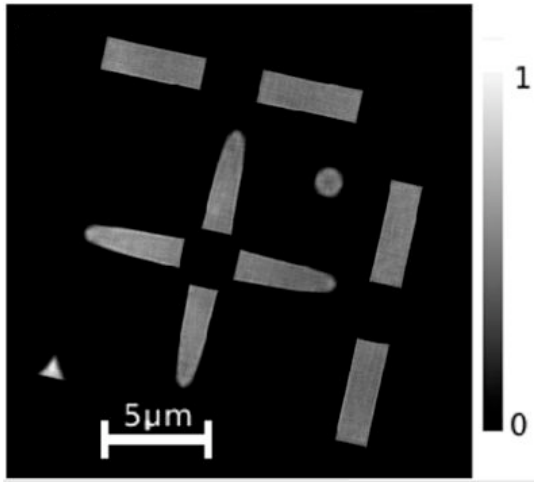

Reconstruction incorporating 3 spatially coherent modes

L. Whitehead, PRL 103, 243902 (2009)

Going broadband: use polychromatic light

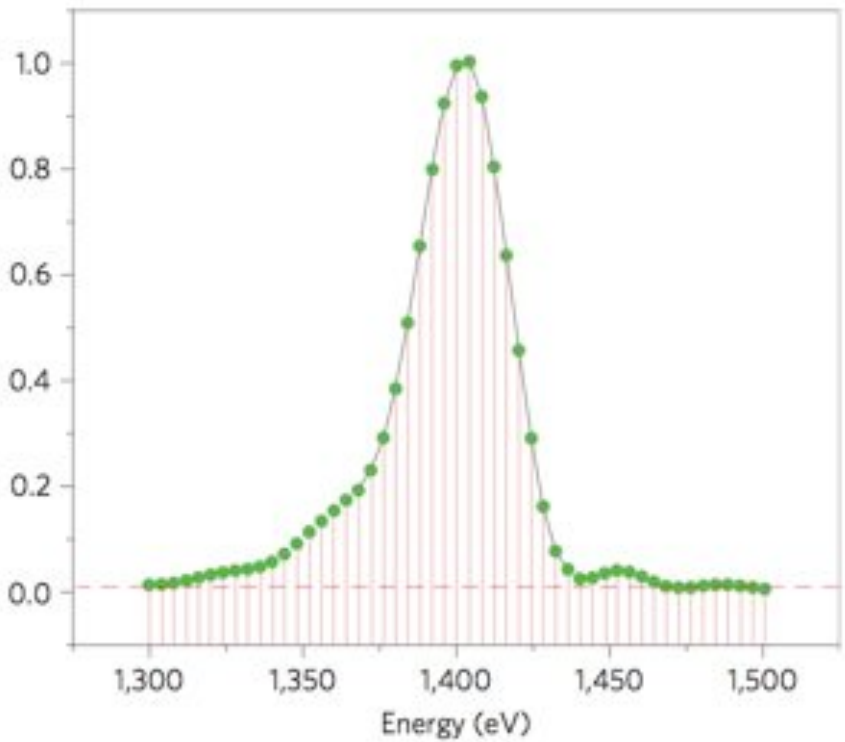

Use of entire first undulator harmonic (~2.5% BW) gives 60x gain in measurement speed.

B. Abbey, Nature Photonics 5, 420 (2011)

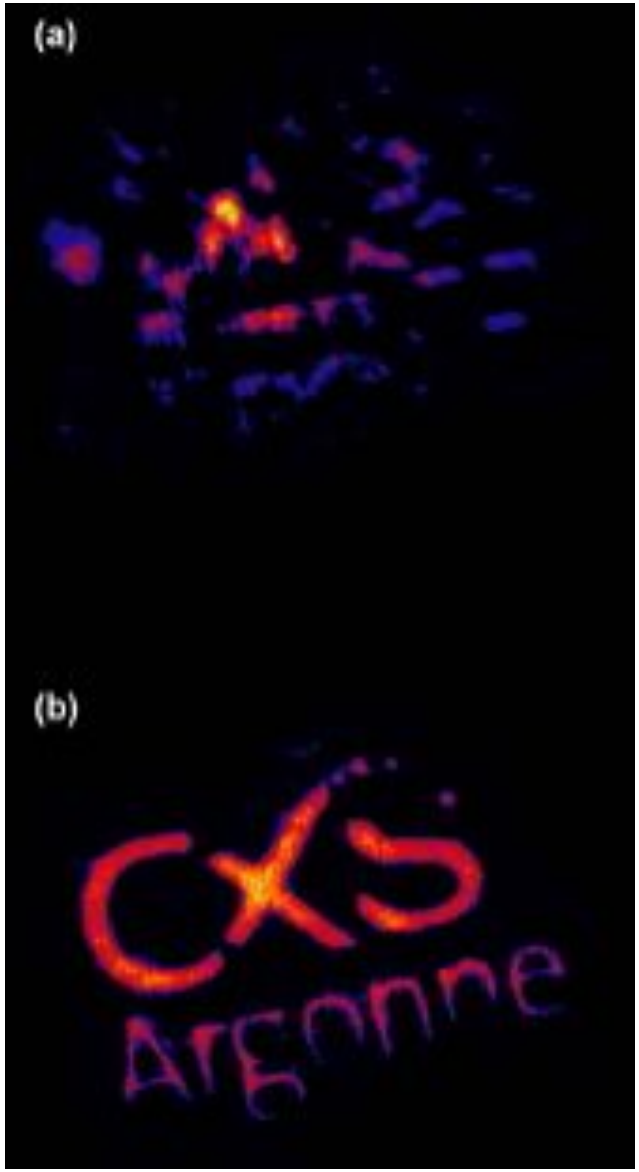

"Mr. Osborne, may I be excused?
My brain is full."

Summary

- Contrast, resolution, sources, optics and detectors; x-ray imaging regimes
- Direct methods: projection and full-field
- Indirect methods: coherent diffractive imaging, ptychography, holography, and time-resolved
- Brighter sources, partially coherent methods

Many thanks to

Ercan Alp

The many people who graciously shared their slides for these lectures

... and thank you!